



Controlled Synthesis of MOF-235 Derivatives for Efficient Dye Removal from Wastewater

Chengrui Xie, BSC, MRes

**A thesis submitted in fulfilment of the requirements for
the degree of Doctor of Philosophy**

August 2024

Abstract

The contamination of water by synthetic dyes has become a significant environmental issue, attracting increasing attention due to the harmful effects of dye-contaminated wastewater on aquatic ecosystems and human health. This has driven the development of advanced materials and technologies aimed at effectively removing dyes from water. Adsorption and catalytic degradation are two promising approaches for this purpose, offering both efficiency and sustainability. To achieve these goals, this work focuses on the synthesis of metal-organic frameworks (MOFs) using a controlled synthesis method and a sustainable synthesis technique, followed by their conversion into porous carbon materials for enhanced dye removal.

A novel controlled synthesis method for MOF-235 was developed to increase the adsorption capacity for methyl orange. A yield of 166.7% was achieved compared to conventional methods. The synthesised MOF-235 exhibits a uniform octahedral shape with a narrow size distribution. Adsorption studies showed a maximum capacity of $1257.7 \text{ mg}\cdot\text{g}^{-1}$, surpassing both the traditionally synthesised MOF-235 ($477 \text{ mg}\cdot\text{g}^{-1}$) and other MOFs. Physical adsorption was confirmed as the primary mechanism, with optimal adsorption conditions identified.

In addition, Fe@C-350, a highly porous carbon adsorbent, was obtained by carbonisation of MOF-235 under an argon atmosphere and showed an increased surface area and pore size. This material showed advanced adsorption efficiency for

methyl orange over a wide pH range with a maximum adsorption capacity of 1666.7 $\text{mg}\cdot\text{g}^{-1}$. Kinetic analysis revealed a fast adsorption rate with a rate constant of 0.025 $\text{g}\cdot\text{mg}^{-1}\cdot\text{min}^{-1}$, which can be attributed to the pore characteristics and abundant active sites. Remarkably, Fe@C-350 retained over 98% of its initial adsorption capacity after 10 regeneration cycles, confirming physical adsorption as the main mechanism.

To further improve the removal efficiency of methyl orange while reducing the cost of material development, a carbon nanocomposite catalyst (PD-Fe@Cx) was synthesised using terephthalic acid from pyrolysed PET plastic waste, which can be used as a heterogeneous Fenton-like catalyst for methyl orange degradation. PD-Fe@Cx exhibited optimal catalytic activity at a pyrolysis temperature of 350°C and effectively degraded methyl orange in the presence of hydrogen peroxide. The reaction parameters, including initial dye concentration, H₂O₂ dosage and pH, were optimised, with PD-Fe@C350 achieving 99.9% methyl orange degradation at a rate constant of 1.171 min^{-1} under optimal conditions. This approach not only utilises the properties of MOF carbons, but also promotes sustainability through the reuse of PET waste for environmental remediation.

In summary, this study makes an important contribution by developing highly efficient MOF-based porous carbon materials and PET-based catalysts for the effective removal and degradation of synthetic dyes and provides a sustainable solution to water pollution. Further work is needed to optimise the synthesis

processes for industrial applications, in particular to improve material stability and scalability. In addition, the extension of this approach to other environmental pollutants will be crucial to advance the sustainability and efficiency of these materials in real-world applications.

Achievements

Journal publications

Xie, C.R., Song, Y.X., Yang, G., Sun, C.G., Luo, X. and Wu, T., 2024. Porous carbon derived from MOF-235 for the adsorption of methyl orange with high capacity. *Materials Today Communications*, p.110843.

Xie, C.R., Song, Y.X., Sun, C.G., Luo, X. and Wu, T., Controlled synthesis of uniform MOF-235 for the adsorption of methyl orange in wastewater with high efficiency and high capacity. (Submitted for review)

Xie, C.R., Meng, Y., Sun, C.G., Luo, X. and Wu, T., Recycled PET Plastic Bottle Derived Carbon for Highly Efficient Heterogeneous Fenton-like Degradation of Methyl Orange. (Prepared for submission)

Hong, Y., **Xie, C.R.**, Chen, W., Luo, X., Shi, K.Q. and Wu, T., 2020. Kinetic study of the pyrolysis of microalgae under nitrogen and CO₂ atmosphere. *Renewable Energy*, 145, pp.2159-2168.

Jiang, P., **Xie, C.R.**, Luo, C.L., Meng, W., Yang, G., Yu, G.S., Gong, Y., Xu, M. and Wu, T., 2021. Distribution and modes of occurrence of heavy metals in opposed multi-burner coal-water-slurry gasification plants. *Fuel*, 303, p.121163.

Lan, D.W., Zhu, H.W., Zhang, J.W., **Xie, C.R.**, Wang, F., Zheng, Y.Y., Guo, Z.Y., Xu, M.X. and Wu, T., 2024. Heterojunction of UiO-66 and porous g-C₃N₄ for

boosted photocatalytic removal of organic dye. *Applied Surface Science*, 655, p.159623.

Lan, D.W., Zhu, H.W., Zhang, J.W., **Xie, C.R.**, Wang, F., Zheng, Y.Y., Guo, Z.Y., Xu, M.X. and Wu, T., 2024. Green One-Pot Synthesis of Mesoporous g-C₃N₄ for Promoted Organic Dyes Photodegradation in Wastewater Treatment. *Industrial & Engineering Chemistry Research*, 63(8), pp.3491-3503.

Patents

An iron-based MOF material and its preparation method and application. 一种铁基 MOF 材料及其制备方法和用途, 2022. Application Number: ZL202211553559.8.

An electroplating wastewater treatment system. 一种电镀废水处理系统, 2022. Application Number: ZL202223351959.9.

Acknowledgement

First, I would like to deeply thank my PhD supervisors, Prof. Wu Tao, Dr Luo Xiang and Prof. Sun Chenggong, for their tireless support and selfless guidance. Over the past four years, Prof. Wu Tao has been instrumental in shaping both the experimental design and the writing of my thesis. Working with them has enriched my academic journey at the University of Nottingham Ningbo China, and their encouragement has played a crucial role in the completion of my thesis.

My special thanks go to the dedicated contributors who have provided invaluable help and insightful suggestions during my research and experiments. I also thank all my colleagues and friends — Dr Yang Gang, Dr Luo Chunlin, Dr Liu Shuai, Dr Mu Xueliang, Dr Yu Jiahui, Dr Liu Shu, Wang Fan, Zheng Yueying, Chen Quhan, Zhang Jianwen, Zhu Huiwen, Lan Dawei, Guo Zeyu, Yan Zijun, Wan Cong and many others — for their continuous support.

I appreciate the contributions of Karen Ning, Julian Zhu, Jane Zhang, Karey Shan, Helen Xu and others. A special mention goes to Carey Tao, Kelly Yao, William Zhang and many others for their significant contributions to the safety and management of the lab.

Above all, my deepest appreciation goes to my family. I am grateful to my parents for providing a supportive environment for me to pursue my goal. I am grateful to my sister for giving me very valuable advice at many moments. I would like to

thank my wife, and her family for their unwavering support and encouragement, which has been my constant source of strength. They are and will always be my motivation.

List of Figures

Figure 1.1 Frequency of publications on dye removal since 1991 to 2024 (Aug.) with the selected keyword 'Dye Removal'.....	3
Figure 1.2 Thesis structure.	10
Figure 3.1 Oil bath device (synthesis temperature = 80° C, synthesis time = 24 h).....	64
Figure 3.2 Adsorption test device.	65
Figure 3.3 Photoactivity test device.	67
Figure 3.4 Dye removal capacity evaluation rig.....	68
Figure 3.5 Principle of HPLC-MS.....	68
Figure 4.1 Schematic of the synthesis of MOF-235 under continuous strong stirring.....	77
Figure 4.2 SEM images of MOF-235 prepared by controlled synthesis method (a, b), MOF-235 synthesized by traditional hydrothermal method and (d) MOF-235 SEM image reported by others [157].	83
Figure 4.3 Comparison of synthesis efficiency: controlled synthesis method and traditional solvothermal method.	84
Figure 4.4 (a) XRD pattern of MOF-235 synthesized by oil bath method, (b) FTIR spectrum of control synthesized MOF-235.....	86
Figure 4.5 Influence of initial pH on adsorption (C_0 = initial concentration, V = solution volume, W = adsorbent mass, t = adsorption time, T = adsorption temperature).....	91

Figure 4.6 Influence of initial methyl orange concentration on adsorption ($V =$ solution volume, $W =$ adsorbent mass).....	92
Figure 4.7 Langmuir and Freundlich models of methyl orange adsorption on MOF-235.....	94
Figure 4.8 Results of the (a) pseudo-first-order and (b) pseudo-second-order kinetics models at a temperature of $25 \pm 1 \text{ }^\circ \text{C}$	102
Figure 4.9 Interconversion of methyl orange under acidic and alkaline conditions.	104
Figure 4.10 ESI mass spectra of methyl orange which (a) before adsorption and (b) after adsorption.	105
Figure 4.11 FTIR spectrum of methyl orange, MOF-235 and MOF-235 after absorbing methyl orange.	106
Figure 5.1 Synthesis process of MOF-235 and carbonised Fe@C-350.....	111
Figure 5.2 (a) TG result ($40\sim 500 \text{ }^\circ \text{C}$) of MOF-235 (b) Thermogravimetric-differential thermal analysis (TGA-DTA) curves of the Fe@C-350 in the range between room temperature ($25 \text{ }^\circ \text{C}$) and $350 \text{ }^\circ \text{C}$ and (c) MO adsorption capacities for MOF-235 carbonised at 330 to $500 \text{ }^\circ \text{C}$	119
Figure 5.3 TG results ($40\sim 350 \text{ }^\circ \text{C}$, keep $350 \text{ }^\circ \text{C}$ for 1 h) of MOF-235.	120
Figure 5.4 The SEM images of as-prepared (a) and (b) Fe@C-360, (c) and (d) Fe@C-380, (e) and (f) Fe@C-400.	121
Figure 5.5 The XRD spectrum of as-prepared MOF-235 and Fe@C-350..	123
Figure 5.6 The SEM images of as-prepared (a) and (b) Fe@C-330, (c) and (d) Fe@C-340, (e) and (f) Fe@C-350.	124
Figure 5.7 The nitrogen adsorption-desorption isotherm for Fe@C-350. ...	125

Figure 5.8 Langmuir isotherm and Freundlich isotherm models of MO on Fe@C-350 (V = 50 mL, W = 10 mg, pH = 6.8, adsorption time = 24 h).	128
Figure 5.9 (a) Pseudo-first-order kinetic and (b) pseudo-second kinetic models of methyl orange on Fe@C-350 (V = 100 mL, W = 50 mg, temperature = 25 ° C, pH = 6.8).	132
Figure 5.10 Effect of (a) initial concentration, (b) pH on adsorption performance, (c) adsorption time, (d) environment temperature and (e) adsorbents dosage.	136
Figure 5.11 Recyclability of Fe@C-350 after 10 cycles (x = the number of thermal regeneration cycles).	141
Figure 5.12 (a) The initial methyl orange sample and the methyl orange samples after adsorption and desorption in (b) the first regeneration cycle, (c) the ninth regeneration cycle and (d) the tenth regeneration cycle.	141
Figure 5.13 FT-IR spectra of Fe@C-350 and MO-loaded Fe@C-350.	143
Figure 5.14 The ratio of the desorbed methyl orange solution to the initial concentration (100mg • L ⁻¹) after 10 cycles (x = the number of thermal regeneration cycles).	144
Figure 6.1 Sustainable synthesis of PD-Fe@C and its application in the Fenton reaction.	150
Figure 6.2 (a) Comparison of the adsorption and degradation performance of methyl orange at different carbonisation temperatures, (b) fitting kinetic curves, (c) kinetic rates of PD-MOF-235 and its carbonised derivatives, and (d) TGA results of PD-MOF-235.	155

Figure 6.3 SEM images of a) purchased terephthalic acid, b) terephthalic acid obtained from the depolymerisation of PET waste bottles, c) PD-MOF-235, d) PD-Fe@C350..... 157

Figure 6.4 TEM images PD-Fe@C350..... 157

Figure 6.5 XRD patterns of a) PET derived terephthalic acid and purchased terephthalic acid and b) PD-Fe@C350 and PD-MOF-235, FTIR patterns of c) PET derived terephthalic acid and purchased terephthalic acid, d) PD-Fe@C350 and PD-MOF-235..... 162

Figure 6.6 Effect of key parameters on degradation the methyl orange: a) H₂O₂ and catalyst existence; b) initial methyl orange concentration and c) H₂O₂ dosage; d) initial solution pH, and (e) kinetic rates of PD-Fe@C350 in the pH range from 3 to 7. 169

Figure 6.7 (a) XPS survey spectrum of fresh PD-Fe@C350 and photochemical reacted PD-Fe@C350, and (b) Fe 2p spectra of fresh PD-Fe@C350 and photochemical reacted PD-Fe@C350..... 172

List of Tables

Table 1.1 Characteristics of methyl orange [38-40].	6
Table 4.1 Comparison of textural properties of MOF-235 prepared in this and other studies.	89
Table 4.2 Results of factors relevant to the methyl orange adsorption process at three distinct temperatures.	95
Table 4.3 Comparison of various adsorbents in methyl orange adsorption... ..	99
Table 4.4 Parameters associated with the pseudo-first order and pseudo-second order models at a temperature of 25 ± 1 ° C.	101
Table 5.1 BET parameters and methyl orange adsorption capacity for the carbon adsorbents and MOF adsorbents.	126
Table 5.2 Comparative fitting outcomes for the Langmuir and Freundlich adsorption models.	130
Table 5.3 Comparative fitting outcomes for the Pseudo-first-order kinetic and Pseudo-second-second kinetic models.	133
Table 5.4 Comparison of methyl orange adsorption capacity and efficiency of different MOF-based adsorbents.	139

List of Abbreviations

IUPAC International Union of Pure and Applied Chemistry

BET Brunauer–Emmett–Teller

SEM Scanning electron microscopy

TGA/TG Thermogravimetric analysis

XRD X-ray diffraction

TEM Transmission electron microscope

STEM Scanning transmission electron microscope

FT-IR Fourier transform-infrared spectrum

XPS X-ray photoelectron spectroscopy

MOF(s) Metal-organic framework(s)

MDC(s) MOFs derived carbon(s)

DPC derived porous carbon

TOC Total organic carbon

AOP(s) Advanced Oxidation Process(es)

$\cdot\text{OH}$ Hydroxyl radicals

nm Nanometer

NP Nanoparticles

MO Methyl orange

MB Methylene blue

MR Methyl red

PET Polyethylene terephthalate

BDC/TPA Terephthalic acid

BPDC Biphenyl-4,4'-dicarboxylic acid

4,4'-Bipy 4,4'-Bipyridine

H₂O₂ Hydrogen peroxide

TC Tetracycline

Fe²⁺ Ferrous ions

PS Persulfate

CUS Uncoordinated metal sites

FeCl₃ · 6H₂O Ferric chloride hexahydrate

DMF N,N-dimethylformamide

HCl Hydrochloric acid

KOH Potassium hydroxide

List of Content

Abstract	I
Achievements	IV
Acknowledgement.....	VI
List of Figures	VIII
List of Tables	XII
List of Abbreviations.....	XIII
List of Content	XV
Chapter 1. Introduction.....	1
1.1. Background	2
1.2. Aim and Objectives	7
1.3. Thesis Structure.....	8
Chapter 2. Literature Review.....	11
2.1. Dye and Removal Method	12
2.1.1. Dyes	12
2.1.2. Adsorption.....	14
2.1.3. Photo-Fenton Catalysis	23
2.2. Metal Organic Frameworks (MOFs).....	35
2.2.1. Characteristics of MOFs	35
2.2.2. Controlled Synthesis of MOFs.....	38
2.2.3. Sustainable Synthesis of MOFs	41

2.2.4. MOFs for Dye Adsorption.....	44
2.2.5. MOFs for Dye Photo-Fenton Degradation	46
2.2.6. Research Gap	48
2.3. MOFs Derived Carbons.....	49
2.3.1. Characteristics of MOFs-derived Carbons	49
2.3.2. Synthesis of MOFs-derived Carbons.....	51
2.3.3. MOFs-derived Carbons for Dye Adsorption	53
2.3.4. MOFs-derived Carbons for Dye Photo-Fenton Degradation	55
2.3.5. Research Gap	59
2.4. Summary.....	60
Chapter 3. Experimental.....	62
3.1. Materials	63
3.2. Dye Removal Test.....	63
3.2.1. Oil Bath Device	63
3.2.2. Adsorption Test Device.....	64
3.2.3. Photoactivity Test Device	66
3.2.4. Concentration Test Device.....	67
3.3. Characterisation of Adsorbents and Catalysts	69
3.3.1. Structural Analysis.....	70
3.3.2. Surface Area and Porosity Analysis.....	70
3.3.3. Surface Chemical Analysis.....	71

3.3.4. Thermal Analysis	71
3.3.5. Molecular Structure and Bond Analysis	72
3.3.6. Morphology and Microstructure Analysis	73
Chapter 4. Controlled Synthesis of Uniform MOF-235 for the Adsorption of Methyl Orange in Wastewater with High Efficiency and High Capacity	74
4.1 Introduction	74
4.2. Preparation of MOF-235	76
4.3. Characterisation.....	77
4.4. Adsorption Experiments.....	78
4.4.1. Effect of pH.....	79
4.4.2. Effect of Initial Concentration	79
4.5. Adsorption Mechanism	80
4.6. Results and Discussion.....	81
4.6.1. Characterisation.....	81
4.6.2. Adsorption of the Dye	90
4.6.4. Adsorption Kinetics.....	100
4.6.5. Mechanism Study.....	103
4.6.6. Regeneration Study	106
4.7. Conclusions	107
Chapter 5. Porous Carbon Derived from MOF-235 for the Adsorption of Methyl Orange with High Capacity	108

5.1. Introduction	108
5.2. Chemicals	110
5.3. Synthesis.....	110
5.3.1. Preparation of MOF-235	110
5.3.2. Carbonisation Procedures	111
5.4. Characterization.....	111
5.5. Adsorption	112
5.5.1. Initial Concentration Effect	113
5.5.2. Adsorption Isotherm	113
5.5.3. Adsorption Kinetics	114
5.5.4. Effect of the pH	115
5.5.5. Effect of the Adsorbent Dosage.....	115
5.6. Adsorption and Desorption Cyclic Test.....	115
5.7. Results and Discussion	116
5.7.1. Carbonisation Condition.....	116
5.7.2. Characterisation	121
5.7.2 Adsorption Isotherm	127
5.7.3 Adsorption Kinetics	131
5.7.4. Adsorption Performance	134
5.7.5. Cyclic Adsorption-desorption Test	139
5.8. Conclusions	144

Chapter 6. Recycled PET Derived Carbon for Highly Efficient Heterogeneous Fenton-like Degradation of Methyl Orange	145
6.1. Introduction	145
6.2. Chemicals	147
6.3. Synthesis	148
6.3.1. Depolymerization of waste PET Plastic Bottle	148
6.3.2. Synthesis of PD-MOF-235	149
6.3.3. Synthesis of PD-Fe@C350	149
6.4. Characterisation.....	150
6.5. Photo-Fenton Performance Test	151
6.6. Results and discussion	152
6.6.1. Carbonisation Condition	152
6.6.2. Characterisation.....	155
6.6.3. Photocatalytic Performance	162
6.7. Mechanism	171
6.8. Conclusions	174
Chapter 7. Conclusions and Future Work	175
7.1. Conclusions	176
7.2. Future Work.....	177
References	181

Chapter 1.

Introduction

This chapter highlights the importance of methyl orange (MO) removal and explains the main aims and research objectives of the study. It emphasises the urgent need for effective strategies to remove this widespread dye from wastewater. In addition, the chapter provides a comprehensive overview of the structure of the thesis, describing the main sections and the systematic approach of the research. This includes a description of the experimental methods, characterisation techniques and data analysis strategies used. The aim is to provide a clear roadmap for the structure of the study that allows for a thorough understanding of the research process and its contributions to the field of environmental remediation.

1.1. Background

Water is essential for all life on Earth and is one of the features that make the planet Earth unique. Although 97.5 % of the water on the planet is found in the oceans, only 1 % is easily accessible for extraction and utilisation. In recent years, water consumption and pollution from various industries, such as textile, cosmetics, leather, food, pharmaceutical, paint and paper manufacturing, have significantly affected the quality of water resources and exacerbated the global freshwater crisis [1]. In particular, the widespread use of dyes, including methylene blue (MB) [2, 3], rhodamine B (RhB) [4], methyl orange (MO) [5-7], Congo red (CR) [8], methyl red (MR) [9, 10] crystal violet [11, 12] and other type of organic dyes, is one of the main sources of industrial pollution [13]. According to recent statistics, more than 4,500 tonnes of dyes and other pollutants with a high concentration of dyes are discharged into waterways [14-16]. The discharge of this industrial waste not only threatens human health, but also has a serious impact on the environment [17, 18]. As a result, research into dye removal from wastewater has increased. The number of scientific articles with a key word of "dye removal" has increased significantly from 1991 to today (Aug. 2024), a trend that can be clearly seen in Figure 1.1.

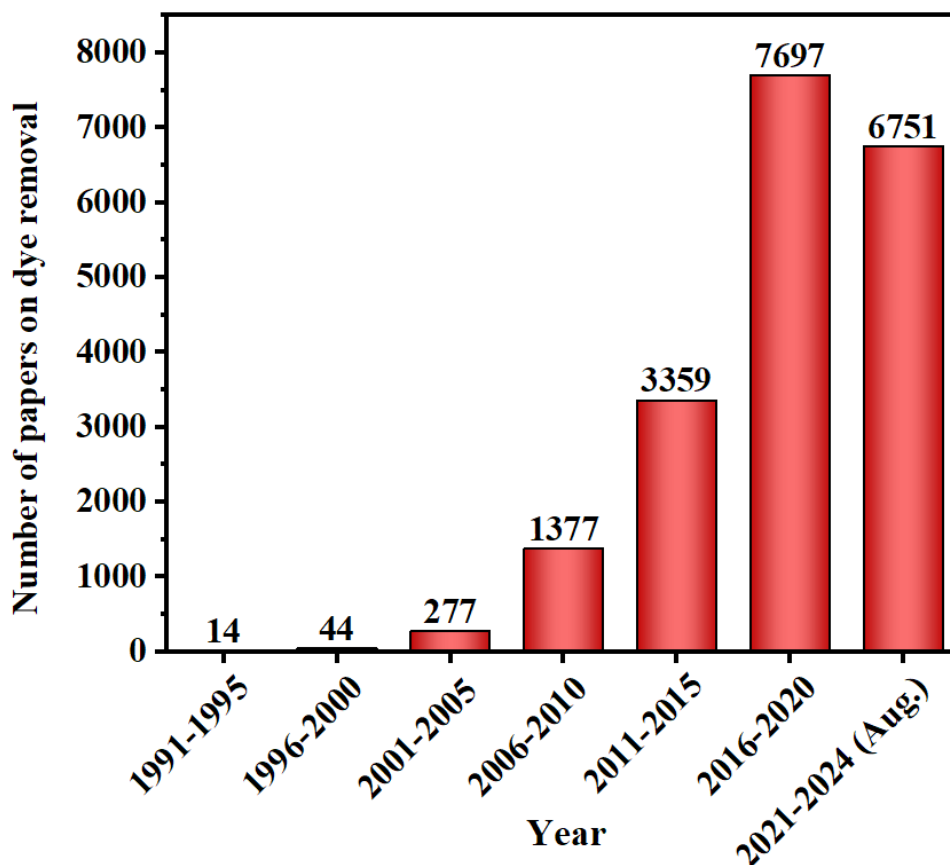


Figure 1.1 Frequency of publications on dye removal since 1991 to 2024 (Aug.) with the selected keyword 'Dye Removal'

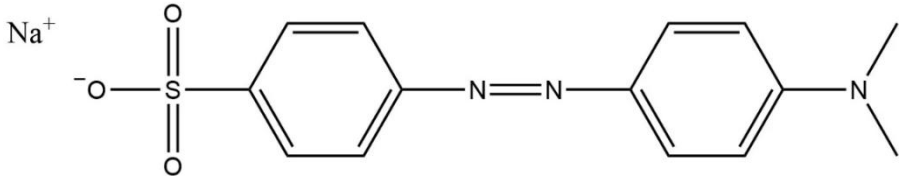
Methyl orange is one of the dyes widely used in the textile industry, which is also commonly used as a pH indicator in titration processes [19, 20]. Table 1.1 shows the detailed the chemical structure and characteristic properties of methyl orange. As shown in Table 1.1, methyl orange has the molecular formula of $C_{14}H_{14}N_3O_3SNa$ and a molecular weight of $327.33 \text{ g}\cdot\text{mol}^{-1}$. The presence of the azo group ($N=N$) in methyl orange combined with its low biodegradability raises serious environmental concerns. This dye may have

acute and/or chronic effects on exposed organisms, depending on the concentration and duration of exposure. These effects may directly or indirectly threaten human health and adversely affect the natural environment [19].

A variety of technologies have been developed and used for the removal of methyl orange. These include methods such as adsorption [5], coagulation [21], advanced oxidation processes (AOPs) [22] and membrane separation processes [23, 24]. Of these processes, adsorption is considered one of the most efficient advanced treatment methods to treat wastewater containing methyl orange. Adsorption offers several advantages: it is easy to handle, highly effective, economical and offers flexibility in design and operation as well as the production of high-quality purified products [25]. Another important advantage of adsorption technology is that the properties of regeneration and recovery of adsorbents, i.e. they can be reused after certain regeneration processes [26]. Besides adsorption, Advanced Oxidation Process technologies, including ozone [27-29], photocatalysis [30-32], Fenton [33, 34] and photo-Fenton [35], have also attracted considerable interest in the treatment of methyl orange-containing wastewater due to their strong oxidising capacity, complete degradation of organic pollutants and the advantage of not causing secondary pollution [36]. In addition, Advanced

Oxidation Processes are also considered one of the most potential technologies due to the problems associated with other methods. For example, physical and chemical methods such as coagulation and flocculation produce large amounts of sludge, while biological methods have long reaction times that can affect process stability and lead to unreliable performance [37]. Fenton and photo-Fenton oxidation methods, characterised by their ability to operate at ambient temperature and atmospheric pressure, as well as their superior oxidation capabilities, have been widely used in wastewater treatment. The advantage of this technology is that it utilises environmentally friendly materials and can operate under different oxidation conditions — using agents such as hydrogen peroxide, ozone or oxygen — tailored to specific process requirements.

Table 1.1 Characteristics of methyl orange [38-40].

Molecular Structure	
IUPAC (International Union of Pure and Applied Chemistry) name	Sodium-4-(4-dimethylamino phenyl diazenyl) benzenesulfonate
Molecular formula	$C_{14}H_{14}N_3SO_3Na$
Molecular weight ($g \cdot mol^{-1}$)	327.33
Molecular size (\AA)	$15.8 \times 6.5 \times 2.6$
Colour & form	Orange-yellow powder or crystalline scales
Type	Anionic dye

1.2. Aim and Objectives

The aim of this research is to advance the sustainable production and application of metal-organic frameworks (MOFs) and their derived porous carbon materials for the efficient removal of methyl orange from wastewater. In this approach, PET waste bottles are used as a sustainable raw material for the synthesis of MOFs and MOF derivatives and their potential as adsorbents and photo-Fenton catalysts for the remediation of organic dye impurities is explored. The particular focus is the production of MOF-235 adsorbents using controlled synthesis techniques that are uniform and have a narrow size distribution, and on the production of iron-rich MOFs-derived carbons nanomaterials using MOF-235 as a precursor through the carbonisation process. In addition, the research explores sustainable synthesis methods for the production of MOF-235-derived carbons using recycled PET plastic waste as a raw material. The resulting MOFs-derived carbons will be investigated both as a physical barrier adsorbent to isolate methyl orange and as a Fenton catalyst that promotes methyl orange degradation. Overall, this study aims to develop sustainable methods for environmental remediation of methyl orange pollutants using MOF-235 and MOFs-derived carbons.

This study is structured around three principal objectives:

1. To Investigate the effect of controlled synthesis on MOF-235's characteristics and adsorption capacity for methyl orange.
2. To determine the suitable carbonisation temperature and investigate the performance and mechanism of methyl orange adsorption by MOF-235-derived MOFs-derived carbon.
3. To investigate the application of using terephthalic acid, derived from recycled PET waste plastic bottles, as a precursor for synthesizing MOF-235 and MOFs-derived carbon, and conducting comparative studies on their performance in photo-Fenton oxidation reactions for methyl orange removal.

1.3. Thesis Structure

This research is systematically organized into seven chapters, each addressing distinct facets of the study.

The thesis begins in **Chapter 1**, which examines the environmental impact of methyl orange and emphasises the urgent need for effective treatment methods for this dye in wastewater. **Chapter 2** then provides a comprehensive overview of various dyes and dye removal technologies, focusing on adsorption and photo-Fenton technologies, and discusses the properties and applications of MOF materials and MOF-derived carbon materials in these

technologies. The chapter also addresses the current challenges in dye wastewater treatment. **Chapter 3** describes the standard characterisation techniques and tools used in this study to provide a basis for the experimental approaches used in the study. **Chapter 4** then focuses on the use of MOF-235 as an adsorbent for methyl orange and presents a novel solvothermal method for the controlled synthesis of MOF-235 with uniform particle size and distribution. It combines experimental and characterisation techniques to explore the properties of MOF-235 and investigate the adsorption process and mechanisms for the removal of methyl orange. Building on this, **Chapter 5** deals with the adsorption of methyl orange by MOF carbon obtained from MOF-235, investigating the optimal carbonisation temperature and studying the adsorption mechanism by integrated experimental and characterisation methods. **Chapter 6** shifts the focus to the sustainable synthesis of MOF carbon from MOF-235, specifically the use of MOF carbon from PET waste bottles for the photo-Fenton degradation of methyl orange, and attempts to determine the optimal reaction conditions for this process. Finally, **Chapter 7** summarises the overall conclusions of the study, recognises its limitations and suggests directions for future research in this field. The structure of the thesis is shown in Figure 1.2.

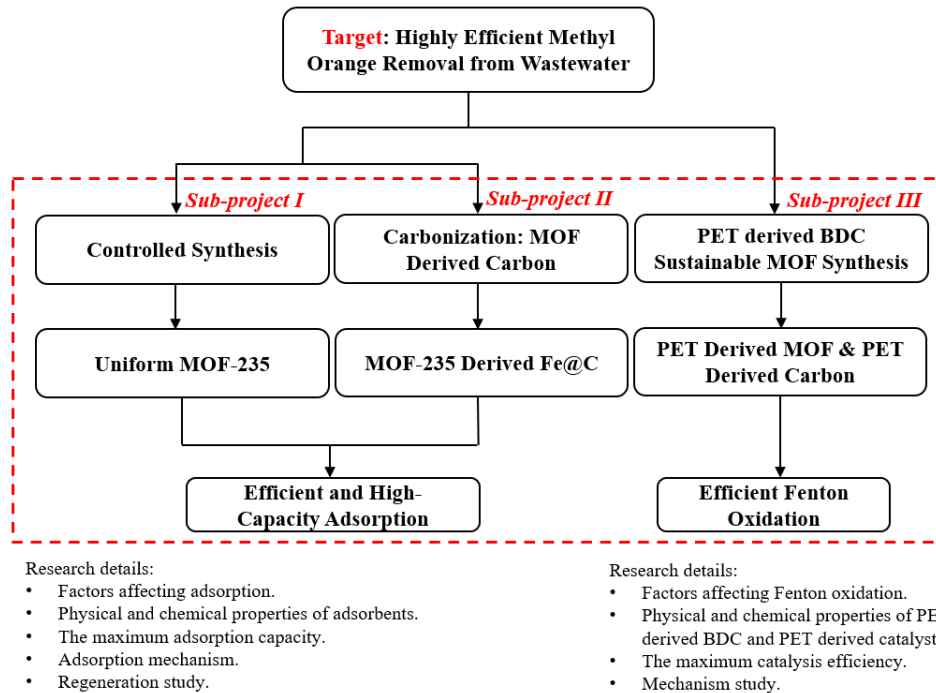


Figure 1.2 Thesis structure.

Chapter 2.

Literature Review

This chapter provides a comprehensive overview of the basic principles and recent advances in the field of dye removal from aqueous environments. In particular, it focuses on the latest developments in the application of MOFs and MOFs-derived carbons for the removal of methyl orange. Through a comprehensive review of current research, the chapter addresses two primary techniques for methyl orange removal: adsorption and heterogeneous photo-Fenton catalysis. It provides a detailed explanation of the mechanisms underlying these processes and the factors that influence their performance. In addition, this chapter highlights the potential of MOFs and MOFs-derived carbons as highly efficient adsorbents and catalysts that open new perspectives for the sustainable practise of dye reduction. This discussion emphasises the importance of these materials in the development of environmentally friendly solutions for water treatment and contributes to the advancement of environmental remediation technologies.

2.1. Dye and Removal Method

In this section, the basic background of dyes and the researched removal methods (with a focus on adsorption and photocatalytic Fenton catalysis) are discussed in detail. This includes an overview of the dyes commonly used in industry and their environmental impact, in particular their persistence and toxicity in aquatic ecosystems. In addition, the principles of adsorption and photocatalytic Fenton processes are examined and it is shown how these methods effectively degrade or remove dyes from wastewater. By combining theoretical knowledge with practical applications, this discussion aims to provide a comprehensive understanding of the current challenges and potential solutions in the field of dye pollution control.

2.1.1. Dyes

2.1.1.1. Background

Dyeing has played a decisive role in industrial civilisation for decades. It is used to give colour to clothing, textiles and various other materials [41]. Nevertheless, the widespread use of synthetic dyes in the recent centuries led to considerable social and ecological problems [42]. Many of these concerns arise from the fact that synthetic colourants are often produced using toxic chemicals that have serious effects on human health and the environment.

Dyes are classified according to their chemical composition, their application techniques and their colour properties. Direct dyes, for example, are applied directly to the substrates, while reactive dyes form covalent bonds with their target materials [43]. A major problem with synthetic dyes is their potential health and environmental hazards. Many contain toxic chemicals that can irritate the skin, cause respiratory problems and increase the risk of cancer [44, 45]. In addition, the synthesis, application and disposal of dyes cause considerable environmental pollution due to the high water and energy consumption and the release of contaminating chemicals into water and soil [46]. The development of new materials and technologies for the efficient processing of industrial dyes is necessary.

2.1.1.2. Methyl Orange

Anionic azo dyes, which are used in the synthetic dye industry and in various related applications, occupy a decisive position [47, 48]. Their limited efficiency in the dyeing of natural fibres leads to a pronounced abundance in the wastewater of textile production plants. Notable among these dyes is methyl orange, scientifically known as sodium-4-(4-dimethylamino phenyl diazenyl) benzenesulfonate. It is an organically produced, water-soluble dye which, when dissolved in water, has a bright orange colour. It is not only used in the textile industry, but also serves as a pH indicator in titration processes

[19, 20]. As shown in Table 1, the molecular structure of methyl orange and related azo dyes comprises aromatic rings and -N=N azo bonds. These structural features make these compounds an environmental and biosafety concern due to their potential toxicity, carcinogenicity and teratogenicity [19]. Therefore, this study focuses on methyl orange as a representative pollutant, and the molecular dimension of methyl orange is estimated to be about 6-8 nm [49]. Various remediation techniques have been investigated for the removal of methyl orange dye from water, which has been introduced in the previous chapter one.

To summarise, methyl orange, a synthetic dye, has been used in many different areas throughout history. However, its widespread use has brought with it a number of environmental and societal challenges. Despite numerous industrial approaches to address methyl orange, there is an urgent need for novel materials and methods aimed at effective remediation of this dye.

2.1.2. Adsorption

To achieve dye removal from wastewater, diverse technologies have been produced, each offering unique benefits and drawbacks. These methods can be broadly divided into three main categories: physical, chemical and biological approaches [50]. Previous research has investigated the potential advantages and possible disadvantages of these methods and provides

important information for the selection of suitable dye removal technologies. The study by Salleh et al. (2011) evaluates different dye removal technologies [47]. Membrane filtration is efficient, but leads to significant sludge production. Ion exchange can be easily regenerated, but is less effective with many dyes, and irradiation only works well on a laboratory scale due to the high oxygen requirement. Electrokinetic coagulation and simple oxidation are cost-effective, but suffer from the high amount of sludge and the need for activating agents. The Fenton reagent is chemically suitable but also produces sludge, while ozonation does not increase the sludge volume but is hampered by the short half-life of ozone. Photochemical methods avoid sludge but risk the formation of by-products. Sodium hypochlorite effectively breaks azo bonds but releases aromatic amines. Electrochemical destruction avoids chemicals and sludge, but loses effectiveness at higher flow rates. Biological treatments with white rot fungus or specific microbes provide natural degradation but are slow and sometimes ineffective for azo dyes under aerobic conditions. Microbial biomass is selective but not consistently effective, especially for toxic dyes. Anaerobic systems decolourise well but emit harmful hydrogen sulphide and methane. Efficiency, cost and environmental considerations are weighed against each technology, highlighting the need for customised wastewater treatment solutions.

Among these dye removal techniques, adsorption is a widely used process in water treatment to remove pollutants such as dyes, heavy metals and organic compounds [51]. Dye adsorption is a popular and cost-effective method to remove dyes from wastewater in an environmentally friendly way. The principle of dye adsorption is based on the affinity of certain materials for certain dyes, which is due to the presence of functional groups on the surface of the adsorbent that can interact with the dye molecules through various forces. The mechanism of dye adsorption involves several steps, including the physical and chemical interactions between the dye molecules and the adsorbent material [52]. The efficiency of dye adsorption is influenced by several factors, including the type of adsorption material, the concentration of the dye in the water, the pH value of the water and the temperature. The properties of the adsorption material, such as its surface area, pore size and functional groups, can also influence the adsorption capacity of the material.

2.1.2.1. Factors Affecting Dye Adsorption

The effectiveness of dye adsorption depends on a number of variables, such as the pH value, the initial dye concentration, the adsorbent dosage, the solution temperature, and the contact time. Fine-tuning these factors is crucial as it can significantly increase the ability of the adsorbent to absorb dyes.

pH

The initial pH value of a solution plays a decisive role in the adsorption capacity of dyes [53]. This is because the pH can change the electrostatic charge of the dye molecules on their surface, which in turn affects how strongly they interact with the adsorbent [54]. In the adsorption process, the interaction between the charged surface of the dye molecules and the surface charge of the adsorbent is important. In particular, if the pH value of the solution is above the zero charge point of the adsorbent (pH_{pzc}), the surface of the adsorbent becomes negatively charged, which increases the adsorption of cationic (positively charged) dyes due to the strong electrostatic attraction at a high pH value. If the pH of the solution is below the pH_{pzc} , on the other hand, the surface of the adsorbent takes on a positive charge and thus creates favourable conditions for the adsorption of anionic (negatively charged) dye, as these are attracted to the positively charged surface of the adsorbent [55].

The influence of pH on MOFs for dye removal of dyes from water has been well studied. MOF-235, for example, shows pH-sensitive behaviour in the removal of methyl orange. Studies have shown that MOF-235 reaches its highest adsorption efficiency for methyl orange at a pH of 4, an acidic state. However, as the pH increases, the adsorption capacity for methyl orange decreases. This trend is due to the fact that the surface charge of MOF-235

becomes increasingly negative at higher pH values, resulting in stronger electrostatic repulsion with methyl orange molecules that are negatively charged at high pH [5]. In contrast, the removal efficiency for methylene blue (MB), a cationic dye, is the opposite. Another study showed that, under alkaline conditions (high pH), the negatively charged surface of $\text{Fe}_3\text{O}_4@\text{AMCA-MIL53}(\text{Al})$ increases its affinity for positively charged MB molecules and thus improves the removal efficiency. At lower pH values, the MOF surface becomes positively charged due to the adsorption of H^+ ions or their interaction with the surface hydroxyl groups, reducing the ability to adsorb MB [56]. This shows how the pH value has a decisive influence on the surface charge of adsorbents and their interaction with various dye molecules. By precisely adjusting the pH value of the solution, it is possible to adjust the adsorption efficiency of MOFs for certain dyes and thus optimise their removal from the water.

Initial Dye Concentration

In wastewater treatment, the initial concentration of the dye plays a decisive role in the transfer of the dye molecules to the adsorbent. This occurs because the dye concentration has a direct effect on the saturation of the adsorbent and its maximum adsorption capacity, which is limited by the adsorption area and pore size available on the adsorbent [57]. In general, the initial concentration

of the dye increases, the rate of adsorption slows down due to the adsorbent's active sites moving closer to saturation. However, under certain conditions, a higher initial dye concentration can improve the driving force for mass transfer and thus increase the adsorption capacity of MOFs [58]. A previous study on the adsorption of MB by the Uio-66 MOF have shown, for example, that an increase in the initial concentration leads to a higher uptake of MB, which indicates a better mass transfer at higher concentrations. Nevertheless, the efficiency of adsorption may decrease due to the repulsion between the MB molecules and the progressive saturation of the surface of the Uio-66 adsorbent's surface. Therefore, in dye adsorption processes in wastewater, while adsorption initially increases with increasing concentration [59]. However, as soon as the concentration reaches the point where the available binding sites are saturated, it decreases, leading to repulsive interactions between the adsorbed dye molecules and reducing the ability for further adsorption.

Adsorbent Dosage

When treating dye wastewater, the amount of adsorbent used has an influence on the rate of dye removal. In general, higher adsorbent dosages improve dye elimination as they provide more sites for adsorption. A previous study demonstrated this by showing that increasing the amount of $\text{Fe}_3\text{O}_4@\text{MIL-}$

100(Fe) resulted in a higher rate of methyl red (MR) removal, primarily due to the increase in surface area and available adsorption sites at higher dosages [10].

However, it is important to note that while the total amount of dye removed may increase with more adsorbent, the efficiency of removal per unit adsorbent may decrease. This is because with larger amounts of adsorbent, not all adsorption sites are effectively utilised and the diffusion of dye molecules to these sites may slow down, resulting in less dye being adsorbed per gramme [60]. In addition, while a higher adsorbent dose can increase the rate of dye removal, it can also increase the cost of treatment and the amount of sludge produced after adsorption. Determining the most efficient adsorbent dosage is therefore essential for cost-effective and environmentally friendly dye removal. A careful balance needs to be struck between the amount of adsorbent used and the adsorption efficiency achieved to ensure that the process is economically viable and environmentally responsible.

Solution Temperature

The temperature of the adsorption environment has a considerable influence on the adsorption efficiency of adsorbents [61]. The reason for this is that the adsorption process of dyes on MOFs can be either endothermic or exothermic, depending on whether it involves physical or chemical adsorption [62].

Chemical adsorption often involves the formation of strong chemical bonds. It is an endothermic process, i.e. the adsorption efficiency increases with temperature. This can be attributed to the increased mobility of the dye molecules and a larger number of active adsorption sites. For example, a study showed that the adsorption of malachite green on MIL-100(Fe) is an endothermic process in which the adsorption capacity increases with temperature. The principle underlying this adsorption behaviour is that the increase in temperature causes the transfer of water molecules from the open metal sites into MIL-100(Fe), causing them to interact with the Lewis acidic Fe sites and the basic $-N(CH_3)_2$ groups in malachite green molecules, leading to an increase in system entropy [63].

In physical adsorption or exothermic processes, on the other hand, the adsorption efficiency generally decreases with increasing temperature. This is supported by previous studies, which indicated that in exothermic adsorption processes, an increase in temperature can weaken the interaction forces between the dye molecules and the active sites on the adsorbent surface, leading to a reduction in adsorption capacity [47]. The reason for this is that higher temperatures can increase the kinetic energy between the adsorbent and the dye molecules and thus reduce their mutual attraction.

These results emphasise the need to consider the thermodynamic properties of the adsorption process and the effects of ambient temperature on adsorption efficiency when developing and selecting adsorbents for dye removal. Understanding these factors is crucial for optimising treatment conditions and improving dye removal efficiency.

Contact Time

The duration of the contact time required to achieve adsorption equilibrium is a critical factor in the selection of adsorbents, as it determines the optimum adsorption effect within the shortest possible time. This aspect is particularly important in the development of water treatment systems, where the processing time directly influences both the efficiency and cost-effectiveness of operation. MOFs and MOFs-derived carbons are particularly characterised by their ability to reach adsorption equilibrium quickly. This rapid equilibrium capability makes them outstanding options for water treatment and a variety of other applications, increasing their practicality and attractiveness in environmental engineering and industrial processes.

The speed at which an adsorbent reaches equilibrium affects not only the speed of the treatment process, but also the efficiency of regeneration and reuse of the adsorbent. A longer equilibrium time slows down the regeneration process and makes the adsorbent less useful for real applications. Therefore,

fast response and short equilibrium times are essential for improving process efficiency. In a study by Zhang et al. (2018), for example, Zn-MOF was found to reduce the MB concentration by 98% within 60 minutes [64]. Similarly, $\text{H}_6\text{P}_2\text{W}_{18}\text{O}_{62}/\text{MOF-5}$ showed a removal efficiency of 97% for the same dye and achieved this within just 10 minutes [65]. The rapid realisation of this remarkable adsorption capacity underlines the importance of studying contact time in the adsorption process and confirms its applicability in the real world.

2.1.3. Photo-Fenton Catalysis

With rapid economic growth, accelerated industrialisation and increasing urbanisation, water pollution has become a serious global environmental problem. In particular, the widespread use of synthetic organic compounds, especially industrial dyes, poses a major challenge due to their high stability and low biodegradability in the environment, making them difficult to remove by conventional wastewater treatment methods and exacerbating the extent of water pollution. Therefore, it is necessary to develop effective water treatment methods to remove these organic dye pollutants.

To address this challenge, various water treatment technologies have been explored in the past, including physical, biological and chemical methods aimed at improving the efficiency of removal of these recalcitrant organic dyes [66-68]. Among the numerous water treatment technologies, Advanced

Oxidation Processes (AOPs) are being intensively researched and used due to their high efficiency in removing organic dye [69]. Although the traditional Fenton reaction is favoured due to its simple operating conditions, its limitations, such as a narrow pH operating range and difficulties in recovering and reusing the catalyst, limit its application. Against this background, researchers have begun to explore the combination of the Fenton reaction with photocatalytic technology to improve the removal efficiency of organic pollutants through synergistic effects while overcoming the inherent disadvantages of the Fenton reaction. In this context, MOFs, especially iron-based MOFs (Fe-MOFs) and iron-based MOF derivatives (Fe-MOF derivatives), have shown significant catalytic activity in photo-Fenton systems due to their structural diversity, high specific surface area and excellent chemical stability. Under illumination, Fe-MOFs and Fe-MOF derivatives can generate many reactive oxygen species, which have a strong oxidising ability and can efficiently degrade organic pollutants in water. Therefore, the application of Fe-MOFs and Fe-MOF derivatives in photocatalysis and Fenton reaction has attracted much attention.

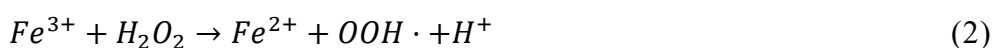
This section provides an overview of the application of Fe-MOFs and Fe-MOF derivatives in photo-Fenton systems, analyses the key factors affecting the efficiency of photodegradation of organic dye pollutants, and discusses in detail the mechanisms of action of Fe-MOFs and Fe-MOF derivatives in the

photo-Fenton reaction. It also highlights the key issues and challenges of current research and the potential and direction for the future development of Fe-MOFs and Fe-MOFs derivatives in environmental remediation. By discussing these key points, it aims to provide a theoretical basis and technical guidance for further improving the application efficiency of Fe-MOFs and Fe-MOFs derivatives in photo-Fenton systems and expanding their application in environmental remediation.

2.1.3.1. Principle of Fenton Reaction

In essence, the Fenton reaction involves the decomposition of hydrogen peroxide (H_2O_2) by iron(II) ions (Fe^{2+}) to form hydroxyl radicals ($\cdot OH$). The hydroxyl radicals are highly reactive and can oxidise a broad spectrum of organic pollutants, which makes them efficient for dye degradation of dyes [8].

The primary reactions involved are:



Remarkably, the direct Fenton process faces challenges such as the need for acidic conditions and the inefficiency of iron salt catalysts in the reaction.

2.1.3.2. Factors Affecting Photo-Fenton Dye Degradation

The efficiency of the removal of organic dye is significantly influenced by external environmental factors. Therefore, it is important to fully understand these influences when developing and using iron-based catalysts and the photo-Fenton process. To optimise the use of iron-based catalysts and ensure the effectiveness of the Photo-Fenton process, five key categories of external environmental factors are examined in detail in this section.

pH

In photo-Fenton systems, the pH value of the reaction medium has a decisive influence on the catalytic process. This effect is manifested in various ways, including changes in the surface charge properties of the catalyst, its chemical stability, the forms of the active species present and the redox potential. pH fluctuations have a direct influence on the formation of $\cdot\text{OH}$ radicals, the main oxidising agents in the Fenton reaction, which are known for their strong oxidative decomposition of organic pollutants. Under acidic conditions, the redox potential of $\cdot\text{OH}$ radicals is increased, which promotes electron transfer within the $\text{Fe}^{3+}/\text{Fe}^{2+}$ system and facilitates the dissolution of iron ions. This not only supports the homogeneous Fenton reaction, but also improves the efficiency of the catalyser in the degradation of pollutants [70]. Previous research has investigated the influence of initial pH on the catalytic

degradation of tetracycline (TC) by MIL-88A [71], further supporting this hypothesis. Their results showed that the degradation efficiency was highest at a pH of 3, which emphasises the importance of iron ion dissolution under acidic conditions for driving the Fenton reaction. In addition, an acidic environment promotes the effective activation of persulphate (PS), which increases the oxidative capacity of the system.

In highly acidic environments, the structural integrity of certain catalysts can be compromised by proton-induced decomposition, leading to a significant reduction in the iron content of the catalyst. Such phenomena were observed in the photo-Fenton reaction for formaldehyde remediation, where MIL-100(Fe) showed reduced efficacy in acidic environments, as opposed to pH 6.6 [72]. This decrease in effectiveness is attributed to the interaction between water molecules and the uncoordinated metal sites, which triggers the release of H^+ ions and further decreases the pH value. The carboxylic acid linkers present in the MOF structure are susceptible to protonation, leading to deterioration of the structure. Therefore, increasing the initial pH of the solution from 3 to 6.6 resulted in increased structural resistance and increased efficiency of the photocatalyst. This underlines the high susceptibility of Fe-MOFs to destabilisation under highly acidic conditions.

At elevated pH values, the stability of hydrogen peroxide (H_2O_2) decreases, which leads to its decomposition into oxygen (O_2) and water (H_2O). At the same time, iron-based catalysts tend to produce less reactive iron species and precipitate as hydroxide oxides. This scenario inhibits the conversion rate of Fe^{3+} to Fe^{2+} ions [73]. As the pH rises, the binding sites of the Fe^{3+} ions increasingly combine with OH^- ions, significantly limiting the interaction between Fe^{3+} ions and H_2O_2 , which reduces the effectiveness of pollutant degradation. In addition, highly alkaline conditions can jeopardise the structural integrity of iron-based catalysts. Studies by Liu et al [74], including X-ray powder diffraction (XRD) analyses of the M88/GO-9 composite before and after a photocatalytic reaction at pH 11, indicate possible partial degradation of the material under these conditions. These observations underline the crucial importance of pH optimisation in the application of Fe-MOFs as catalysts in advanced oxidation processes in order to maintain both catalytic performance and material stability.



The pH value has a considerable influence on the surface potential of materials, whereby the surface beyond the isoelectric point assumes a negative charge. In earlier studies, for example, the isoelectric point of MIL-

53(Fe) was determined at a pH value of 5.3 [75]. Below this pH, in acidic environments, the surface of MIL-53(Fe) becomes positively charged, which facilitates the formation of strong hydrogen bonds with H^+ ions. This positive charge prevents the O=O bond in peroxymonosulfate (PMS) from interacting with the surface of MIL-53(Fe). In addition, pH influences the predominant forms of contaminants; for example, tetracycline (TC) is protonated (TCH_3^+) at pH values below 3.3, but becomes a monoanion (TC^-) above pH 7.7 [76]. It has also been found that the adsorption efficiency of MIL-53(Fe) for pollutants decreases at higher pH values [77, 78]. This decrease in adsorption is attributed to the fact that chlorobenzoic acid (CA) is mainly present in its anionic form under alkaline conditions, while the surface of MIL-53(Fe) is increasingly negatively charged, leading to electrostatic repulsion between the negatively charged MIL-53(Fe) and the CA anions.

Temperature

The temperature of the solution has a significant influence on the efficiency of the catalyst-activated photo-Fenton reactions. Higher temperatures improve the transfer rates of the reaction molecules and electrons, accelerating the activation of the catalyst and the overall reaction. A study has shown that the use of MIL-101(Fe) to activate persulphate for the degradation of tri(2-chloroethyl)phosphate is more efficient at 308 K than at 288 K or 298

K [79]. Beyond a certain temperature, however, the efficiency of the reaction decreases, which is probably due to the exothermic nature of the Fenton reaction, where higher temperatures can reduce the production of $\cdot\text{OH}$ radicals. Previous studies have also shown that increasing the reaction temperature during the removal of total organic carbon (TOC) with Fe/MIL-47 reduces the efficiency of TOC removal [80]. This reduction is attributed to the accelerated decomposition of hydrogen peroxide (H_2O_2) at higher temperatures, which limits the availability of $\cdot\text{OH}$ radicals that are critical for the thorough removal of organic dye contaminants.

These findings suggest that while a moderate increase in temperature can increase the efficiency of photo-Fenton reactions, further increases could reduce efficiency by inhibiting the formation of $\cdot\text{OH}$ radicals. Therefore, controlling the optimal reaction temperature and extending the temperature range for effective application are crucial for maximising the performance of the catalyst-activated photo-Fenton system in the treatment of dye effluents.

Light Conditions

The performance of the photo-Fenton reaction is highly influenced by the properties of the light source used, in particular its wavelength and light intensity. The ability of a photocatalyst to facilitate degradation depends largely on its specific properties, which determine which wavelengths it can

absorb efficiently. Photocatalysts with a band gap energy above 3 eV (which corresponds to wavelengths below 400 nm) require ultraviolet light for activation, while those with a band gap energy below 3 eV (which corresponds to wavelengths above 400 nm) can be activated by visible light [81]. Iron-based catalysts, such as Fe-MOFs, are usually activated by visible light, especially at wavelengths beyond 420 nm, and only rarely by ultraviolet light due to their lower band gap energy [82]. However, the effectiveness of the light source also depends on whether its wavelength matches the absorption spectrum of the material. A previous study has shown that GO@MIL-101(Fe) was not activated for TCEP degradation in long wavelength visible light, but showed clear activation in short wavelength visible light [83].

A higher light intensity increases the photon density on the catalyst surface, providing more energy and high-energy electrons for the photo-Fenton reaction. Higher light intensity increases the production of electron-hole pairs and reduces the probability of their recombination, thereby improving the efficiency of the reaction. Nevertheless, the energy requirement of the light source in photocatalytic processes is a significant factor in energy consumption, which poses a challenge to the advancement of photocatalytic technology. The development of photocatalysts that are effective under

natural sunlight is crucial to overcoming this challenge and advancing the field.

Fenton Reagent and Catalyst

In Fenton-like processes, the reaction rate is significantly influenced by the concentration of the catalyst and the Fenton reagent. Within an optimal range, an increased catalyst concentration can improve the efficiency of the catalytic reaction by providing more active sites and promoting the formation of reactive free radicals. For example, a previous study showed that increasing the concentration of $\text{Fe}_3\text{O}_4/\text{MIL-125}$ from $0.05 \text{ g}\cdot\text{L}^{-1}$ to $0.1 \text{ g}\cdot\text{L}^{-1}$ increased the efficiency of tetracycline hydrochloride removal from 89% to 97%, illustrating the benefits of an optimal catalyst concentration [84]. However, increasing the catalyst concentration beyond a certain point, for example to $0.2 \text{ g}\cdot\text{L}^{-1}$, proved to be counterproductive for removal efficiency. There are two main reasons for this: A higher catalyst concentration can lead to greater turbidity of the solution, which scatters the light and reduces the light absorption of the system. In addition, the excessive presence of the catalyst can trigger competitive reactions that limit the availability of effective free radicals and thus reduce the overall catalytic efficiency.

Fenton reagents such as H_2O_2 and PS serve as powerful electron acceptors in photocatalytic processes that significantly improve the degradation of organic

pollutants. These reagents function by activating MOFs to produce strong oxidative radicals, including $\cdot\text{OH}$ and $\cdot\text{SO}_4^-$. Previous research [85] showed that increasing the H_2O_2 concentration from 0.5 mM to 5 mM significantly improved the photo-Fenton degradation efficiency of tetracycline hydrochloride (TC-HCl) during the first 15 minutes. After this period, the degradation rate levelled off due to the rapid degradation of H_2O_2 . Furthermore, a H_2O_2 concentration of 8 mM decreased the degradation efficiency, possibly due to the saturation of the catalyst active sites and the overproduction of radicals that exceeded the utilisation capacity of the system. Excess H_2O_2 can act as a radical scavenger and convert reactive hydroxyl radicals into less effective peroxide radicals (equation). Similarly, previous research [71] observed that increasing the PS concentration up to 4 mM improved the formation of $\cdot\text{SO}_4$ radicals and pollutant degradation. However, increasing the PS concentration to 8 mM led to a decrease in the degradation rate, probably due to competitive reactions and the formation of unwanted by-products. These examples illustrate that while a moderate increase in the concentration of the Fenton reagent can be beneficial, excessive concentrations can impair the photocatalytic process.





Ions in Aquatic Environments

In the practise of wastewater treatment, the uptake of organic compounds and various ions influences the effectiveness of the catalysts in the Photo-Fenton system. These influences range from pH changes to the binding of free radicals and the degradation of H₂O₂. Although most cations have minimal influence on the reaction dynamics, certain metal cations that can react with H₂O₂ can accelerate pollutant degradation by supporting the activation of the Fenton reagents. Conversely, anions can occupy the active sites on the catalyst surface, act as radical scavengers or compete with free radicals for reactive sites, thereby reducing the efficiency of the photo-Fenton reaction. A previous study on α -Fe₂O_{3-x} synthesised from Fe-MOF modified with benzimidazole has highlighted the significant influence of coexisting ions on the α -Fe₂O_{3-x} photo-Fenton degradation pathway of MB [86]. In particular, Cl⁻ as \cdot OH acceptor forms less reactive chlorinated radical anions, while the introduction of 10 mM HCO₃⁻ reduced the MB degradation rate to only 11% within 40 min. This result indicates that HCO₃⁻ not only scavenges \cdot OH radicals but also impairs MB removal by shifting the pH of the solution towards alkalinity. Understanding the differential effects of different anions

is therefore crucial for developing strategies to remove specific organic contaminants to ensure that the Photo-Fenton system remains effective for wastewater treatment.

2.2. Metal Organic Frameworks (MOFs)

The removal of dyes from wastewater is a critical challenge in environmental engineering that can be effectively addressed by adsorption and heterogeneous Fenton catalysis. These methods are highly efficient and widely used in wastewater treatment due to their ability to handle a wide range of contaminants. From these removal techniques, the focus shifts to the use of MOFs, which represent a promising class of materials in this field. The following sections look at the properties of MOFs, their widespread use in dye removal and the potential for their sustainable synthesis.

2.2.1. Characteristics of MOFs

MOFs are known for their vast specific surface areas, sometimes exceeding $10,000 \text{ m}^2 \cdot \text{g}^{-1}$. These extensive surface areas are formed by linking metal ions with organic molecules [87]. By carefully selecting these metal ions and organic molecules, scientists can engineer MOFs with tailored structural properties. The choice of organic molecules is particularly important for the heat and water resistance of MOFs and their ability to adsorb pollutants.

Commonly used organic ligands in MOF construction include glutaric acid, 4,4'-bipy (4,4'-bipyridine), BDC (1,4-benzenedicarboxylic acid/terephthalic acid), BTC (1,3,5-benzenetricarboxylic acid), imidazole, pyrazine, triazole, and BPDC (biphenyl-4,4'-dicarboxylic acid) [88-90]. These ligands are fundamental in forming the diverse and functional structures of MOFs, significantly enhancing their adsorption capacities by creating well-ordered porous frameworks.

The stability of MOFs in water is often undermined by the weak bonds between metal ions and organic molecules [91]. Strengthening these bonds can increase the water resistance of MOFs. In addition, the incorporation of specific functional groups into the organic molecules can make the MOFs more hydrophobic and thus increase their water stability. The choice of metal ions in MOFs affects their structural robustness. MOFs consisting of multiple metal ions are generally more stable as they have stronger metal-metal bonds and are less likely to decompose. In addition, interactions such as π - π stacking and hydrogen bonding within the molecules are crucial for improving the resistance of MOFs in an aqueous environment.

The exceptional ability of MOFs to remove dye pollutants from wastewater is due to their highly porous structure, which significantly improves the interaction between pollutants and adsorption sites and thus increases the

efficiency of the adsorption process [92]. MOFs are particularly suitable for dye treatment of dye wastewater as the ligands in their structure provide an abundance of adsorption sites and they are highly porous. This porosity facilitates the effective absorption of dye contaminants from the water, making MOFs an excellent option for the purification of dye wastewater sources.

While MOFs are comparable to many conventional adsorbents in removal of dye pollutants, they have different properties that offer further advantages. Firstly, open metal sites in MOFs serve as additional adsorption points that increase the uptake capacity for pollutants. Secondly, MOFs can be selectively targeted at specific pollutants by functionalising their pores. This utilises various intermolecular forces such as electrostatic attraction, hydrogen bonding, hydrophobic interactions, acid-base interactions and π - π stacking. These interactions significantly improve the adsorption capacity of MOFs. Finally, the large surface area of MOFs provides numerous active sites for adsorption, facilitating the effective uptake and removal of more pollutant molecules. These structural properties emphasise the great potential of MOFs as adsorbents for the treatment of dye effluents.

The adsorption mechanism of MOFs in dye removal is similar to that of conventional adsorbents, but has significant differences due to the embedded

functional ligand groups and the presence of metal ions or clusters in the MOF structure [93]. These features enable various interactions between dye molecules and MOFs, such as electrostatic attraction, hydrogen bonding, hydrophobic effects, acid-base interactions and π - π stacking. These complicated interactions significantly increase the adsorption capacity of MOFs for dyes and show excellent efficiency in removing dye impurities from water.

2.2.2. Controlled Synthesis of MOFs

The development of effective synthesis methods and the precise control of reaction conditions are crucial in MOF research [94]. Several synthesis methods, including those for HKUST-1, MIL-101, UiO-66, ZIF-8 and MOF-5, have been explored. The discussion has shown the importance of reaction conditions to achieve high yield and desired properties. Regulation of reactant concentrations is critical to prevent unwanted side reactions and improve product selectivity. Temperature and pressure are important variables that influence the reaction rate and crystal growth. In addition, stirring speed and reaction time have been identified as key factors influencing the morphology and size distribution of MOFs.

Overall, the discussion highlighted the importance of understanding the various factors that influence the synthesis of MOFs and the need to optimise

the reaction conditions to achieve the desired properties. The synthesis methods presented, the factors influencing MOF synthesis and the importance of controlling the reaction conditions are discussed below.

MOF Synthesis Methods

This section covers different MOF synthesis methods, such as solvothermal synthesis, microwave-assisted synthesis, hydrothermal synthesis, mechanochemical synthesis, and others. Examples for each method are provided, alongside a discussion of their benefits and drawbacks. Hydrothermal and solvothermal syntheses are highlighted as important subfields within inorganic synthesis [95]. In hydrothermal synthesis, chemical compounds are produced by reactions in an aqueous solution at temperatures above the boiling point of water, while solvothermal synthesis takes place in a non-aqueous solution at elevated temperatures. Both methods facilitate the chemical production, synthesis and construction of unique compounds or substances by the solution route. By lowering the reaction temperature, these techniques offer a gentler alternative for reactions in the solid state. An important aspect of hydrothermal and solvothermal systems is their non-ideal and non-equilibrium states in which water and other solvents can be activated under high temperature and pressure conditions. Hydrothermal and solvothermal reactions are becoming increasingly

important for the production of various functional inorganic materials with specialised compositions, structures and morphologies, including nano- and ultrafine powders, sol-gels, non-crystalline states, inorganic membranes and single crystals. These methods effectively bridge the gap between synthetic chemistry and the physical properties of the materials produced. Compared to other synthesis techniques, hydrothermal and solvothermal methods offer clear advantages and enable the production of a wide range of materials and crystals that are used in numerous technological fields. The resulting materials often exhibit unique and superior chemical and physical properties.

Hydrothermal and solvothermal chemistry enable unique synthetic reactions that are not possible with reactions in the solid state due to the vaporisation of reactants at high temperatures. These methods enable the creation of new materials with unique valence states, metastable structures, condensed and aggregated states and materials with low melting points, high vapour pressures and low thermal stability. In addition, these techniques facilitate the growth of perfect single crystals with thermodynamic equilibrium defects, controllable morphology and particle size, and direct ion doping during the synthetic reaction.

This section provides an overview of the main synthesis techniques for MOFs, including hydrothermal and solvothermal methods. Hydrothermal and

solvothermal approaches are versatile for the preparation of various crystalline materials. The optimal technique depends on the target application and the desired MOF properties. With these methods, the chemical and physical properties can be adjusted by manipulating the synthesis conditions. Overall, they offer viable options for the production of MOFs with customised structures and functions. Further research to optimise the syntheses will expand the scope and utility of MOFs accessible through these platforms.

2.2.3. Sustainable Synthesis of MOFs

In today's materials science landscape, the importance of sustainability in materials synthesis is increasingly recognised [96-98]. As the environmental impact of conventional synthesis methods becomes ever more apparent, the search for sustainable alternatives is becoming increasingly urgent. This is particularly true for MOFs, which have attracted considerable interest due to their unique properties and diverse applications. However, conventional MOF synthesis is often associated with energy-intensive processes and the use of harmful solvents, leading to significant environmental problems. Therefore, the pursuit of sustainable synthesis methods for MOFs is crucial to meet the demand for these versatile materials while protecting the environment.

The sustainable synthesis of MOFs from polyethylene terephthalate (PET) waste is based on the principles of green chemistry and resource recovery [99, 100]. PET, a type of polyester, consists of repeating units of terephthalic acid and ethylene glycol. Under certain conditions, PET can be depolymerised to recover these monomer components. Terephthalic acid in particular can serve as an organic ligand in the formation of MOFs and thus offers a valuable use for PET waste [101, 102]. The chemical process for synthesising MOFs from PET waste involves several steps. First, PET waste is depolymerised under alkaline conditions to obtain terephthalic acid and ethylene glycol. This depolymerisation process usually requires the use of a strong base, such as sodium hydroxide, and heat. The resulting terephthalic acid is then isolated and purified. The purified terephthalic acid is then used as an organic ligand in the synthesis of MOFs. This usually involves the reaction of the terephthalic acid with a suitable metal ion or cluster under controlled conditions. The sustainable synthesis of MOFs from PET waste has been the focus of several innovative studies, each of which has contributed to different applications. Recent studies have shown the potential of upcycling PET waste into MOFs for advanced applications. In one work, a Zn-MOF or MOF-5 was produced from PET, which is proving to be a promising material for high performance supercapacitor application [103]. Another synthesised Ni/La extracted Al_2O_3 from PET waste was found to be an efficient catalyst for

hydrogen production [104]. Taken together, these innovations underscore the value of PET waste as a platform for synthesising MOFs with tailored properties for energy storage, catalysis, nanocomposites and more. Further research utilising this strategy to sustainably convert plastic waste into functional nanomaterials will advance the goals of the circular economy.

The sustainable synthesis of MOFs from PET waste represents a significant advance in waste management strategies [104]. This innovative approach is not only in line with the principles of a circular economy, but also offers a competitive advantage over conventional MOF synthesis methods. By converting PET waste, a common environmental pollutant, into valuable MOFs, this method avoids the high costs associated with conventional organic ligands, thus improving cost efficiency. In addition, MOFs derived from PET waste exhibit promising properties, such as high surface area and improved separation ability, making them suitable for various applications. This approach also contributes to environmental protection by facilitating the reduction of PET waste, a major concern in today's waste management industry. Despite these compelling advantages, the method needs further scientific research to fully realise its potential and solve any emerging problems.

2.2.4. MOFs for Dye Adsorption

The increase in industrial and agricultural activities in recent years has contributed significantly to the widespread pollution of water bodies with organic pollutants, highlighting the urgent need for effective and sustainable water purification solutions [105]. Among the various methods investigated for the treatment of organically polluted wastewater, adsorption, Advanced Oxidation Processes (AOPs), membrane filtration and biodegradation have been shown to reduce pollutant concentrations to levels that are safe for the environment. Each of these methods has its own strengths and weaknesses, which points to the need for novel materials that can improve the effectiveness and sustainability of water treatment methods.

In this context, MOFs have attracted considerable attention as promising materials for the removal of dyes from wastewater. MOFs offer several advantages in water treatment, including their high porosity and surface area for effective pollutant binding and the ability to tailor their chemical properties to different pollutants [106]. Some MOFs also exhibit catalytic activity that facilitates the degradation of pollutants through advanced oxidation processes, actively removing pollutants rather than just trapping them [107]. The structural robustness of MOFs in aqueous environments and their potential for regeneration and reutilisation also promote their application

for industrial water purification strategies [108]. The structural diversity of MOFs, resulting from the wide range of possible metal and linker combinations, gives them the flexibility to be used in various water treatment scenarios, from selective adsorption of pollutants to catalysing their oxidative degradation. MOFs are versatile, with potential applications in adsorption [109], separation [110], catalysis (including photocatalysis and biocatalysis) [111]. They can be synthesised by a variety of methods, including solvothermal, hydrothermal, mechanochemical, sonochemical, spray drying, sol-gel and flow chemistry techniques, demonstrating the adaptability of MOFs to different manufacturing requirements [112]. One of the main advantages of MOFs compared to conventional adsorbents is their efficiency in regeneration, which requires relatively little energy [113]. This advantage, combined with their high thermal and mechanical stability, makes MOFs exceptionally suitable for the removal of contaminants from aquatic environments. These properties emphasise the potential of MOFs as effective materials for the purification of water bodies and address the urgent need for sustainable and efficient solutions to the problem of dye effluent pollution.

In summary, MOFs have attracted considerable attention due to their potential in addressing environmental problems in recent decades, particularly in the purification of wastewater through the adsorption of pollutants. Dye effluents from the textile industry dye and conventional methods have often been

insufficient to effectively remove these pollutants from water bodies. Since the ability of MOFs to adsorb and remove dye (MO) from water was first reported in 2010 [114], a wealth of research has emerged investigating their efficiency and adaptability in this context. This section provides an overview of unmodified and modified MOFs as adsorbents for MO dye. This section addresses the inherent properties and performance of MOFs and focuses on recent developments in dye removal of dyes from aquatic environments using various MOF structures. In addition, the effects of key operating parameters such as pH, adsorbent dosage, contact time and initial dye concentration on the effectiveness of MOFs in dye. Through this discussion, this section highlights the advances and potential of MOFs in the purification of water bodies from dye contaminants.

2.2.5. MOFs for Dye Photo-Fenton Degradation

Using different organic ligands, a wide range of Fe-MOFs were developed to investigate their potential for catalytic Fenton degradation of dye contaminants in aquatic environments [82].

By strategically combining carefully designed organic ligands with iron sources, researchers can achieve exceptional control over the structural and functional properties of Fe-MOFs. For example, the integration of benzene-1,4-dicarboxylic acid (H₂BDC) with octahedral FeO₄(OH)₂ chains leads to

the flexible MIL-53(Fe) structure [115]. In addition, the MIL-88 A(Fe) series MOFs are prepared by the association of $[\text{Fe}_3(\mu_3\text{-O})(\text{COO})_6]$ clusters with linear dicarboxylic acid ligands of different lengths [116], while MIL-101(Fe) is synthesized by combining the same $[\text{Fe}_3(\mu_3\text{-O})(\text{COO})_6]$ secondary building units (SBUs) with terephthalic acid ligands [117].

By precisely regulating the synthesis conditions, including temperature, reaction time and solvent type in hydrothermal methods, Viswanathan and his team were able to produce MIL-88 A(Fe) particles with different morphologies [116]. Their results indicated that rod-shaped particles exhibited improved photocatalytic performance due to their smaller size and lower electron-hole recombination rate. Nevertheless, the continuous consumption of Fe(II) within the material can lead to a reduction in the reaction rate. To investigating the application of Fe-MOFs in photocatalysis, Wu and colleagues conducted experiments on the degradation of tetracycline hydrochloride (TC-HCl) using the MIL-101(Fe)/photo/ H_2O_2 system [118]. They discovered that visible light effectively promotes the Fe(II)/Fe(III) cycle in Fe-O cluster-based photo-Fenton systems, thereby accelerating the degradation rate of TC-HCl. Xing and his team synthesised a two-dimensional $\text{Fe}_3(\text{HITP})_2$ MOF with FeN_4 active sites and excellent conductivity by incorporating specific organic linkers [119]. This design has further accelerated the Fe(III)/Fe(II) cycle and shows significant potential for

environmental remediation. These studies not only demonstrate the effectiveness of Fe-MOFs in degrading organic pollutants, but also highlight the potential of optimising the Fe(III)/Fe(II) cycle through material design to improve photocatalytic performance.

2.2.6. Research Gap

In summary, extensive literature research on MOFs has highlighted their significant potential in the adsorption and catalytic removal of organic pollutants, such as dyes, from aqueous solutions. The versatility and effectiveness of MOFs emphasise their promise as robust materials for environmental remediation technologies. However, there are still some research gaps that should be explored further. First, the synthesis of MOFs relies predominantly on traditional solvothermal methods, where synthesis conditions often cannot be precisely controlled. This limitation presents a critical opportunity for further research, particularly for the development of synthesis techniques that allow for more precise control, thus enabling the creation of MOFs with customised properties for specific applications. Secondly, the high cost of raw materials such as terephthalic acid, which is commonly used to synthesise many MOFs, remains a major challenge. A promising approach to solve this problem is the sustainable synthesis of MOFs, in particular through the depolymerisation of PET to obtain high-

purity terephthalic acid. This method not only offers the opportunity to reduce the costs associated with MOF production, but also contributes to the recycling of plastic waste and is therefore in line with global sustainability goals.

2.3. MOFs Derived Carbons

2.3.1. Characteristics of MOFs-derived Carbons

MOFs are a special category of materials that have attracted the attention of the scientific community due to their unique properties, such as high porosity, large surface area and customisable chemical functionality. However, despite these favourable properties, MOFs face significant problems. These include intrinsic instability, problems with stability under certain conditions (e.g. high temperatures and high humidity) and the limitation that they only have microporous structures, which limits their potential applications [91, 120].

To overcome these obstacles, a novel class of materials, MOF-derived carbon, has been created. MOFs-derived carbons are formed by the carbonisation of MOFs, a process that generally involves the pyrolysis of the MOF in an inert atmosphere. This transformation results in a carbon material that retains the porosity and structure of the original MOF, but also acquires new properties characteristic of carbon materials [121, 122].

Interestingly, MOFs can be directly converted into porous carbon materials by pyrolysis. Considering the structured spatial arrangement and careful metal ion framework of MOF precursors, it is plausible that porous carbon from MOFs may exhibit superior adsorptive properties [123-125]. These carbon materials are of great interest in analytical science, not only because of their unique chemical properties, but also because of their versatility as adsorbents. Among the MOFs that have been investigated for MO adsorption, MOF-235 is characterised by its suitable adsorption sites and ideal pore configuration for MO adsorption [5]. So far, the potential of using porous carbon from MOF-235 for dye adsorption of dyes has not been explored. Therefore, this study focusses on the use of MOF-235 as a starting material for the production of porous carbon.

To summarise, MOF-derived carbon materials represent an intriguing class of materials that combine the advantages of MOFs, including high porosity and tunable functionality. This distinctive blend of properties paves the way for novel applications in catalysis and adsorption. Therefore, MOFs-derived carbons represent a promising avenue for future research in the field of porous materials.

2.3.2. Synthesis of MOFs-derived Carbons

Currently, there are two main methods to extract carbon from MOFs: (a) direct carbonisation of MOF precursors and (b) incorporation of external organic materials as a carbon source and co-carbonisation with MOFs to produce carbonised products. Below you will find a detailed description of the direct carbonisation of MOFs:

2.3.2.1. Direct Carbonisation of MOFs

MOFs contain a significant amount of organic ligands that can be converted into nanostructured porous carbon or metal compounds at different temperatures during pyrolysis. By carefully controlling the temperature and atmosphere during the carbonisation process, the original structure and functionality of the MOFs can be maintained, significantly improving the specific surface area, pore volume and properties of the porous structure [126, 127]. For example, in carbonised MOF-5, which is obtained from MOF-5 and treated at 1000°C in an argon atmosphere, the surface area increases from 477 m²/g to 1884 m²/g, as reported by Kukulka et al. [128]. MC produced from MOF-5 carbonised at 600 and 800 °C in a nitrogen atmosphere achieves a surface area of 1812 m²/g, which is a significant improvement according to Hu et al. [126]. In contrast, MPC obtained from MIL-100(Fe) and carbonised at 700°C in a nitrogen atmosphere retains a relatively lower surface area of

132 m²/g, as found by Zhang et al. [129]. A major advantage of the direct carbonisation method is its simplicity. The resulting carbon materials have a more ordered and uniform pore structure than conventional commercial activated carbon.

2.3.2.2. Co-pyrolysis of MOFs and Other Precursors

By co-pyrolysis of MOFs with other carbon-based materials, biomass or synthetic polymers, structurally diverse carbon materials can be created. This approach enables the modulation and functionalisation of material properties during the carbonisation process. For example, the NPC obtained from MOF-5 and FA at 1000°C shows that higher carbonisation temperatures correlate with a larger specific surface area, as observed by Liu et al. [130]. Another NPC variant from MOF-5 and FA carbonised at temperatures between 530 and 1000°C shows improved specific surface area, mesopore distribution and conductivity, as reported by Liu et al. [131]. MOF-74-C prepared from MOF-74 and FA at 450°C shows increased pore sizes according to Wei et al. [132]. Finally, Ni/NC derived from Ni-MOF-74 and FA at 450/600°C shows improved dispersion of Ni particles, expanded pore size distribution and increased pore size, as found by Ning et al. [133]. These results highlight the significant influence of carbonisation conditions on the physical properties and performance of MOF carbons. The structural diversity of these materials

leads to unique properties that are suitable for different applications. Co-pyrolysis has considerable advantages. For example, the co-pyrolysis method increases the specific surface area and pore volume of the resulting materials and optimises their structure and performance through the selective addition of different precursors.

2.3.3. MOFs-derived Carbons for Dye Adsorption

Due to their unique properties, MOFs-derived carbons have proven to be effective adsorbents for organic pollutants in water. Their high porosity and large surface area provide ample adsorption sites and increase capacity [134, 135]. The ability to adjust the pore size and structure of MOFs-derived carbons enables optimisation for specific pollutants and thus increases selectivity. The incorporation of heteroatoms during carbonisation can create active sites that increase adsorption and catalysis efficiency [136, 137]. The durability of MOFs-derived carbons under different conditions ensures their effectiveness in different environments. In addition, their potential for regeneration and reuse emphasises their suitability for practical water treatment applications [122, 138]. Therefore, MOFs-derived carbons are very promising for the adsorption of organic pollutants from water. Recent research has identified four main elements that significantly influence the efficiency of MOFs-derived carbons in dye adsorption of dyes: the specific

MOF used, the parameters of the carbonisation process, the post-synthetic modifications made to the MOFs-derived carbons and the intrinsic properties of the pollutant in question.

The choice of MOF precursors is crucial for the properties of the resulting MOFs-derived carbons. Different MOFs with their unique metal centres and organic linkers can influence the porosity, surface area and chemical functionality of MOFs-derived carbons. For example, recent scientific studies have shown that MOFs-derived carbons have significant potential for the adsorption and catalysis of organic pollutants from aqueous environments. MDC-1000, a material derived from MOF-5 (Zn) carbonised at temperatures of 800 to 1000°C, has an impressively high surface area of 1337 m²·g⁻¹ and is characterised by its ability to remove MB with an exceptional adsorption capacity of 2723.88 m²·g⁻¹ [139]. MPCs derived from MOF-5 (Fe) is subjected to a two-step carbonisation process (200°C for 1 hour, followed by 500°C for 1 hour), resulting in a surface area of 104 m²·g⁻¹ and an adsorption capacity of 113.00 m²·g⁻¹ for 4-nitrophenol [140]. Finally, ZIF-8/AG-CA, which is produced from ZIF-8 and carbonised at an elevated temperature of 900°C, has a surface area of 516 m²·g⁻¹ and is particularly effective in adsorbing organic solvents. It can absorb 30 to 60 times its own weight [141].

In summary, the effectiveness of MOFs-derived carbons in adsorbing organic pollutants from aqueous environments is strongly influenced by the choice of MOF precursors, the carbonisation parameters and the pollutant properties. The proven versatility and high adsorption capacities of MOFs-derived carbons emphasise their potential for practical applications in water treatment. The importance of carbonation conditions for optimising the properties and performance of MOFs-derived carbons was highlighted. Future research should aim to fine-tune these parameters to further improve the performance of MOFs-derived carbons and investigate their regeneration and reuse potential to assess sustainability. The considerable potential of MOFs-derived carbons for the adsorption of organic pollutants from water deserves additional scientific attention.

2.3.4. MOFs-derived Carbons for Dye Photo-Fenton Degradation

Advanced Oxidation Processes (AOPs) are recognised as effective solutions for the elimination of persistent organic pollutants. These methods, which include photocatalysis and Fenton reactions, are mainly characterised by their ability to initiate hydrogen peroxide (H_2O_2) to form highly active hydroxyl radicals ($\cdot\text{OH}$) and to initiate peroxymonosulphate (PMS) and peroxydisulphate (PDS) to generate active oxygen species (ROS). Compared to traditional homogeneous Fenton methods, heterogeneous Fenton methods

using solid catalysts have been emphasised for their extended pH spectrum, simplified catalyst recovery and improved reusability. In this context, MOFs-derived carbons derived from MOFs have attracted great interest. These substances, which are produced by carbonisation of MOFs, not only retain the porous architecture of the original MOFs, but also exhibit improved catalytic efficiency through the integration of transition metals or metal oxides. These advantages make MOFs-derived carbons superior catalysts for Fenton and Fenton-like oxidation reactions, especially in the purification of organic pollutants in wastewater treatment.

Wang and his team [142] investigated the degradation of norfloxacin (NOR) using a novel iron-based magnetic nanoparticle catalyst embedded in mesoporous carbon (Fe@C 700). The catalyst was prepared by pyrolysis of MIL-101-Fe at 700°C and used in a microwave-assisted Fenton reaction with H₂O₂. It improved the Fe(III)/Fe(II) redox cycle, electron transfer and hydroxyl radical (\cdot OH) production and achieved a degradation efficiency of 95.22% under optimal conditions. The Fe@C 700 catalyst showed excellent stability and reusability over five cycles and was effective over a wide pH range. Similarly, Tang and colleagues [143] created a three-dimensional flower-like catalyst (FeCu@C) embedded with bimetallic iron-copper nanoparticles within a mesoporous carbon shell by thermal decomposition of Fe, Cu-BDC precursors. This catalyst was tested in the Fenton-like

degradation of sulfamethazine (SMT) and showed a complete removal of SMT within 90 minutes and a total organic carbon (TOC) conversion rate of 72.3 % within 240 minutes at a pH of 3. This flower-like carbon structure not only acts as a scaffold for the bimetallic nanoparticles and facilitates the attraction of SMT molecules via π - π interactions, but also increases the degradation efficiency of SMT. The iron and copper nanoparticles contained therein serve as active centres in the Fenton reaction. They promote the formation of $\cdot\text{OH}$ radicals and thus effectively improve the degradability of SMT.

Due to the limitations of the conventional Fenton process, which is only effective in a pH range of 2 to 4, there has been a remarkable shift towards the application of Fenton-like methods based on peroxymonosulphate (PMS) for the efficient and environmentally friendly degradation of persistent pollutants. The conversion of MOFs containing metals such as cobalt (Co) and iron (Fe) by pyrolysis leads to the formation of carbon-based composites in which metal nanoparticles are embedded. The carbonaceous framework of these composites prevents the clumping of metal nanoparticles, while the embedded metals, especially Co and Fe, exhibit exceptional catalytic activity in Fenton-like processes.

By annealing bimetallic core-shell MOFs, Shao et al. [144] successfully synthesised a novel catalyst characterised by a two-dimensional porous carbon architecture decorated with Co-N_x sites and cobalt nanocrystals on a graphene oxide substrate. Nitrogen-containing ligands in the MOFs were observed to release reductive gases during the carbonisation phase, facilitating the on-site evolution of Co²⁺ ions and cobalt nanocrystals in the structure, which is further enhanced by the incorporation of Co-doped carbon nanotubes. This catalyst proved to be highly effective in degrading various phenyl derivatives such as bisphenol A, phenol, biphenyl and naphthalene, utilising its unique structural properties.

Furthermore, the pyrolysis of iron-containing MOFs leads to porous carbon materials doped with Fe/Fe₃C, which are used for the oxidative degradation of aqueous pollutants via Fenton-like reactions. Similarly, porous CoFe₂O₄ nanocarbon catalysts derived from bimetallic Co/Fe MOFs have demonstrated their performance in the activation of PMS for the degradation of bisphenol A (BPA) [145]. Compared to hydrothermally synthesised CoFe₂O₄ nanoparticles, they exhibit a significantly larger specific surface area (60.4 m²·g⁻¹) and pore volume (0.64 cm³·g⁻¹), thereby improving the interaction efficiency with BPA. Electron paramagnetic resonance (EPR) analysis elucidated the key contributions of ·OH and ·SO₄ radicals to the degradation mechanism. After five cycles of degradation, the catalytic

performance of the C-ZIF-67@ZIF-8@GO-900 catalyst decreased only minimally, demonstrating its remarkable catalytic stability.

2.3.5. Research Gap

In summary, after reviewing the extensive literature on MOFs-derived carbons, it is clear that these materials show promise for the adsorption and catalytic removal of organic pollutants, such as dyes, from the aquatic environment. MOFs-derived carbons show better performance than their precursor MOFs in certain applications, emphasising their potential as highly effective materials for environmental remediation. Despite these promising properties, significant research gaps remain to be filled. In particular, targeted MOFs-derived carbons for specific dyes, such as methyl orange, have not yet been explored, indicating an important area for future research. This gap emphasises the need for the development of MOFs-derived carbons tailored for the adsorption and degradation of specific pollutant molecules, which could improve the efficiency and specificity of pollution reduction strategies. In addition, the sustainable synthesis of MOFs using PET as a feedstock to produce high-purity terephthalic acid represents a cost-effective method that could be similarly applied to the synthesis of MOFs-derived carbons. This approach not only promises to reduce the costs associated with the production of MOFs-derived carbons, but is also in line with environmental sustainability

goals as PET waste is recycled. Exploring this route could potentially lead to the development of an economically feasible and environmentally friendly production method for MOFs-derived carbons, which would further increase their applicability and impact in addressing global environmental challenges.

2.4. Summary

This chapter focus on the adsorption and photocatalytic Fenton catalysis of dyes in an aqueous environment, with particular emphasis on the potential of MOFs and MOFs-derived carbons as efficient adsorbents and catalysts. The chapter describes in detail the high surface area, tunable pore size and chemical functionality of these materials and highlights their potential applications in the treatment of dyes in water. It also discusses the potential negative impact of synthetic dyes on the environment and highlights the importance of developing effective dye removal technologies, with adsorption and photocatalytic Fenton catalysis being promising approaches.

The chapter also looks at the unique properties and different synthesis methods of MOFs and emphasises the importance of precisely controlling the synthesis conditions to optimise the performance of MOFs. In addition, a new class of materials, MOFs-derived carbons, is introduced, which can overcome some limitations of MOFs as adsorbents, such as insufficient pore size. Finally, the possibility of a sustainable synthesis of MOFs and MOFs-derived

carbons from PET waste is investigated, which not only improves the environmental friendliness of the materials, but also promotes the recycling of waste into valuable resources. This approach provides a holistic view of the use of innovative materials in environmental remediation and contributes to both pollution reduction and sustainable materials science.

Chapter 3.

Experimental

This chapter provides an overview of the basic experimental tools and primary characterisation methods used to analyse the materials. These techniques are essential for the evaluation of the physical, chemical and optical properties of the synthesised materials. In addition, they play a crucial role in elucidating the relationship between the structural properties of the samples and their performance. By applying these methods, researchers can gain deeper insights into the mechanisms underlying the adsorption and photocatalysis processes and thus improve the understanding of how material properties influence these reactions. This comprehensive characterisation is crucial for optimising material design and improving the effectiveness of the developed systems in practical applications.

3.1. Materials

MO used in this thesis is purchased from Aladdin Chemical reagent Co. (Shanghai, China). Other chemicals, such as iron chloride hexahydrate ($\text{FeCl}_3 \cdot 6\text{H}_2\text{O}$), N,N-Dimethylformamide (DMF, 99%), Ethanol (99%), p-Phthalic acid (TPA, 99%) were purchased from Aladdin Chemical reagent Co., Ltd (Shanghai, China) and Shanghai Macklin Biochemical Technology Co., Ltd (Shanghai, China). The waste PET bottles used as feedstock in this study were obtained from Sam's Supermarket, Wal-Mart Department Store Co., Ltd. All chemicals used in this study were used without further purification.

3.2. Dye Removal Test

3.2.1. Oil Bath Device

The oil bath method was primarily used to produce the materials, which makes it possible to customise the structures of the samples produced by modifying the synthesis parameters. In a standard procedure, the precursors were dissolved in a suitable solvent to obtain a uniform solution. This solution was then placed in an oil bath apparatus where continuous stirring was carried out at a controlled temperature to facilitate the synthesis process. This method allowed precise control of the reaction conditions, such as temperature and mixing speed, which are critical to achieving the desired material properties.

The detailed set-up and process of this method is shown in Figure 3.1 and illustrates its role in the production of high-quality materials with customised properties.



Figure 3.1 Oil bath device (synthesis temperature = 80°C, synthesis time = 24 h).

3.2.2. Adsorption Test Device

The adsorption experiment serves as a crucial method for evaluating the effectiveness of the synthesised adsorbents. In this study, a thermostatic

oscillator was used to precisely regulate both the temperature and the oscillation rate during the experiments. These factors are of great importance as they strongly influence the adsorption process and ensure that the experiments are carried out under optimal conditions to obtain accurate and reliable results. The use of the thermostatic oscillator allows for consistent environmental control, which is essential for replication and comparison of experimental results. The design and function of this device is shown in Figure 3.2 to illustrate its role in facilitating the adsorption experiments.

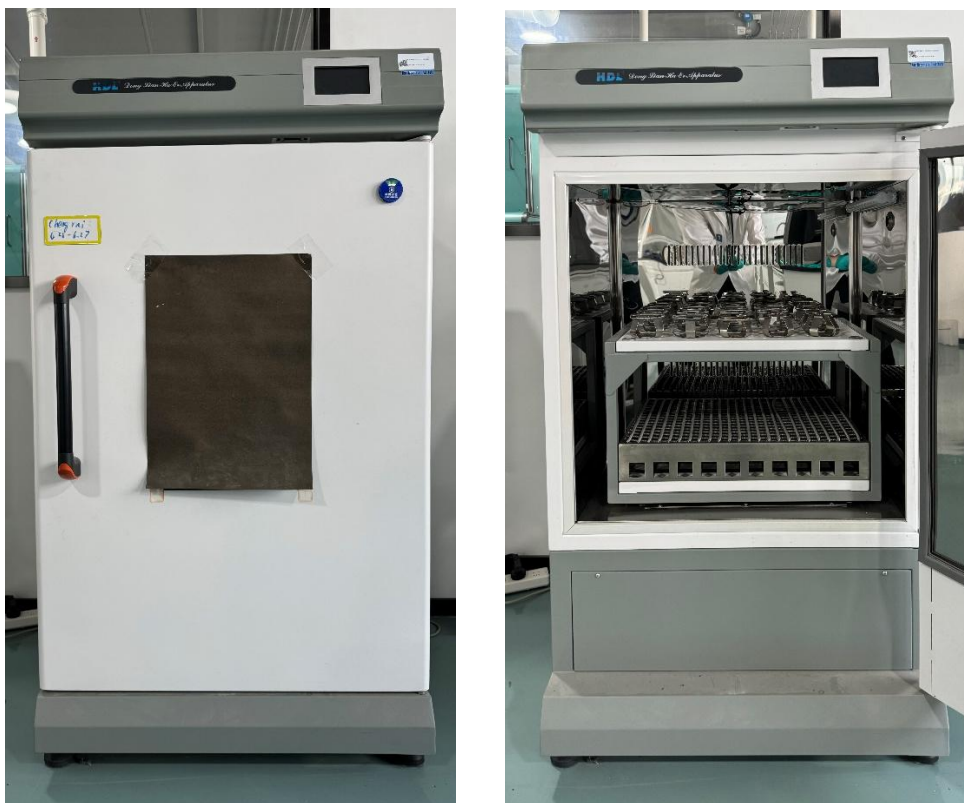


Figure 3.2 Adsorption test device.

3.2.3. Photoactivity Test Device

Photoactivity tests are fundamental experiments in photocatalysis that are crucial for evaluating the performance of photocatalytic materials. In this study, a simple photocatalytic reactor was built to perform these experiments. As shown in Figure 3.3, the setup included a xenon (Xe) lamp, a magnetic stirrer and a dark metal cover. The Xe lamp served as a source of simulated visible light and was fitted with a special filter to ensure an appropriate wavelength. The magnetic stirrer ensured thorough mixing of the reaction mixture and promoted uniform interaction between the photocatalyst and the reactants. The dark metal cover shielded the reactor from external natural light sources, preventing interference with the photocatalytic process. This controlled setup was essential to obtain accurate and reliable measurements of photocatalytic activity.

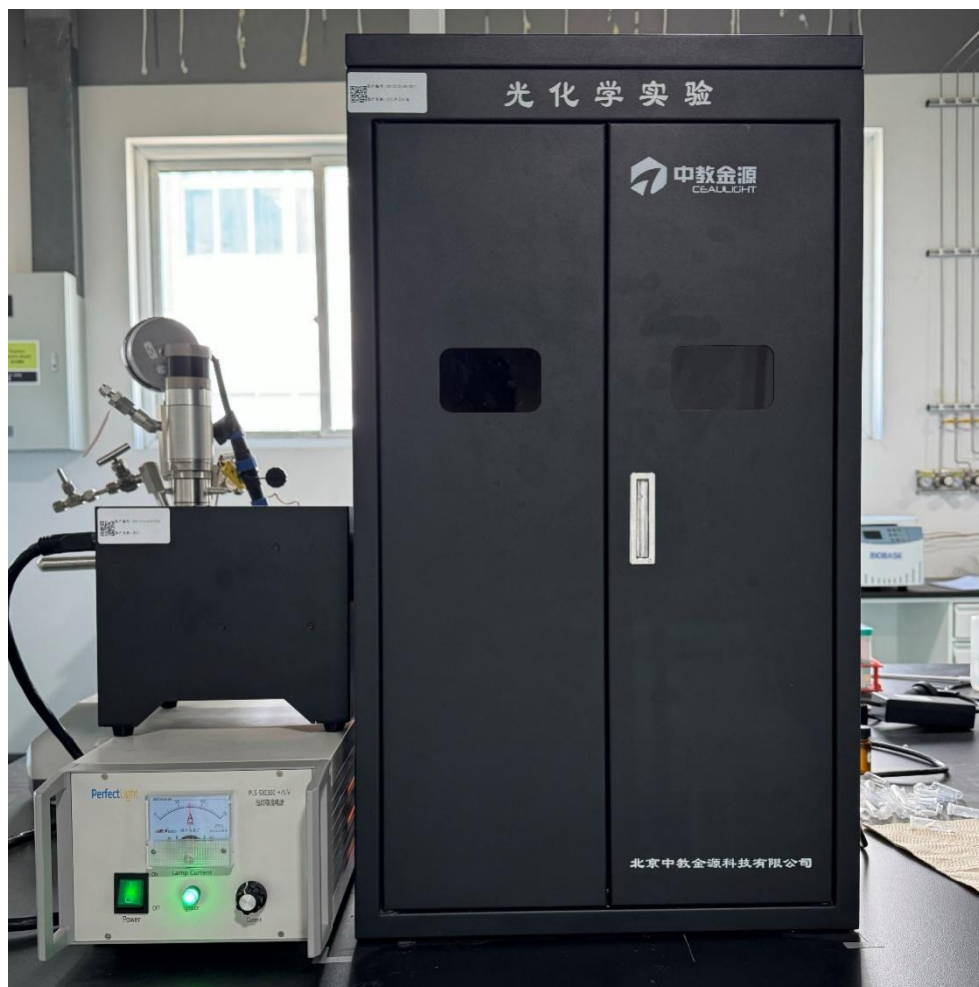


Figure 3.3 Photoactivity test device.

3.2.4. Concentration Test Device

The removal of methyl orange dye by the synthesised adsorbents and catalysts was investigated using UV spectrophotometry and batch experiments. Prior to analysis, all materials were dried overnight at 80°C in a vacuum and stored in a desiccator. A solution volume of 4 mL was used for the tests and a blank sample was measured before each analysis to obtain a spectral baseline. The adsorbent/catalyst/adsorbate mixtures were shaken with an automatic

thermostatic shaker. The residual dye concentrations in the collected solutions were quantified by UV-Vis spectroscopy at 465 nm.



Figure 3.4 Dye removal capacity evaluation rig.

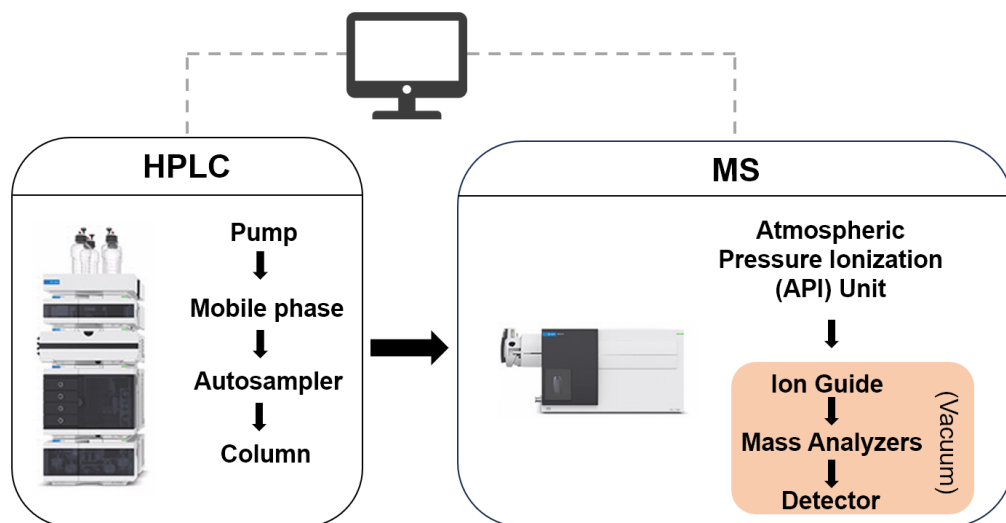


Figure 3.5 Principle of HPLC-MS.

In mass spectrometric analysis, ions are generated from a sample in the gas/liquid phase, usually by electron ionisation. The ions are separated according to the mass-to-charge ratio (m/z) and their relative abundances are

determined. This produces a mass spectrum that shows the intensity of the ion signal as a function of m/z .

In this study, liquid chromatography-mass spectrometry (LC-MS) was used to elucidate the mechanism of methyl orange treatment by the synthesised adsorbents and catalysts. LC-MS analysis was performed on untreated methyl orange solutions and on solutions after adsorption/catalytic treatment. After a 2-hour adsorption period, the treated and untreated samples were carefully collected and adjusted to a pH of 6.8 with 0.01 M NaOH prior to analysis. The mobile phase was a mixture of acetonitrile and ammonium acetate (0.01 mM, pH 6.8) (30:70 v/v) passed through a Waters ACQUITY UPLC BEH C18 column (2.1 x 50 mm, 1.7 μm) at a flow rate of 0.2 $\text{mL}\cdot\text{min}^{-1}$. Controlled conditions included a sample temperature of $15 \pm 5^\circ\text{C}$, a column temperature of $40 \pm 5^\circ\text{C}$, a capillary voltage of -2.8 kV, a sampling cone of 29.0 V, a threshold of 150°C and a desolvation temperature of 400°C . The gas flows for the cone and desolvation were set to 50.0 and 800.0 $\text{L}\cdot\text{h}^{-1}$ respectively.

3.3. Characterisation of Adsorbents and Catalysts

The adsorbents and catalysts in this study were analysed using a variety of characterisation techniques. These techniques provided comprehensive analyses and insights into the structure of the materials, specific surface area

and pore size, surface chemical properties, thermal properties, molecular structure and chemical bonding, morphology and microstructure.

3.3.1. Structural Analysis

Material phase and structural analysis was conducted utilizing powder X-ray diffraction (XRD) on a Bruker D8 advance A25 instrument. The scan type selected was coupled two Theta/Theta, with two Theta ranging from 5° to 100° in steps of 0.01° and an interval of 0.1 s, following previously established protocols. For the analysis, 1 to 2 g of the sample was loaded into the sample holder. It was imperative to ensure that the sample was finely powdered, presenting a flat surface, before proceeding with the testing. This methodological approach adheres to established practices for accurate and reliable phase characterization through XRD techniques.

3.3.2. Surface Area and Porosity Analysis

The porosity and surface area of MOFs and their derivatives were evaluated using BET specific surface area analysis, employing the Micromeritics Tristar II 3020 instrument. Comprehensive adsorption and desorption profiles, alongside BET and Langmuir surface areas, BJH pore volumes, distribution, and porosity data were obtained from the analysed results. Samples were prepared by weighing approximately 0.3 g and subjected to a degassing

temperature of 150°C for 24 hours. Subsequently, the analysis was conducted at a testing temperature of 77 K.

3.3.3. Surface Chemical Analysis

X-ray photoelectron spectroscopy (XPS) is a widely used technique for analysing the chemical properties of the surface of materials. In this thesis, XPS analyses were performed using an ESCALAB 250Xi spectrometer (Thermo Scientific, USA) with a monochromatic Al Ka X-ray source. The results obtained were then standardised by adjusting the C 1s signal to 284.8 eV.

3.3.4. Thermal Analysis

The study of MOFs by thermogravimetric analysis (TG) proves to be a crucial way to understand their carbonisation processes. In this experimental protocol, a sample with an initial weight of about 15-20 mg is weighed before the carefully orchestrated heating procedure begins. In the first phase, the temperature is gradually increased from room temperature to 105°C to drive out the remaining moisture. Two different series of experiments are then carried out: firstly, a temperature rise to 350°C, which is maintained for 120 minutes; secondly, a temperature rise to 500°C. The use of high purity nitrogen (99.999%, Linde) during the intrinsic analysis in combination with

a controlled heating rate of 20°C per minute ensures a systematic exploration of the thermal response of the MOF. This comprehensive approach aims to explore the intricacies of MOF carbonisation across different temperature ranges and gain valuable insights into the thermal behaviour and potential applications.

3.3.5. Molecular Structure and Bond Analysis

The sustainable raw materials of the MOF, as well as the MOF and its derivative samples, underwent analysis using a Fourier transform infrared spectroscopy (FTIR) (Bruker Vertex 70 from the United States). The FTIR measurements were conducted with a sample scan time and background scan time both set at 40 minutes. The wave number was configured to range from 400 to 4000 cm^{-1} . To enable accurate and consistent measurements, all samples were carefully prepared as a fine powder and then pressed into a circular mould with an inner diameter of 1 cm for 5 minutes at a pressure of 3 MPa. This FTIR analysis aims to decipher the molecular composition and structural features of the sustainable raw materials, MOFs and their derivatives, providing valuable insights into their chemical properties and functional groups.

3.3.6. Morphology and Microstructure Analysis

The morphology of the MOFs and the samples prepared from them was analysed using scanning electron microscopy (SEM) (Sigma VP device from Zeiss, Germany). The SEM analysis was performed at a test voltage of 2 to 5 kV and a working length of approximately 7.5 mm. The SEM images were recorded with a secondary electron detector (SE2 in the control panel). In addition, the metal composition of the MOFs was determined by energy dispersive X-ray spectroscopy (EDS) in conjunction with SEM observation of the recorded images. X-ray generation during EDS analysis was performed at a voltage of 15-20 kV. This comprehensive approach allows a detailed exploration of the morphological features and elemental composition of MOFs and their derivatives and provides valuable insights into their structural properties.

Chapter 4.

Controlled Synthesis of Uniform MOF-235 for the Adsorption of Methyl Orange in Wastewater with High Efficiency and High Capacity

4.1 Introduction

Wastewater from the textile industry is a major problem worldwide, as more than 700,000 tonnes of dyes are produced every year [146]. methyl orange, an acidic anionic azo dye [147, 148], accounts for a significant proportion of this dye-containing wastewater and is used extensively in the textile industry [19]. Due to their mutagenic, toxic and oncogenic properties, methyl orange released into water pose a serious challenge to the environment and human health [149]. It is therefore necessary to develop novel adsorbents that are highly efficient in removing methyl orange from wastewater.

Various methods have been developed to treat dye wastewater before it is released into the environment, including photocatalytic degradation, electrochemical hybrid degradation and adsorption [148, 150-153]. Due to its high efficiency and cost-effectiveness, adsorption is widely applied for the removal of azo dyes in the aquatic environment [51, 154]. Metal-organic frameworks (MOFs), which are known for their large surface area, adaptable

structure and good thermal and chemical stability, have been effectively used as adsorbents for removing azo dyes from wastewater [155].

To date, many MOFs have been used for removing methyl orange from wastewater and have shown different adsorption capacities, for example, PED-MIL-101 (adsorption capacity: $194 \text{ mg}\cdot\text{g}^{-1}$), ED-MIL-101 ($160 \text{ mg}\cdot\text{g}^{-1}$), MIL-101 ($114 \text{ mg}\cdot\text{g}^{-1}$) [114]. Most MOF materials have limited adsorption capacity in the field of methyl orange adsorption. MOF-235 stands out from other MOFs due to its high concentration of aromatic rings, which promote dye adsorption through π - π structures resulting from strong hydrophobic interactions between the dye and the MOF. The maximum adsorption capacity of MOF-235 for methyl orange has been reported as $477 \text{ mg}\cdot\text{g}^{-1}$ [5]. This result could be further improved due to its non-uniform shape. In addition, early studies have confirmed that the controlled synthesis process can also significantly increase the production yield of MOF [94, 156]. Therefore, it is necessary to develop a new method for the controlled synthesis of MOF-235 to increase the yield and significantly improve its capacity in methyl orange adsorption.

The specific mechanism of the adsorption behaviour of MOF-235 towards methyl orange has not been thoroughly investigated. Previous research showed that the adsorption of methyl orange on MOF-235 is driven by

electrostatic interactions between the surface of the adsorbents dye and dye molecules [5]. Therefore, further research is needed to verify whether chemical reactions are involved in the adsorption process of MOF-235. In addition, research into the adsorption potential of MOF-235 for other organic dyes is also of great importance.

In this study, a solvothermal method for the controlled synthesis of MOF-235 with defined morphology and size distribution was developed as an adsorbent with improved capacity for the adsorption of methyl orange from wastewater. The physical and chemical properties of the MOF-235 were characterised. The adsorption kinetics and adsorption isotherms of the MOF-235 material were investigated. Optimal adsorption conditions were investigated. In addition, the mechanism of adsorption of methyl orange onto MOF-235 was investigated.

4.2. Preparation of MOF-235

All chemicals (terephthalic acid (TPA), $\text{FeCl}_3 \cdot 6\text{H}_2\text{O}$, N, N-dimethylformamide (DMF) and ethanol) reached 99% purity and were purchased by Aladdin Chemical Reagent Co. in Shanghai, China. To synthesise MOF-235, 0.6 g of TPA and 0.6 g of $\text{FeCl}_3 \cdot 6\text{H}_2\text{O}$ were dissolved in 180 ml of DMF and sonicated for one hour. Then, 60 ml of ethanol was added to the reaction solution and the mixture containing 240 ml of the

solution was placed in an apparatus with oil bath and magnetic stirring before heating at a temperature of 353 K for 24 hours. After drying in a freeze dryer, the orange-coloured powder was washed with a mixture of DMF and ethanol (Figure 4.1).

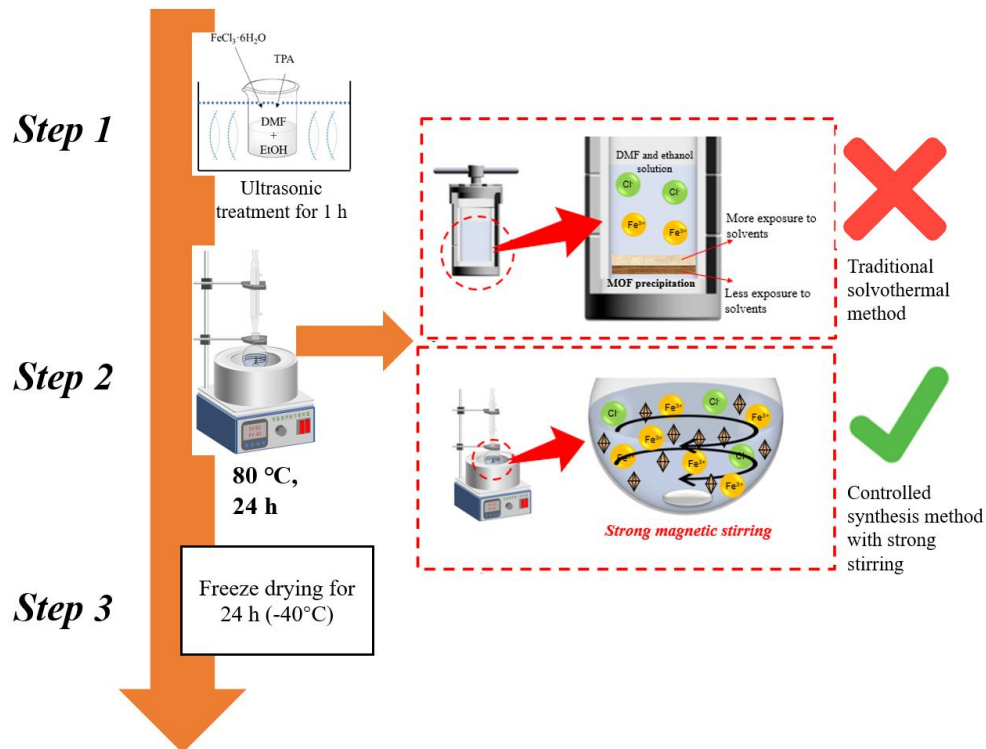


Figure 4.1 Schematic of the synthesis of MOF-235 under continuous strong stirring.

4.3. Characterisation

In order to investigate the change in the functional group, the adsorbents were analysed using Fourier transform infrared spectroscopy (Thermo Fisher Scientific, Nicolet iS50 FT-IR) in the wavenumber range from 4000 to 400 cm⁻¹. Scanning electron microscopy (SEM, Regulus 8100, Japan Hitachi)

was used to analyse the morphology of the material. The crystal structure was determined using an X-ray diffractometer (Smart Lab (3 KW), Japan Rigaku). The X-ray diffraction (XRD) patterns were then identified (40 kV, 30 mA, scan step = 0.02° , 2θ range was from 5 to 40°). The textural properties of the adsorbents, such as pore volume and pore size Brunauer – Emmett – Teller (BET, 3 Flex America Micromeritics) surface analysis of the synthesised adsorbents were measured by nitrogen adsorption/desorption method at 77 K. To evaluate the thermal stability, the prepared sample was heated in a nitrogen atmosphere ($50 \text{ ml}\cdot\text{min}^{-1}$) at a rate of 2K min^{-1} from 30 to 500°C using a thermogravimetric analyser (TGA, 3+ Switzerland Mettler Toledo). UPLCMS (Waters Acquity UPLC Hclass-Waters SO Detector 2) was used to investigate the mechanism of MO removal from the MOF-235 synthesised in this study.

4.4. Adsorption Experiments

The adsorption of methyl orange on MOF-235 was analysed by UV-vis spectrophotometry and batch tests. Prior to testing, all adsorbents were fully dried overnight and stored in a vacuum oven. Comprehensive studies were conducted to investigate the effects of solution pH, initial dye concentration and adsorption temperature on methyl orange removal. The adsorbent-adsorbate mixtures were stirred for 60 minutes using an automatic

thermostatic shaker. The dye concentration was then measured by UV-vis spectroscopy at a wavelength of 465 nm.

4.4.1. Effect of pH

A range of 3 to 11 was used to investigate the effects of initial pH on the adsorption efficiency of MOF-235. About 50 mL of $100 \text{ mg}\cdot\text{L}^{-1}$ MO solution was added to a flask containing 0.02 g of adsorbent and stirred at 150 rpm for 24 hours at a stable room temperature. 0.1 M NaOH or 0.1 M HCl solution was used to adjust the pH of the dye solution before adsorption. After adsorption, the adsorbent was isolated using a centrifuge.

4.4.2. Effect of Initial Concentration

To study the effect of the initial dye concentration, 100 mL amber bottles containing 50 mL of the methyl orange solution at a concentration of 20 to $800 \text{ mg}\cdot\text{L}^{-1}$ were used. To each bottle, 20 mg of MOF-235 was added. The mixture was then transferred to a shaking incubator, which was operated at 3 different temperature (15, 25, 35 °C) and 150 rpm for 24 hours. The samples were then filtered through a centrifuge. A UV-vis spectrophotometer with a wavelength of 465 nm was used to determine the concentration of MO before and after adsorption. The amount of methyl orange adsorbed on MOF-235 was analysed using equation,

$$q_e = \frac{(C_0 - C_e)V}{W} \quad (9)$$

where q_e : amount of methyl orange compounds adsorbed at equilibrium ($\text{mg}\cdot\text{g}^{-1}$); C_0 : initial dye concentrations ($\text{mg}\cdot\text{L}^{-1}$); C_e : equilibrium concentrations after adsorption ($\text{mg}\cdot\text{L}^{-1}$); W : the mass of MOF-235 used in the process (g); V : solution volume (L).

4.5. Adsorption Mechanism

Liquid chromatography-mass spectrometry (LC-MS) analysis was used in this study to determine whether the adsorption of methyl orange by MOF-235 in this study was due to a physical or chemical process. Both the untreated methyl orange solution and the methyl orange solution after treatment with MOF-235 were subjected to LC-MS analysis. Samples were carefully taken from both the untreated and adsorbed methyl orange solution after a 2-hour adsorption period. Prior to the assay, the pH of the treated methyl orange solution was adjusted to 6.8 with NaOH (0.01 M). The mobile phase consisted of a 30:70 ($\text{vol}\cdot\text{vol}^{-1}$) mixture of acetonitrile and 0.01 mM ammonium acetate ($\text{pH} = 6.8$) and was administered at a flow rate of $0.2 \text{ ml}\cdot\text{min}^{-1}$. A reversed phase column, namely Waters ACQUITY UPLC® BEH C18 $1.7 \mu\text{m}$ $2.1*50$ mm, was used. The analysis was performed under controlled temperature conditions, with the sample temperature maintained at $15 \pm 5^\circ\text{C}$ and the column temperature at $40 \pm 5^\circ\text{C}$. The capillary (kV) was set to 2.80, the

sampling cone to 29.00, the threshold temperature ($^{\circ}\text{C}$) to 150, and the desolvation temperature ($^{\circ}\text{C}$) to 400. The cone gas flow ($\text{L}\cdot\text{H}^{-1}$) and the desolvation gas flow ($\text{L}\cdot\text{Hr}^{-1}$) were set to 50.0 and 800.0, respectively.

4.6. Results and Discussion

4.6.1. Characterisation.

The sample prepared in this study was also analysed by SEM to show its morphology and particle size, as shown in Figure 4.2. It is clear that the MOF-235 has a well-crystallised octahedral shape and a generally uniform size distribution with few deviations, compared to Figure 4.2 (d), an SEM image of high-purity MOF-235 from previous publications [157]. The magnified SEM image in Figure 4.2 (a) shows that a particle size distribution of 800 nm prevails for the MOF-235 crystals, which is much smaller and more uniform than the MOF-235 particles prepared by the classical solvothermal approach (Figure 4.2 (c)) and the previous study (Figure 4.2 (d)). Figure 4.2 (b) shows that the MOF-235 synthesised during a controlled synthesis time of 24 hours has a broader particle size distribution, ranging up to 1.3 μm . This indicates that a longer synthesis time provides sufficient time for the development and enlargement of the crystalline structures.

This study compares the quality of products synthesised using the traditional solvothermal method and a controlled synthesis approach under identical raw

material and synthesis temperature conditions over different synthesis durations. As can be seen in Figure 4.3, the controlled synthesis method, which was facilitated by improved mass transfer through vigorous stirring, achieved the product quality observed with the traditional solvothermal method after 10 hours within only 4 hours of synthesis time. After 24 hours of synthesis, the MOF-235 produced by the controlled synthesis was of 1.67 times higher quality than that produced by the traditional solvothermal method. The SEM images confirm that the controlled synthesis results in MOF-235 that is uniform and has a narrow size distribution.

The introduction of stirring into the synthesis process improves mass transfer, ensures an even distribution of reactants and prevents localised fluctuations in concentration. This promotes synchronous nucleation, leading to the formation of more uniform nuclei and consequently particles of uniform size and shape. Agitation also optimises nucleation kinetics by distributing heat, preventing supersaturation and reducing the risk of explosive nucleation. This controlled process improves particle homogeneity and reduces multimodal size distributions. In addition, agitation facilitates sustainable crystal growth by increasing the mass transfer rate to the crystal surface, ensuring an adequate supply of material to each nucleus and preventing stagnation or defects. Furthermore, agitation reduces secondary nucleation, maintaining the

monodispersity of the particles and further improving the overall yield and quality of the product.

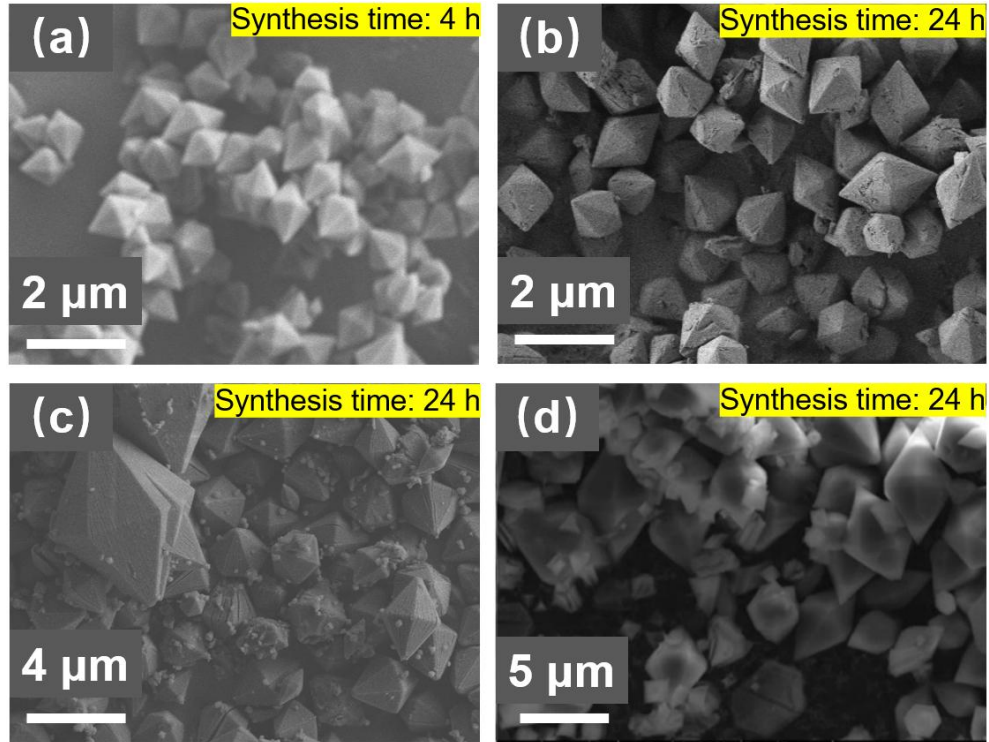


Figure 4.2 SEM images of MOF-235 prepared by controlled synthesis method (a, b), MOF-235 synthesized by traditional hydrothermal method and (d) MOF-235 SEM image reported by others [157].

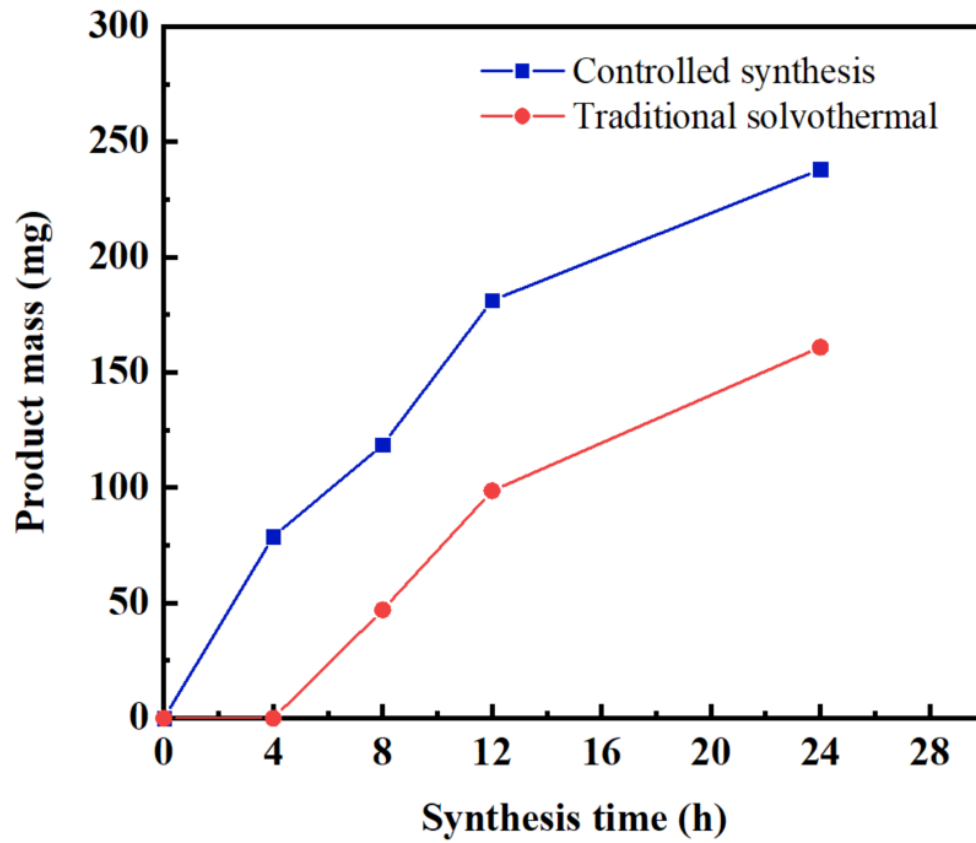


Figure 4.3 Comparison of synthesis efficiency: controlled synthesis method and traditional solvothermal method.

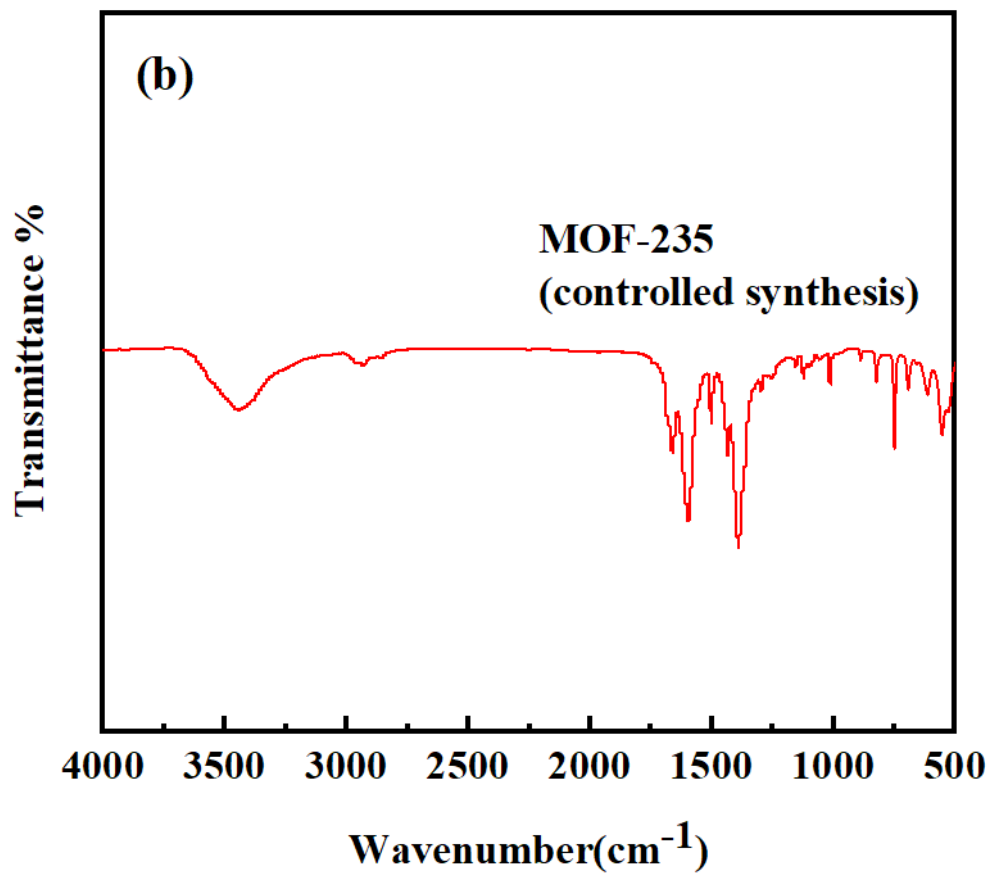
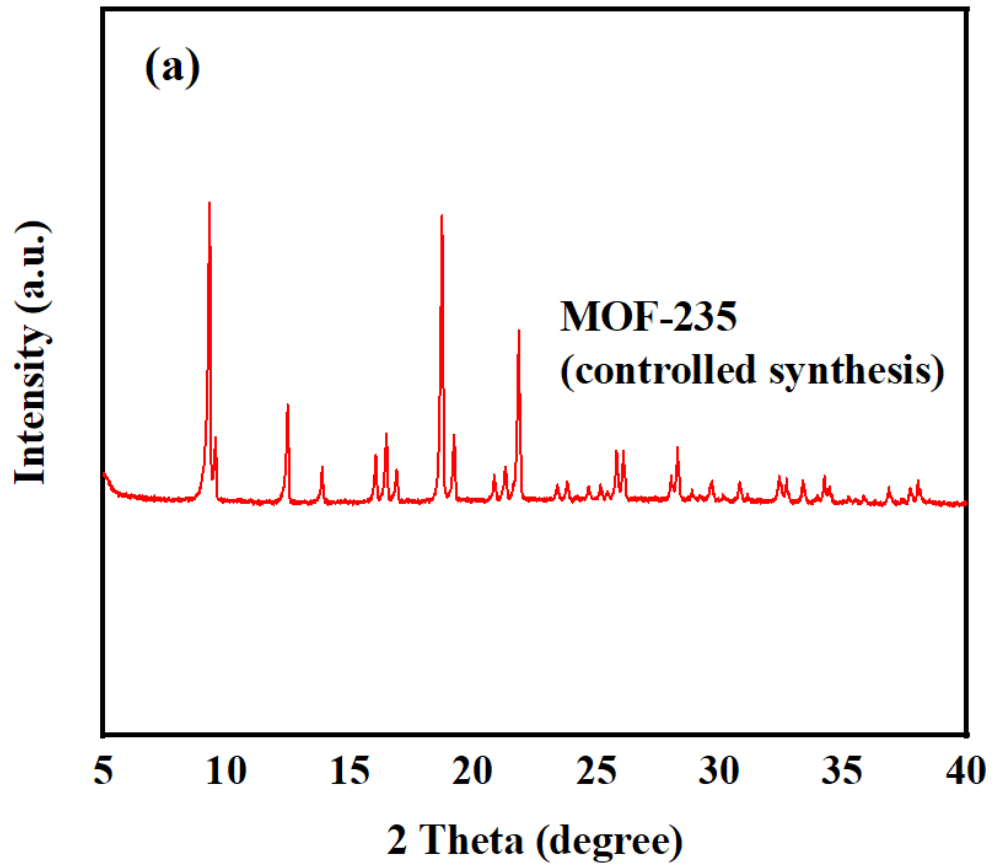


Figure 4.4 (a) XRD pattern of MOF-235 synthesized by oil bath method, (b) FTIR spectrum of control synthesized MOF-235.

Figure 4.4 (a) illustrates that the sample has a pure MOF-235 crystal structure. The main peaks are observed at 2θ angles of 12.6° , 19° and 22° . Furthermore, a prominent peak at 9.4° corresponds to the main peak (101) of MOF-235, which underlines its importance for the characterisation of the crystal structure [158]. The FT-IR spectrum of MOF-235 is shown in Figure 4.4 (b). The FTIR spectrum of the materials prepared in this study contains main peaks at 554 cm^{-1} (S), 750 cm^{-1} (S), 823 cm^{-1} (m), 1014 cm^{-1} (m), 1597 cm^{-1} (VS), 1390 cm^{-1} (VS), 2935 cm^{-1} (W), 3442 cm^{-1} (m), which are consistent with the values for MOF-235 from previous studies [5]. S stands for strong, m stands for medium, VS stands for very strong and W stands for weak. As shown in Fig. 4(b), the stretching vibrations of C=O, C—O and C—H in terephthalic acid are responsible for the adsorption maxima at 1597 cm^{-1} , 1390 cm^{-1} and 750 cm^{-1} , respectively. In addition, the vibrational absorption peak of Fe—O—Fe at 554 cm^{-1} is representative of MOF-235 in its normal form. It can be concluded that the obtained MOF-235 has shown its unique crystalline structure, phase properties and the special features of its chemical composition and functional groups by controlling the synthesis process.

The surface areas of MOF-235 were determined using the nitrogen adsorption-desorption method. Table 4.1 shows the Brunauer-Emmett-Teller (BET) surface area as well as the pore diameter and pore volume of MOF-235. It is noteworthy that the surface area in this study ($10.95 \text{ m}^2 \cdot \text{g}^{-1}$) is very low. This could be due to the high purity of MOF-235 in this study, as the adsorption capacity for MO is significantly influenced by the purity of MOF-235. Often synthesised MOF-235 is impure and may contain both MOF-235 and MIL-101. Previous studies have shown that higher amounts of MOF-235 lead to a lower surface area, while the presence of MIL-101 can increase it [157]. However, the smaller pore diameter of MIL-101 (2.63 nm) leads to a poorer methyl orange adsorption capacity ($q_e=232.55 \text{ mg} \cdot \text{g}^{-1}$) [159], which explains why MOF-235 with larger surface areas showed a lower methyl orange adsorption capacity in previous studies [160]. In contrast, the MOF-235 from this study has a higher purity, as indicated by its low BET surface area.

MOF 235 has pores with a diameter of 9.9 nm, which indicates that the material is mesoporous and has a good permeation capacity for adsorption. Since the molecular size of methyl orange is 2.6 nm [153], the mesoporous MOF-235 prepared in this study is suitable for use as an adsorbent for methyl orange and is expected to have a high adsorption capacity. In summary, the MOF-235 prepared by a controlled synthesis process exhibits remarkable

uniformity of particle size and pore distribution, which is favourable for the adsorption of methyl orange.

Table 4.1 Comparison of textural properties of MOF-235 prepared in this and other studies.

MOF	Synthesis Method	BET surface area ($\text{m}^2 \cdot \text{g}^{-1}$)	Average pore volume ($\text{cm}^3 \cdot \text{g}^{-1}$)	Average pore diameter (nm)	Ref.
MOF-235	Controlled synthesis	10.95	0.027	9.9	This study
MOF-235	Solvothermal method	190	0.125	2.64	[160]
MOF-235	Microwave-assisted method	148	0.075	-	[150]

4.6.2. Adsorption of the Dye

4.6.2.1. Effect of pH Value

The influence of the initial pH value on the adsorption performance of MOF-235 was investigated in a pH range from 3 to 11. Approximately 50 mL of methyl orange solution ($100 \text{ mg} \cdot \text{L}^{-1}$) was placed in a flask containing 0.02 g of adsorbent for 24 hours at a constant stirring speed of 150 rpm at $25 \pm 1 \text{ }^\circ\text{C}$. Either 0.1 M NaOH or 0.1 M HCl was used to adjust the pH of the solution. The adsorbent was separated from the solution by a centrifuge. In most cases, the pH of the solution played an important role in determining the adsorption of dyes [15]. Figure 4.5 shows that the adsorption efficiency of MOF-235 for methyl orange decreases from 95.78% to 88.88% in a pH range of 3.0 to 10.0. However, at a pH of 11.0, the adsorption rate decreased drastically to 22.77%. This indicates that the adsorption efficiency remains relatively stable between pH 3.0 and 10.0. Under acidic conditions, the increased positive charge density in the solution causes the surface of MOF-235 to become positively charged, which improves the adsorption of methyl orange. Conversely, as the pH increases, the concentration of OH^- increases, especially between pH 10 and 11, causing the surface of MOF-235 to become negatively charged, which significantly reduces the adsorption efficiency. The experimental data clearly show that MOF-235 exhibits optimal adsorption performance for methyl orange within an initial solution pH range of 3.0 to 10.0.

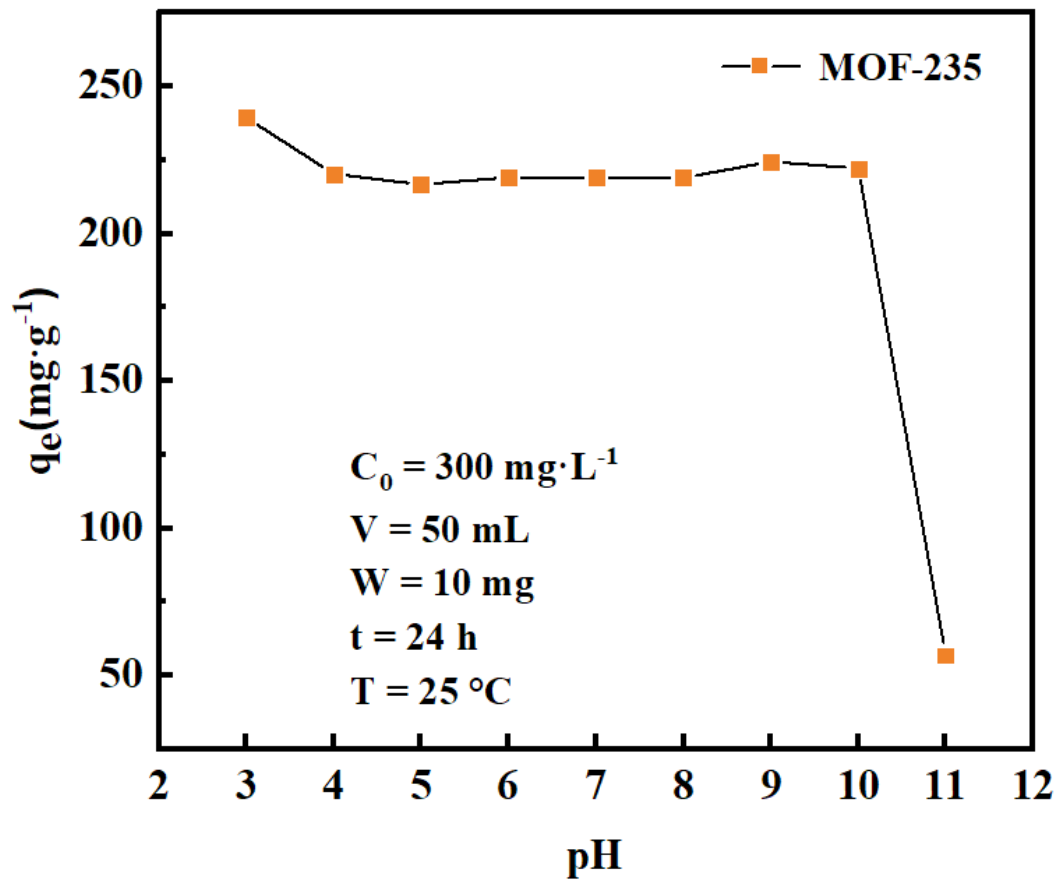


Figure 4.5 Influence of initial pH on adsorption (C_0 = initial concentration, V = solution volume, W = adsorbent mass, t = adsorption time, T = adsorption temperature).

4.6.2.2. Effect of Initial Concentration

Figure 4.6 illustrates the effect of the different initial methyl orange concentrations on the adsorption of methyl orange by MOF-235 at 15°C, 25°C and 35°C. The adsorption capacity increased with the initial methyl orange concentration from 20 to 800 mg·L⁻¹, which can be attributed to the higher driving force overcoming the mass transfer resistance at higher concentrations.

However, the capacity stagnated near 600 to 800 $\text{mg}\cdot\text{L}^{-1}$ as the active sites were saturated, indicating a limited number of active sites available for adsorption. Equilibrium is reached when all sites are occupied. At the same initial concentration of methyl orange, MOF-235 shows better adsorption at lower temperatures, indicating that the adsorption process is exothermic. This indicates that the adsorption of methyl orange by MOF-235 is primarily a physical adsorption process. This observation is consistent with other studies [5] [148].

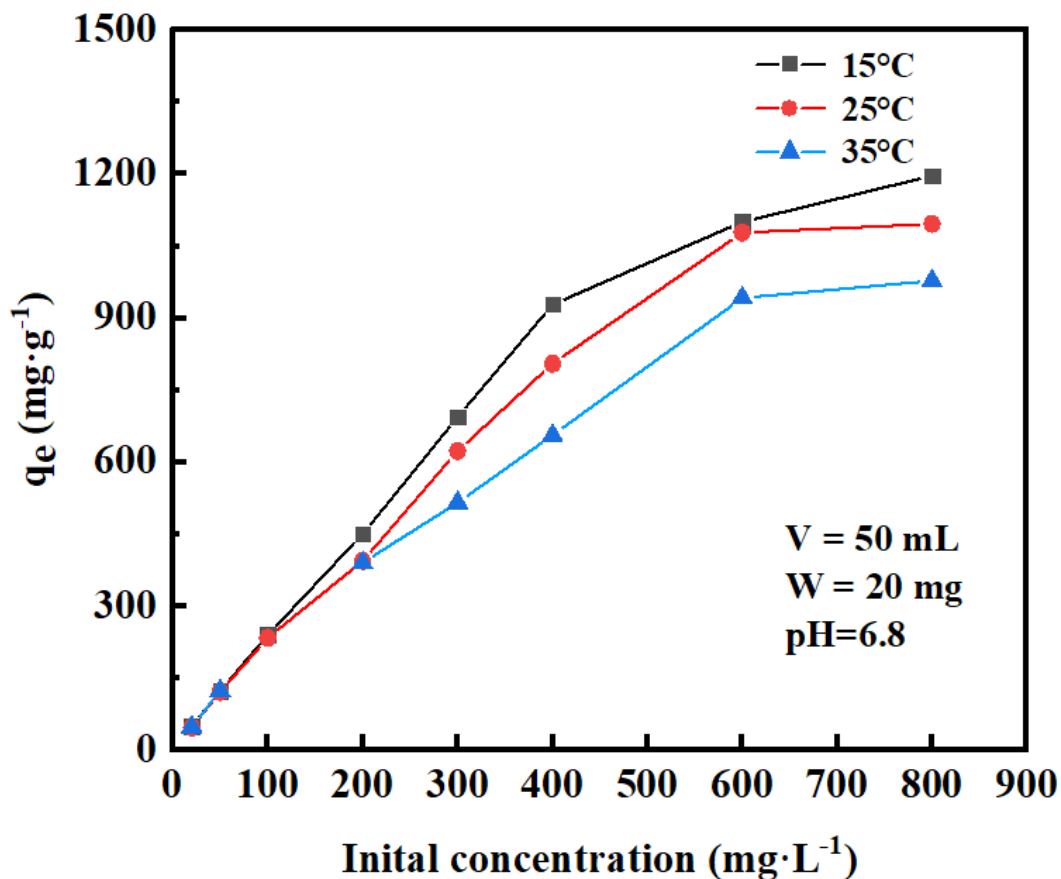


Figure 4.6 Influence of initial methyl orange concentration on adsorption ($V =$ solution volume, $W =$ adsorbent mass).

4.6.2.3. Adsorption Isotherms

The adsorption isotherms provide information about the surface properties, the adsorption processes and the efficiency of the adsorbent. In the experiments with the adsorption isotherms, the initial concentrations of methyl orange ranged from 20 to 800 mg·L⁻¹. In addition, the initial pH was set to 6.8 and the adsorption temperature was set to 3 different temperatures (15, 25 and 35°C). The Langmuir and Freundlich isotherm models are shown as follows:

$$\frac{C_e}{q_e} = \frac{1}{q_{max}K_L} + \frac{C_e}{q_{max}} \quad (10)$$

$$\ln q_e = \ln K_F + \frac{1}{n} \ln C_e \quad (11)$$

where C_e : equilibrium concentrations after adsorption (mg·L⁻¹), q_e : amount of methyl orange compounds adsorbed at equilibrium (mg·g⁻¹), q_{max} : the maximum adsorption capacity of the adsorbate (mg·g⁻¹), K_L : the Langmuir constant (L·mg⁻¹), K_F : the Freundlich constant and $1/n$: the heterogeneity factor.

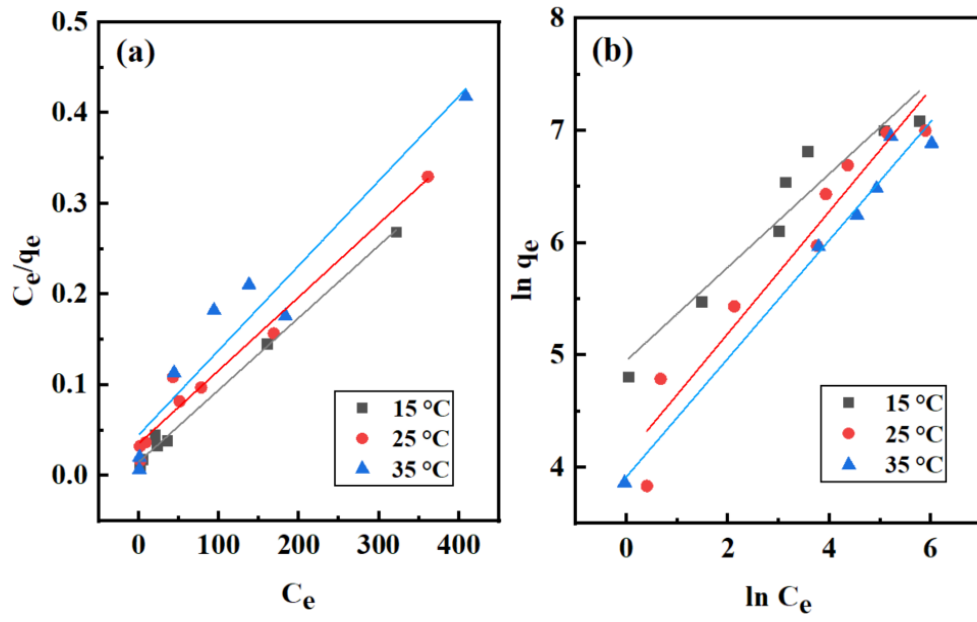


Figure 4.7 Langmuir and Freundlich models of methyl orange adsorption on MOF-235.

Table 4.2 Results of factors relevant to the methyl orange adsorption process at three distinct temperatures.

Adsorbent	Temperature (°C)	Langmuir model			Freundlich model			
		q_{\max} (mg·g ⁻¹)	K_L (L·mg ⁻¹)	R^2	K_F (mg·g ⁻¹) (L·mg ⁻¹) ^{1/n}	1/n	n	R^2
MOF-235	15	1257.7	0.053	0.995	102.6	0.495	2.020	0.913
	25	1237.1	0.023	0.969	60.7	0.544	1.837	0.935
	35	1071.2	0.021	0.927	80.8	0.432	2.316	0.918

The Langmuir isotherm model showed that MOF-235 reached a maximum adsorption capacity (q_{\max}) of $1257.7 \text{ mg}\cdot\text{g}^{-1}$ at 15°C , indicating a significant adsorption capacity. As the temperature increased to 25°C and 35°C , q_{\max} decreased to $1237.1 \text{ mg}\cdot\text{g}^{-1}$ and $1071.2 \text{ mg}\cdot\text{g}^{-1}$, respectively. This decrease in q_{\max} was accompanied by a decrease in the Langmuir constant (K_L), with values of $0.053 \text{ L}\cdot\text{mg}^{-1}$ at 15°C , $0.023 \text{ L}\cdot\text{mg}^{-1}$ at 25°C , and $0.021 \text{ L}\cdot\text{mg}^{-1}$ at 35°C . This trend indicates a decrease in adsorption affinity with increasing temperature. In general, a decrease in K_L with increasing temperature indicates that the adsorption process is exothermic, i.e. that the process releases heat as it occurs. This is consistent with previous studies on the adsorption of methyl orange on MOF-235 [5].

Further analysis of the variation of K_L with temperature may shed light on its physical significance. The decrease in K_L could be related to changes in the surface energy of MOF-235, in particular the deprotonation of the surface functional groups at higher temperatures. Such changes likely reduce the adsorption affinity of MOF-235, which is confirmed by the observed decrease in q_{\max} at higher temperatures. In addition, temperature increases could affect the pore structure and surface hydration of MOF-235. Higher temperatures can reduce surface hydration and thus weaken the interaction between the dye molecules and the adsorbent, further reducing the adsorption capacity. In addition, temperature can cause structural changes in MOF-235, such as changes in pore size distribution or surface functionality, which could also contribute to the observed decrease in adsorption capacity.

The results of this study show a significant improvement in q_{\max} compared to previous reports (see Table 4.3), indicating that the controlled synthesis method used in this study results in a more effective methyl orange adsorption capacity than the traditional solvothermal method. The controlled synthesis method, which involves more stirring, likely promotes more uniform dispersion of reactants, which improves the overall adsorption properties of MOF-235.

The adsorption of methyl orange on MOF-235 was also evaluated using Freundlich's isothermal model at 15°C, 25°C and 35°C. The Freundlich parameters derived were: $K_F = 102.6$ and $n = 2.020$ at 15°C; $K_F = 60.7$ and $n = 1.837$ at 25°C; and $K_F = 80.8$ and $n = 2.316$ at 35°C. The relative constancy of K_F over the temperature range indicates that the adsorption process remains strong between 15°C and 35°C, further supporting the presence of significant adsorption. The intensity parameter n , which remains above 1 at all temperatures, indicates a heterogeneous adsorption surface, suggesting that adsorption occurs at multiple sites on the MOF-235 surface. Changes in n with temperature likely reflect variations in the nature of surface interactions or the distribution of adsorption sites. Higher n values at higher temperatures (2.316 at 35°C) indicate a more favourable adsorption process under these conditions. The value of the regression coefficient (R^2) emphasises the effectiveness of the Langmuir isotherm model in describing adsorption, especially at lower temperatures. This indicates that the adsorption of methyl orange by MOF-235 occurs primarily by monolayer adsorption.

4.6.2.3. Comparison of Adsorption Capacity

Table 4.3 shows the adsorption capacities of the MOF-235 produced in this study compared to the data reported by other researchers. It can be seen that the MOF-235 used in this study has a methyl orange adsorption capacity of $1257.7 \text{ mg}\cdot\text{g}^{-1}$, which is much higher than that of other HOFs (hydrogen-bonded frameworks), COFs (covalent organic frameworks) and MOF materials when the synthesis and experimental conditions are carefully controlled. As described in the previous sections, the suitability of MOF-235 for methyl orange adsorption is enhanced by its larger pore diameter, which is why its adsorption capacity for methyl orange is much higher than that of other MOFs, as shown in Table 4.3. In this study, the controlled synthesis of MOF-235 further enhanced the advantage of pore diameter. This indicates that the controlled synthesis of MOF-235 is promising for use in wastewater treatment.

Table 4.3 Comparison of various adsorbents in methyl orange adsorption.

Adsorbents type	Adsorbents name	Pore diameter (nm)	q_{\max} ($\text{mg}\cdot\text{g}^{-1}$)	Source
HOFs (hydrogen-bonded frameworks)	PFC-1	\	252	[161]
COFs (covalent organic frameworks)	CCOF (cationic COF)	\	196.08	[162]
	ICOFs (Ionic covalent organic frameworks)	2.05	290	[163]
MOFs (metal organic frameworks)	MIL-101	1.6	114	[114]
	UiO-66	2.331	83.7	[164]
	MIL-100 (Fe)	2.9	211.8	[165]
	MOF-235	\	477	[5]
	MOF-235 by controlled synthesis technique	9.9	1257.7	This work

4.6.4. Adsorption Kinetics

The adsorption of methyl orange ($C_0 = 300 \text{ mg}\cdot\text{L}^{-1}$) on MOF-235 was performed for 30 minutes. Additionally, the initial pH was controlled at 6.8, with the adsorption temperature set at room temperature (25°C).

The quantity of adsorbate adsorbed q_t ($\text{mg}\cdot\text{g}^{-1}$) was determined by using the following model,

$$q_t = \frac{(C_0 - C_t)V}{W} \quad (12)$$

where q_t : the amount of methyl orange adsorbed at a given time ($\text{mg}\cdot\text{g}^{-1}$), C_t : the solution concentrations at the corresponding time ($\text{mg}\cdot\text{L}^{-1}$), V : the solution volume (L).

In this study, both pseudo-first-order and pseudo-second-order kinetic models were applied to study the adsorption of methyl orange on MOF-235 with an initial methyl orange concentration of $300 \text{ mg}\cdot\text{L}^{-1}$. The pseudo-first-order model can be expressed by the following linearized integral equation:

$$\log(q_e - q_t) = \log q_e - k_1 \frac{t}{2.303} \quad (13)$$

in which k_1 represents the adsorption rate constant (min^{-1}).

The pseudo-second-order kinetic model can be represented by the following linearized integral equation:

$$\frac{t}{q_t} = \frac{1}{k_2 \cdot q_e^2} + \frac{t}{q_e} \quad (14)$$

where k_2 represents the rate constant of the pseudo-second-order kinetic model.

Table 4.4 provides a comprehensive summary of the kinetic model parameters, while Figure 4.8. illustrates the plots for the pseudo-first-order and pseudo-second-order kinetic models, highlighting the respective rate constants (k_1 and k_2) along with their linear regression correlation coefficients (R^2). The pseudo-second-order model provides a very accurate representation of the adsorption process with an R^2 value of over 0.999. Furthermore, the theoretical equilibrium adsorption capacity (q_e) predicted by this model closely agrees with the experimentally observed q_{\max} values at different initial concentrations of methyl orange. These results indicate that the pseudo-second-order kinetic model describes the adsorption dynamics of methyl orange on MOF-235 better than the pseudo-first-order model.

Table 4.4 Parameters associated with the pseudo-first order and pseudo-second order models at a temperature of 25 ± 1 °C.

Adsorbent	Dye	C_0 ($\text{mg}\cdot\text{L}^{-1}$) ¹⁾	pseudo-first order model		pseudo-second order model	
			k_1	R^2	k_2	R^2
MOF-235	methyl orange	300	0.215	0.9859	0.000533	0.9998

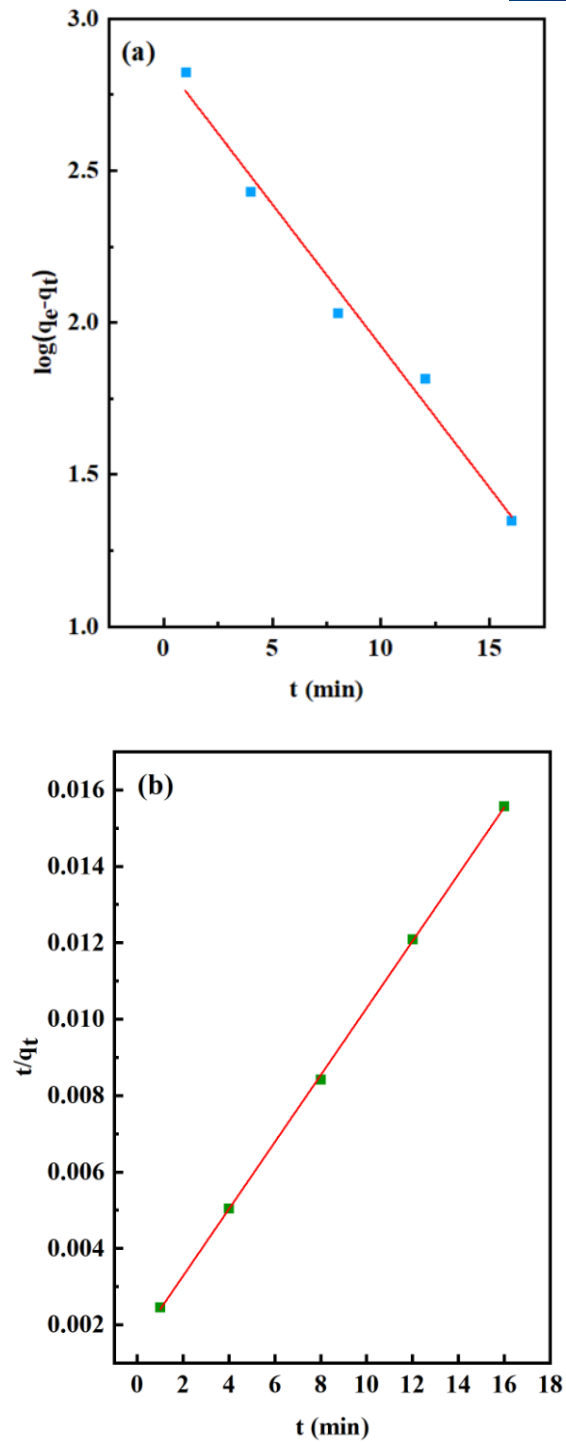


Figure 4.8 Results of the (a) pseudo-first-order and (b) pseudo-second-order kinetics models at a temperature of 25 ± 1 °C.

4.6.5. Mechanism Study

As shown in Figure 4.9, the sodium salt of the sulfonate in methyl orange converts to sulfonic acid in an acidic solution. Therefore, a 0.1 M NaOH solution is used during the LCMS tests to maintain a stable pH before and after adsorption. Figure 4.10 (a) shows the ESI mass spectra of the original methyl orange solution before adsorption, while Figure 4.10 (b) shows the ESI mass spectra after adsorption of methyl orange by MOF-235. The absence of intermediates after adsorption indicates that the methyl orange molecules are not catalytically degraded during the process. Previous studies have shown that the catalytic degradation of methyl orange leads to fragmentation of the molecule ($m/z = 304$) into smaller compounds, as evidenced by the occurrence of six intermediates with m/z values of 290, 217, 202, 113, 109, 97 and 59 [166]. The absence of such intermediates in this study indirectly confirms that MOF-235 adsorbs methyl orange by a physical adsorption mechanism without catalytic degradation of the dye molecule.

FTIR was used to analyse the methyl orange and its samples before and after adsorption on MOF-235 (Figure 4.11). The FTIR spectrum showed the presence of the azo group in methyl orange, with a characteristic peak at 1608 cm^{-1} for the $-\text{N}=\text{N}-$ bond, and the $-\text{C}-\text{N}$ vibrational peak at 1120 cm^{-1} . The ring vibrations of methyl orange were indicated by a peak at 1006 cm^{-1} . The peak at 816 cm^{-1} indicated the existence of a disubstituted benzene ring, confirming the aromatic nature of methyl orange [167]. These peaks were also seen in the FTIR spectrum of MOF-235 after adsorption, as shown in Fig. 9.

These results confirm that methyl orange was successfully adsorbed on MOF-235.

Physical adsorption was further confirmed by desorption experiments in which MOF-235 loaded with methyl orange was resuspended in deionised water, stirred and heated to 80°C, resulting in a distinct bright orange supernatant. The reason that physical adsorption is an exothermic process lies in the interactions between the adsorbent and the adsorbate. If the temperature of the solution increases, this naturally leads to a weakening of these van der Waals forces. This weakening effect in turn promotes desorption, which is further proof that the adsorption mechanism is indeed a physical one. At the same time, the high adsorption capacity of MOF-235 can also be mainly attributed to the electrostatic interactions, the conclusion of which can be linked to previous similar studies [5].

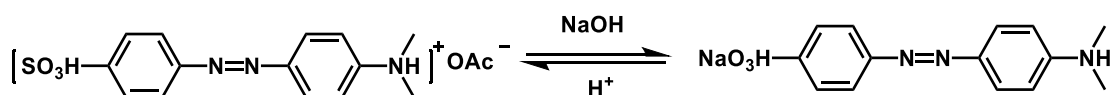


Figure 4.9 Interconversion of methyl orange under acidic and alkaline conditions.

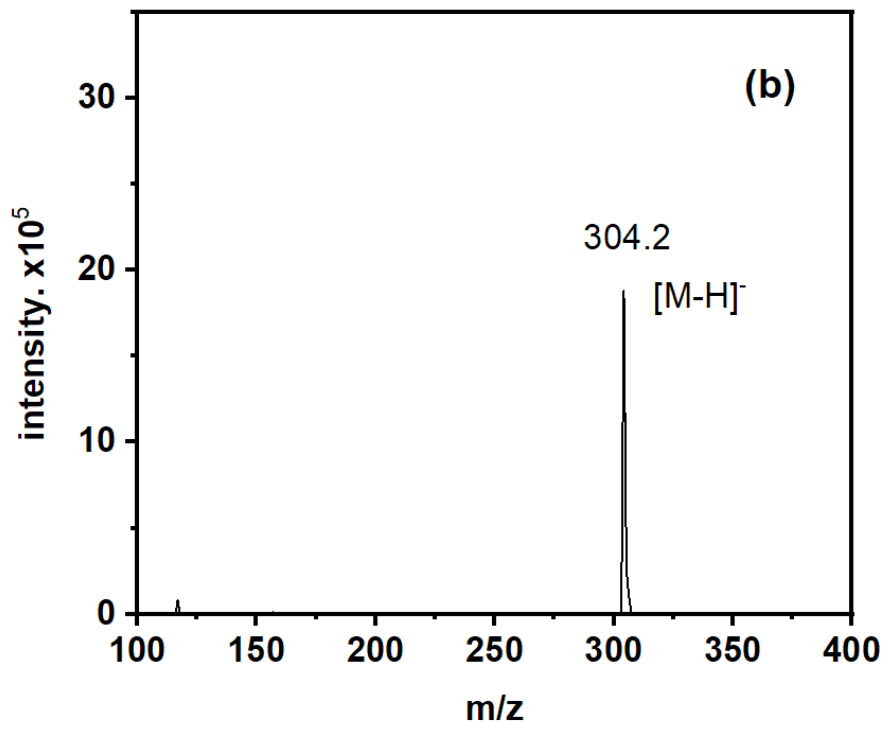
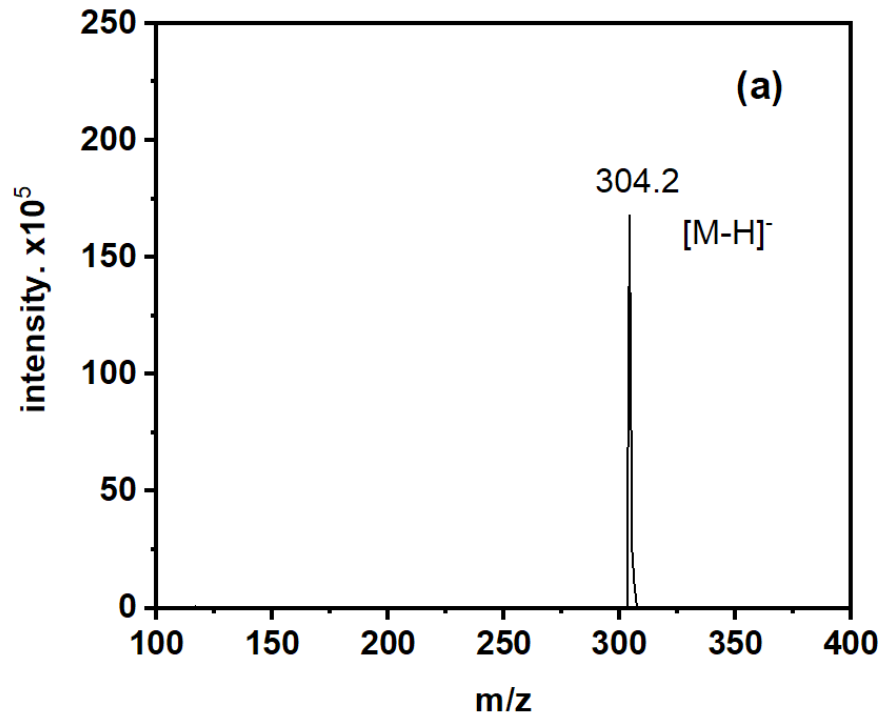


Figure 4.10 ESI mass spectra of methyl orange which (a) before adsorption and (b) after adsorption.

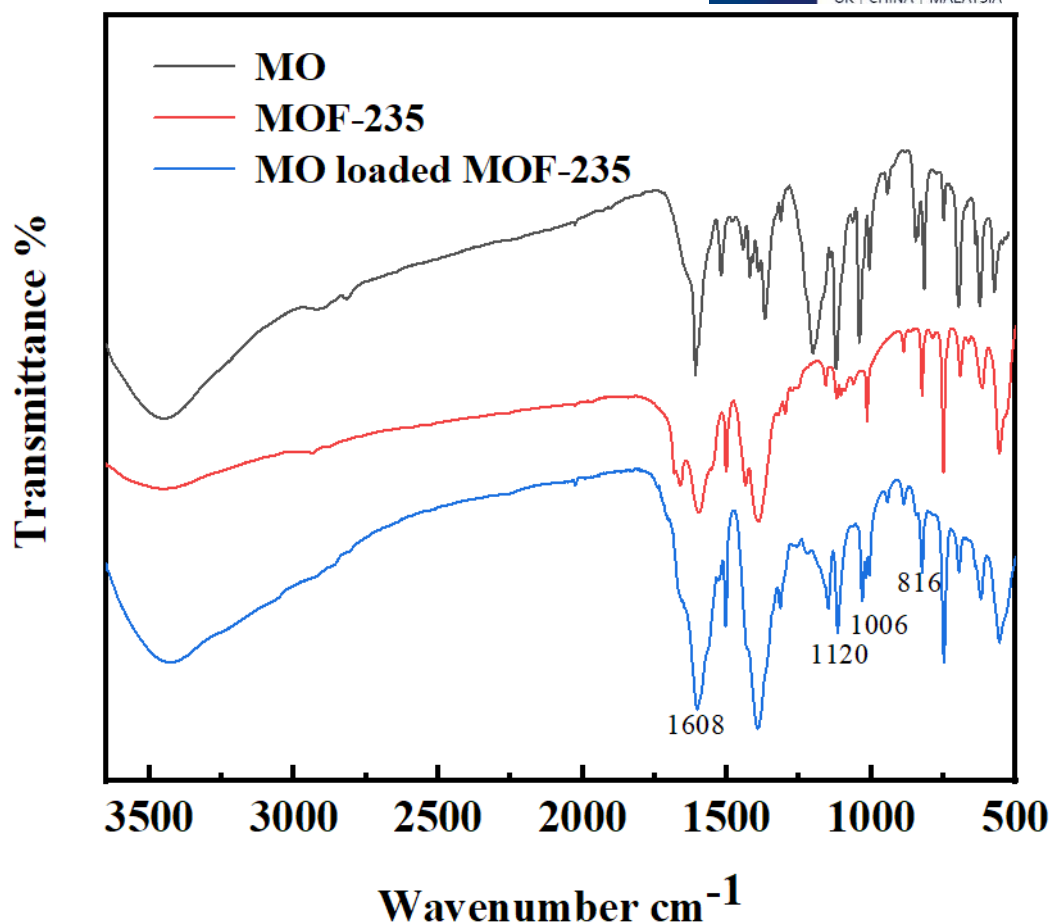


Figure 4.11 FTIR spectrum of methyl orange, MOF-235 and MOF-235 after absorbing methyl orange.

4.6.6. Regeneration Study

To evaluate the reusability of MOF-235, adsorption-desorption experiments were performed. In this study, regeneration of MOF-235 was achieved by ultrasonic treatment with ethanol solution until the solution became completely transparent. The regenerated MOF-235 was then dried at a temperature of 80 °C for 24 hours before the next regeneration cycle began. For each cycle, 5 mg of the regenerated MOF-235 was added to a methyl orange solution (50 mL) with a random concentration of 200 mg·L⁻¹ and adsorbed until equilibrium was reached, which took 24 hours. According to

the experimental results, MOF-235 retains about 80% of its methyl orange adsorption capacity even after four regeneration cycles. These results indicate that the controlled synthesis of MOF-235 not only leads to high adsorption capacity, but also lends itself to easy regeneration and subsequent use to remove methyl orange from the natural environment.

4.7. Conclusions

This chapter concluded with the successful development of a controlled synthesis technique for MOF-235, which is characterised by a uniform, narrow particle size distribution and significantly improved yield. Analytical studies confirmed that the adsorption of methyl orange by MOF-235 is predominantly physical. Significantly, MOF-235 exhibited an exceptionally high adsorption efficiency of $1257.7 \text{ mg}\cdot\text{g}^{-1}$, emphasising its remarkable ability. These favourable properties clearly demonstrate the potential of MOF-235 as an effective adsorbent in the treatment of wastewater contaminated with organic dyes and represent a significant advance in environmental remediation initiatives.

Chapter 5.

Porous Carbon Derived from MOF-235 for the Adsorption of Methyl Orange with High Capacity

5.1. Introduction

Organic dyes are commonly used in the industrial sectors, such as textile, paper, and dyeing [168]. It is reported that approximately 280,000 tons of textile dyes are discharged annually via industrial wastewater [169]. Methyl orange (MO) is an importance dye [170]. The discharge of MO into natural water bodies poses a substantial threat to human health and the ecosystem [171, 172]. The adsorption method has so far attracted significant attention due to its exceptional efficiency, cost-effectiveness, and adaptability; rendering it an exemplary solution for addressing MO pollution [48, 168, 173]. However, the development of cost-effective adsorbents for the remediation of dye-containing wastewater is still a challenge.

Metal-organic frameworks (MOFs) are known for their high porosity, large surface area, and versatile functionalities, which make them highly suitable as precursors for the synthesis of metal-carbon materials by a direct pyrolysis method [122]. To date, MOF-235 has been extensively investigated as a precursor for the synthesis of porous carbon materials due to its favourable adsorption sites and ideal pore configuration [5]. However, the utilization of MOF-derived carbon (MDC), obtained from MOF-235 as a precursor, in dye adsorption, especially for the adsorption of MO, remains unexplored.

Recent studies have emphasised the crucial role of the specific surface area in the adsorption of dyes [174]. While MOF-235 has good adsorption performance for MO [5], its specific surface area is typically only 10-20 m²·g⁻¹ [5, 175]. In addition, previous research has shown that adsorbents with larger pore sizes can improve adsorption capacity for dyes even with similar specific surface area [176]. Therefore, increasing the specific surface area and pore size of MOF-235 by carbonisation treatment is expected to increase its adsorption capacity for MO.

In previous studies, the adsorption of MO by MOF-235 can be described by pseudo-second-order kinetic model (k_2) with a rate constant of 0.0009 g·mg⁻¹·min⁻¹ [5]. In addition, different types of carbon from MOFs have been investigated on their potential in the adsorption of contaminants in wastewater. For instance, previous research has shown that N-NC-800, a nitrogen-doped nanoporous carbon synthesised by the direct carbonisation of an amino-functionalised aluminium terephthalate MOF, was employed to adsorb MO, showing a maximum adsorption capacity of 222.22 mg·g⁻¹ with $k_2 = 0.0081$ g·mg⁻¹·min⁻¹ [177]. However, the common issue of these research is that the adsorbents showed lower adsorption capacities and slow adsorption rates for the adsorption of MO. Thus, it is important to develop new adsorbents that possess high capacity and fast adsorption rates for MO.

At the same time, previous MOF materials show limitations in regeneration and poor structural stability after adsorption of azo dyes. For example, Fe(BTC) retains about 85% efficiency for Orange II after four cycles [152], and Fe₃O₄/Cu₃(BTC)₂ retains about 90% for MB after five cycles [178]. This

shows the necessity of developing adsorbents with high adsorption capacity for azo dyes and excellent structural stability.

This study aims to use MOF-235 as the precursor for the preparation of a porous carbon adsorbent for the removal of MO from wastewater. The structural and physicochemical properties of the porous carbon material were characterised. Detailed investigations were carried out on various parameters such as pH value, initial dye concentration, operating temperature and adsorbent dosage. In order to study the maximum theoretical adsorption capacity, adsorption rate, and adsorption mechanism, the adsorption isotherms and kinetics were analysed. Finally, the cyclic adsorption and desorption test of Fe@C-350 was investigated.

5.2. Chemicals

Iron chloride hexahydrate ($\text{FeCl}_3 \cdot 6\text{H}_2\text{O}$), N,N-Dimethylformamide (DMF, 99%), Ethanol (99%), p-Phthalic acid (TPA, 99%) were purchased from Aladdin Chemical reagent Co. (Shanghai, China). All chemicals used in this study were used without further purification.

5.3. Synthesis

5.3.1. Preparation of MOF-235

To synthesize MOF-235, 0.6 g TPA and 0.6 g $\text{FeCl}_3 \cdot 6\text{H}_2\text{O}$ were first dissolved in 180 mL DMF and sonicated for one hour. Then, 60 mL of ethanol was added to the above-mentioned 180 ml of the reaction solution and the mixture 240 ml of solution was placed in an apparatus with an oil bath and magnetic stirring before being heated at a temperature of 353 K for

24 hours. After the orange powder was dried with a freeze dryer, it was washed with a mixed solution of DMF and ethanol (Fig. 5.2).

5.3.2. Carbonisation Procedures

MOF-235 was carbonised in a tube furnace and heated to different temperatures for 1 hour, with a heating rate of $2\text{ }^{\circ}\text{C}\cdot\text{min}^{-1}$ in an argon atmosphere. All samples are heated from room temperature. The adsorbent prepared after carbonisation was designated as Fe@C-x (x = carbonisation temperature).

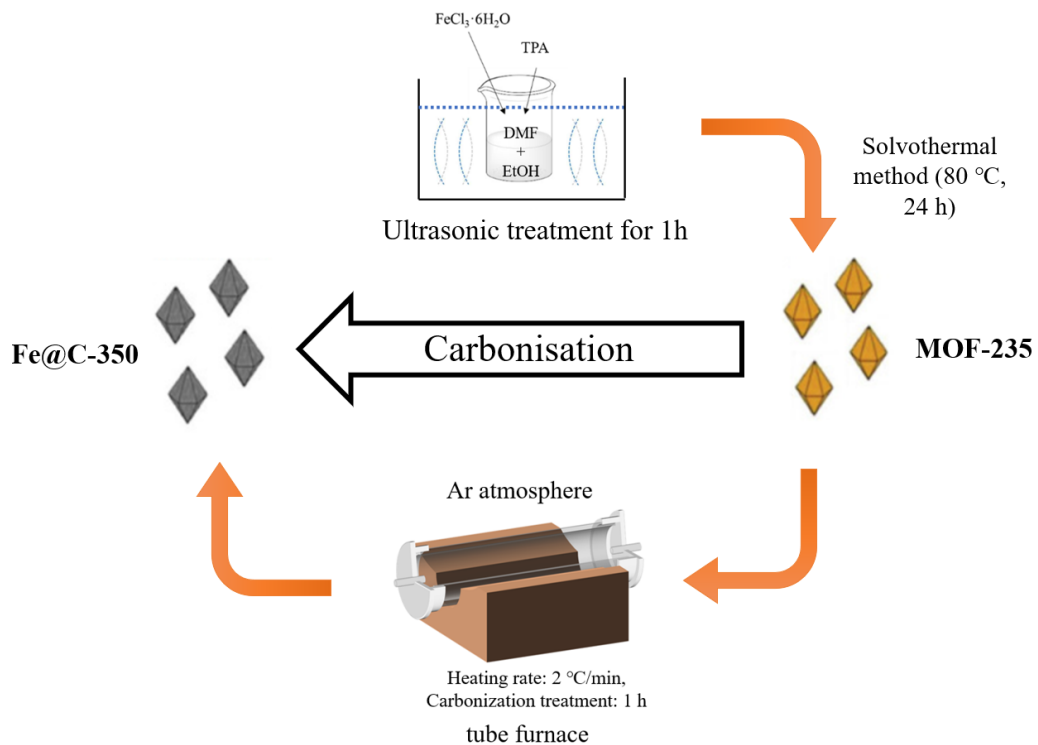


Figure 5.1 Synthesis process of MOF-235 and carbonised Fe@C-350.

5.4. Characterization

To explore alterations in the functional groups of the adsorbents, Fourier Transform Infrared Spectroscopy (FT-IR, Nicolet iS50 FT-IR, Thermo Fisher

Scientific, USA) was utilized, covering a wavenumber range from 4000 to 400 cm^{-1} . The morphology of the materials was examined using Scanning Electron Microscopy (SEM, Regulus 8100, Hitachi, Japan). Additionally, the crystal structure of the adsorbents was characterized using an X-ray Diffractometer (XRD) (Smart Lab (3 KW), Rigaku, Japan). The XRD patterns were then identified using the 2θ range from 5° to 40° (40 kV, 30 mA, scan step = 0.02°). The textural properties of the adsorbents, such as pore volume and pore size Brunauer-Emmett-Teller (BET, 3 Flex America Micromeritics) surface analysis of the synthesized adsorbents were measured by the nitrogen adsorption/desorption method with temperature of 77 K. Thermogravimetric analyses (TGA) of the prepared particles were performed by heating the samples in an inert gas atmosphere ($50 \text{ ml} \cdot \text{min}^{-1}$) at a rate of $2 \text{ K} \cdot \text{min}^{-1}$, ranging from 30°C to 500°C , utilising a TGA instrument (3+ Switzerland Mettler Toledo) to determine the mass loss of the samples.

5.5. Adsorption

The adsorption of methyl orange by MOF-235 and its derivative porous carbon containing adsorbents was investigated by using UV-vis spectrophotometry and batch experiments. Prior to testing, all adsorbents were dried overnight at 80°C under vacuum and stored in a desiccator. Detailed studies were conducted on the effects of initial dye concentration, contact time, solution pH value, and operating temperature on methyl orange uptake. The mixtures of adsorbent and adsorbate were stirred for 60 minutes using an automatic thermostatic shaker. Subsequently, the dye concentration was measured using UV-vis at a wavelength of 465 nm.

5.5.1. Initial Concentration Effect

To find out how the initial concentration of the dye affects adsorption, nine 100 mL amber bottles were prepared in this study, each containing 50 mL of a solution with methyl orange concentrations between 50 and 1000 mg·L⁻¹. For each of these solutions, 30 mg of a single adsorbent was added to the corresponding bottle. The bottles were then placed in a shaking incubator at room temperature (25 °C) and shaken at 150 rpm for 24 hours. The concentrations of methyl orange after adsorption were determined using UV-vis spectroscopy at a wavelength of 465 nm. The amounts of methyl orange adsorbed onto Fe@C-350 were calculated using the equation (9).

5.5.2. Adsorption Isotherm

In the adsorption isotherm tests, 50 mL volumes of methyl orange solutions with concentrations between 50 and 1000 mg·L⁻¹ were utilised. 10 mg Fe@C-350 adsorbent was added and the samples were shaken in the dark. Adsorption was carried out at 15, 25 and 35 °C for 24 hours at 150 rpm. In general, the models of Langmuir and Freundlich describe the basic principles of adsorption, which takes place in single or multiple layers. The Langmuir model shows how molecules attach to solid surfaces. It is characterised by the fact that it focuses on adsorption at uniform sites on a single layer and excludes the possibility of adding further layers. Normally, Langmuir's isothermal model is illustrated by the equation (10), and the Freundlich constants K_F and n were determined by linear regression of the logarithmically transformed data, using the logarithmic form of the equation (11).

In this study, Freundlich constant K_F , the intensity parameter n and the correlation coefficient R^2 together were determined. The K_F value indicates the adsorption capacity and serves as a benchmark for different adsorbents or different conditions within the same adsorbent. At the same time, the parameter n provides information about the type of adsorption, with $n = 1$ indicating linear behaviour and $n < 1$ revealing cooperative adsorption, and $n > 1$ reflecting typical Langmuir behaviour. In addition, a high R^2 value suggests that the Freundlich model is well fitted to the experimental data, which emphasises its relevance for the system under investigation.

5.5.3. Adsorption Kinetics

Kinetic adsorption experiments involving Fe@C-350 were performed on an methyl orange solution with an initial concentration of $200 \text{ mg}\cdot\text{L}^{-1}$, and the adsorption time was from 1 to 720 minutes. Only non-equilibrium adsorption data were used in the kinetic analysis. Two kinetic models were evaluated: the pseudo-first-order model and the pseudo-second-order model. The pseudo-first-order model suggests that the rate of occupation of the adsorption sites is directly proportional to the number of available sites. This is described by the equation (13). Conversely, the pseudo-second-order model is founded on the principle that valence forces, which enable electron exchange or sharing between the methyl orange and iron based adsorbent, control the adsorption rate. It is described by the equation (14).

5.5.4. Effect of the pH

In this study, the pH of the dye solution was adjusted and stabilised with 1 M HCl and NaOH solutions. The effect of pH was analysed at values of 3 to 11. To ensure a constant adsorption time of 24 hours, each 50 mL of MO solution (initial concentration of $300 \text{ mg}\cdot\text{L}^{-1}$) was treated with 30 mg of adsorbent. Before the UV-Vis test was performed with the solution after adsorption, the pH was adjusted to neutral or slightly alkaline to ensure that the maximum absorbance peak at 465 nm was maintained.

5.5.5. Effect of the Adsorbent Dosage

In this study, the dosage was set between $0.2 \text{ g}\cdot\text{L}^{-1}$ and $1.0 \text{ g}\cdot\text{L}^{-1}$ to evaluate the effects of adsorbent dosage on adsorption. The adsorption experiments were performed at a constant temperature of 25°C and an adsorption time of 24 hours. For each experiment, 50 mL of the MO solution with an initial concentration of $200 \text{ mg}\cdot\text{L}^{-1}$ was used.

5.6. Adsorption and Desorption Cyclic Test

During the cyclic adsorption-desorption tests, a mixture is formed by adding 30 mg Fe@C-350 adsorbent to 100 mL of a $100 \text{ mg}\cdot\text{L}^{-1}$ MO solution at a pH of 6.8.

In the first adsorption-desorption process, the mixture is maintained at 25°C for 1 hour to allow adsorption to complete. A small portion of the solution is tested using UV-vis to determine the adsorption capacity. The mixture is then

heated to 60°C for 1 hour to achieve the thermal desorption of MO. This completes the first regeneration cycle.

In the second adsorption-desorption process, the mixture obtained after the first adsorption-desorption process is then cooled naturally to 25°C and stirred for 1 hour so that the MO can be adsorbed again. A small portion of the solution is taken for the UV-vis test to verify the adsorption capacity of the second adsorption-desorption process. This adsorption-desorption process is repeated for a total of 10 desorption-adsorption cycles.

5.7. Results and Discussion

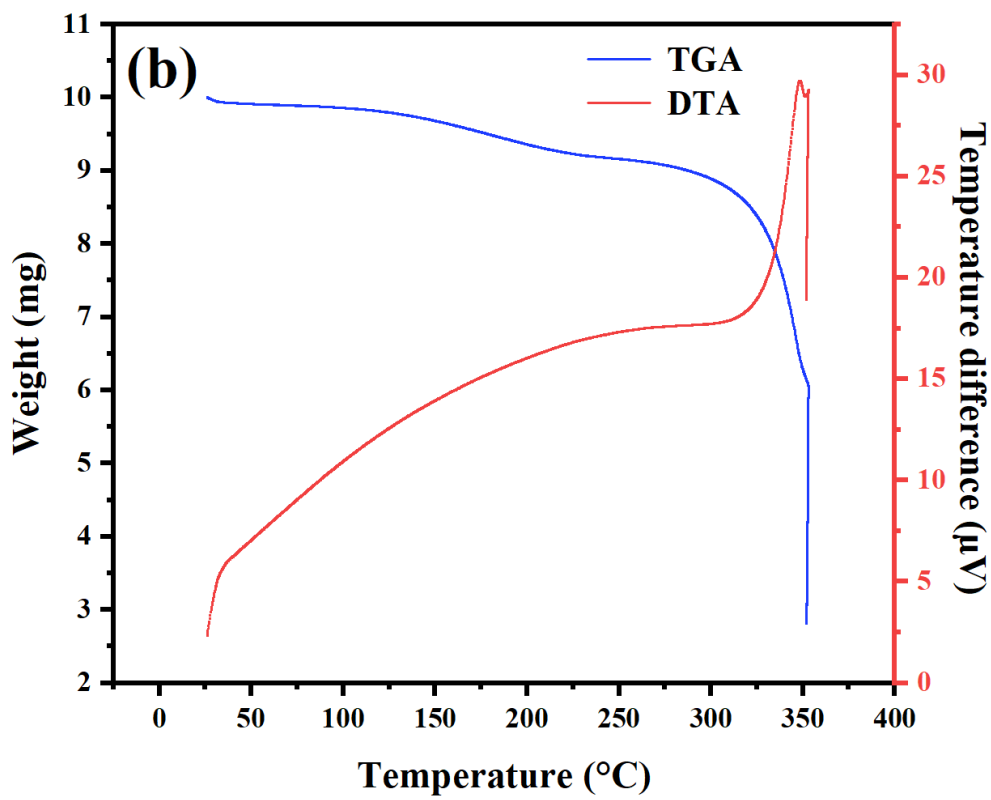
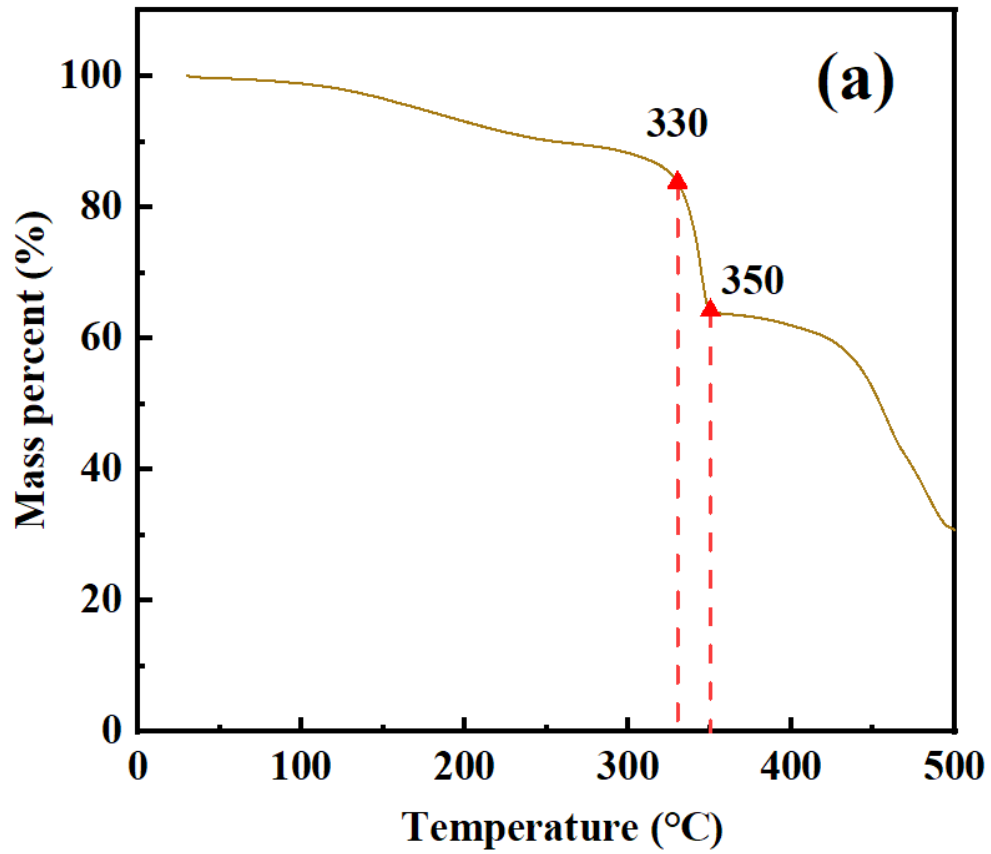
5.7.1. Carbonisation Condition

The thermal degradation of MOF-235 is shown in Figure 5.2 (a). The initial mass loss upon heating started at 100°C, which is probably due to the vaporisation of moisture trapped in the MOF structure. The subsequent degradation takes place between 330°C and 350°C, indicating the decomposition of the hydroxyl groups [179]. Differential thermal analysis (DTA) (Figure 5.2 (b)) shows a slow increase in the DTA curve in the temperature range of 25-310°C, indicating the removal of moisture or other volatile substances (such as solvent molecules in the ligands). The main structure of the material remains stable, with no significant chemical changes or phase transitions observed. Between 310 and 350°C, the Fe atoms in the MOF-235 precursor are oxidized, resulting in an exothermic reaction. Another series of TGA tests were performed to evaluate the structural stability of Fe@C-350 at 350°C (Figure 5.3). The sample is heated from room

temperature to 350°C at a rate of 2°C·min⁻¹ and then held at 350°C for 1 hour.

A noticeable mass reduction occurred when carbonisation stagnated at 350°C for 10 minutes, attributed to the rapid thermal decomposition of the oxygen-containing groups in the organic ligands of TPA and DMF within MOF-235 [180]. A steady mass loss was observed during prolonged carbonisation at a constant 350°C, indicating an incomplete carbonisation process and an evolving structural change. Figure 5.2 (c) shows the methyl orange adsorption capacities at these temperatures, which shows an increase with the porous carbon obtained at treatment temperature between 350 and 500°C. This result is consistent with the TGA results and SEM images (Figure 5.6 and Figure 5.4). It is obvious that a larger surface area and roughness are observed between 350 to 450°C, which favours the adsorption of methyl orange.

The adsorption capacity did not change within the carbonisation temperature range of 350°C to 450°C. Within this temperature, further carbonisation began probably due to the decomposition of TPA, loss of chlorine, decomposition of aromatic rings and further fracturing of the MOF framework [180]. Above 500°C, the adsorption effect decreased significantly due to overpyrolysis, which led to the collapse of the structure. SEM images show the morphological changes at different temperatures. Considering the balance between performance and energy consumption, 350°C was considered as a suitable carbonisation temperature, which offers similar adsorption performance with lower energy consumption for carbonisation. Therefore, Fe@C-350 was selected as the adsorbent for the following experiments.



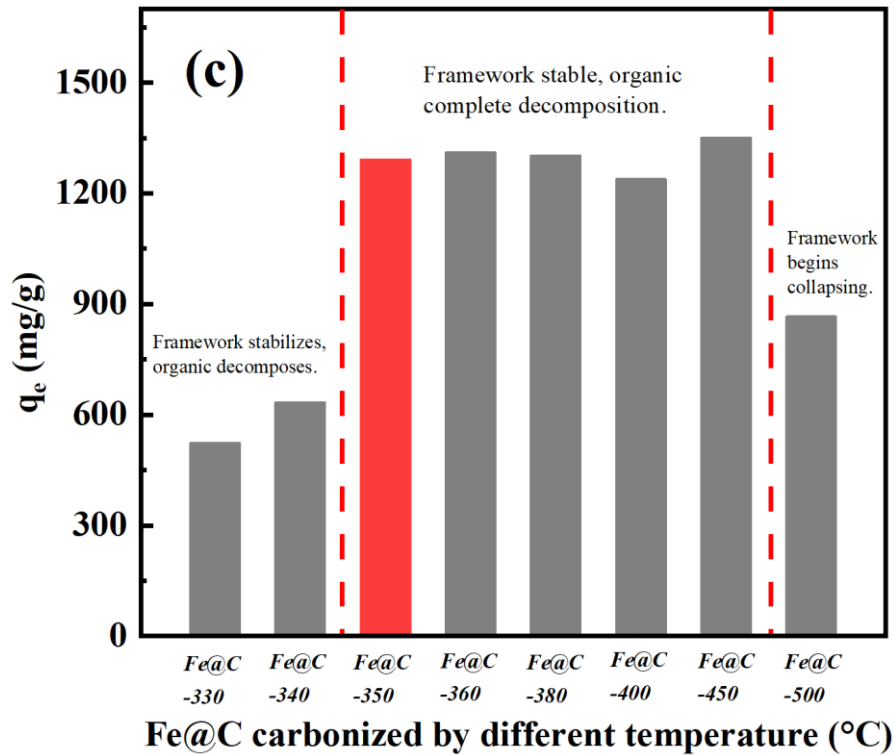


Figure 5.2 (a) TG result (40~500 °C) of MOF-235 (b) Thermogravimetric-differential thermal analysis (TGA-DTA) curves of the Fe@C-350 in the range between room temperature (25 °C) and 350 °C and (c) MO adsorption capacities for MOF-235 carbonised at 330 to 500 °C.

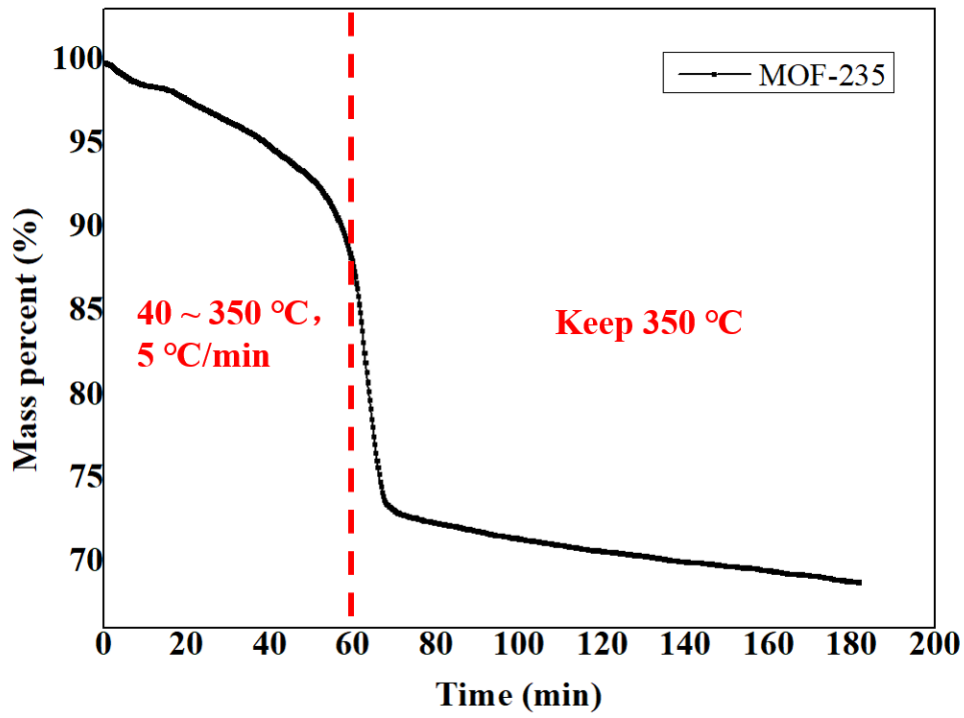
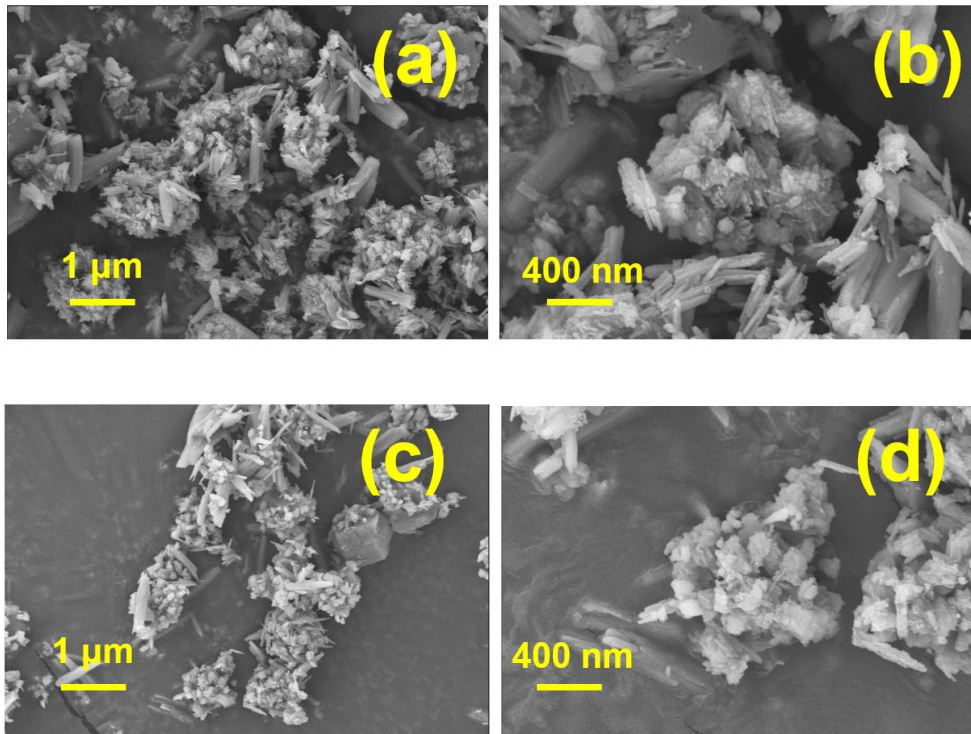


Figure 5.3 TG results (40~350 °C, keep 350 °C for 1 h) of MOF-235.



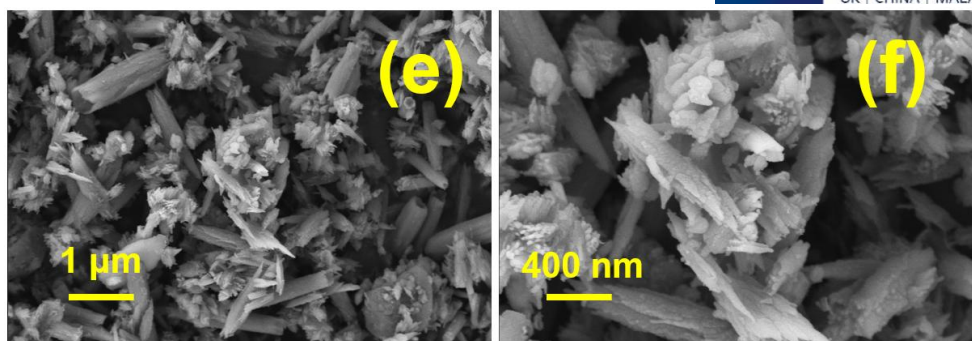


Figure 5.4 The SEM images of as-prepared (a) and (b) Fe@C-360, (c) and (d) Fe@C-380, (e) and (f) Fe@C-400.

5.7.2. Characterisation

XRD analysis of MOF-235 and its carbonised derivative, Fe@C-350, was performed in a 2θ range from 5 to 40° . Figure 5.5 shows the XRD patterns of the synthesised materials. The analysis shows that maghemite predominates in Fe@C-350, which is consistent with previous findings on iron-based carbon materials [181]. It is noteworthy that the characteristic diffraction peaks of the original MOF-235 structure are weakened in the Fe@C-350 pattern, indicating a transformation due to the thermal degradation of the organic ligands and the formation of Fe_2O_3 . This is confirmed by the peak at $2\theta = 30.2^\circ$, which is consistent with JCPDS No. 39-1346. Despite the possible spectral overlap between Fe_2O_3 and Fe_3O_4 in the XRD analysis, Fe_2O_3 is confirmed in the literature as the primary phase in carbonised MOF-235 [181]. Given the carbonisation parameters used here, which are consistent with those of previous studies, Fe_2O_3 is the predominant component in Fe@C-350.

The morphological properties of MOF-235, which was carbonised at temperatures of 330 to 400°C , were analysed using SEM. Figure 5.6 shows that Fe@C-330, Fe@C-340 and Fe@C-350 preserve the essential structure of

MOF-235. Carbonisation leads to a transformation of the originally uniform and flat surface of the MOFs into a more porous and fissured state. The SEM images in Figure 5.5 (a) and (b) indicate the onset of pyrolysis at 330°C, where Fe@C-330 exhibits a sparse pore distribution while the integrity of the metallic framework is preserved. At 340°C, Figure 5.5 (c) and (d) show an increase in porosity in Fe@C-340, confirming the thermogravimetric data. At 350°C, the complete pyrolysis of the organics is evident in Figure 5.5 (e) and (f), resulting in Fe@C-350 with improved surface layering and complexity, which is favourable for adsorption without affecting the structure of the MOF. The optimum carbonisation temperature for methyl orange adsorption capacity derived from SEM observations and thermogravimetric analysis is 350°C. Increasing the carbonisation temperature from 360°C to 400°C leads to further structural degradation of the material, as shown by the decomposition of the OH and Cl groups and the terephthalic acid ligands, as shown in Fig. S3. These results demonstrate the morphological robustness and superiority of Fe@C-350, which will be the focus of subsequent adsorption studies in this research.

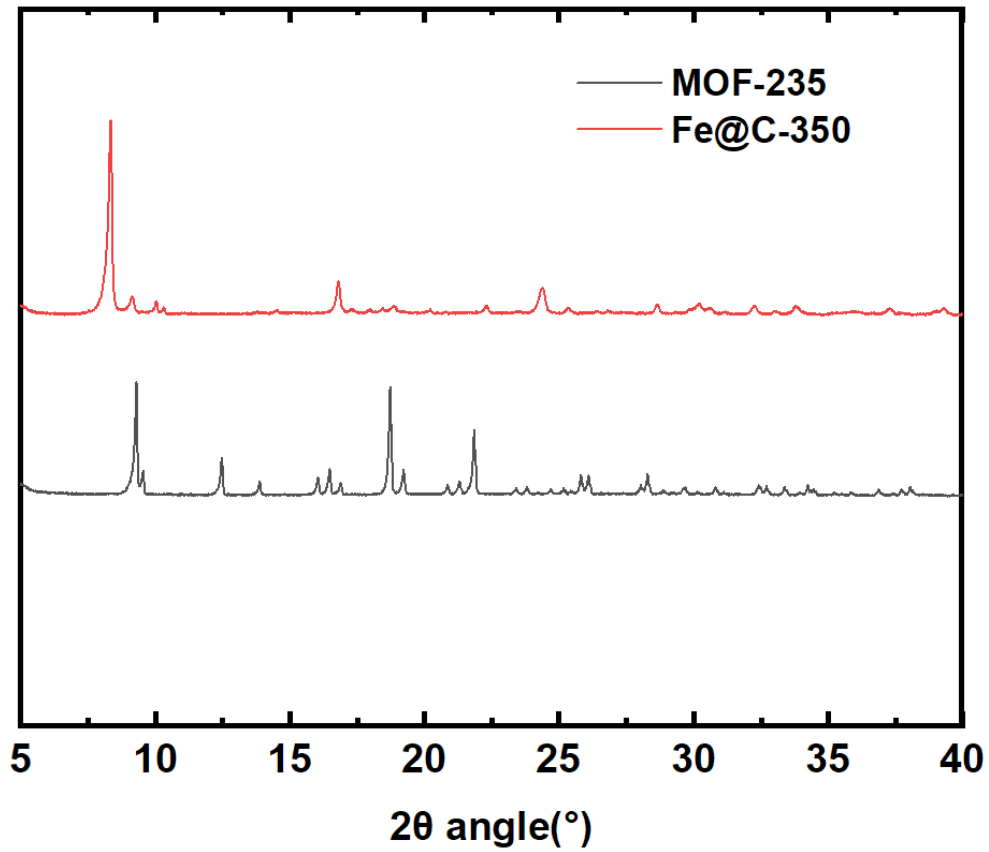
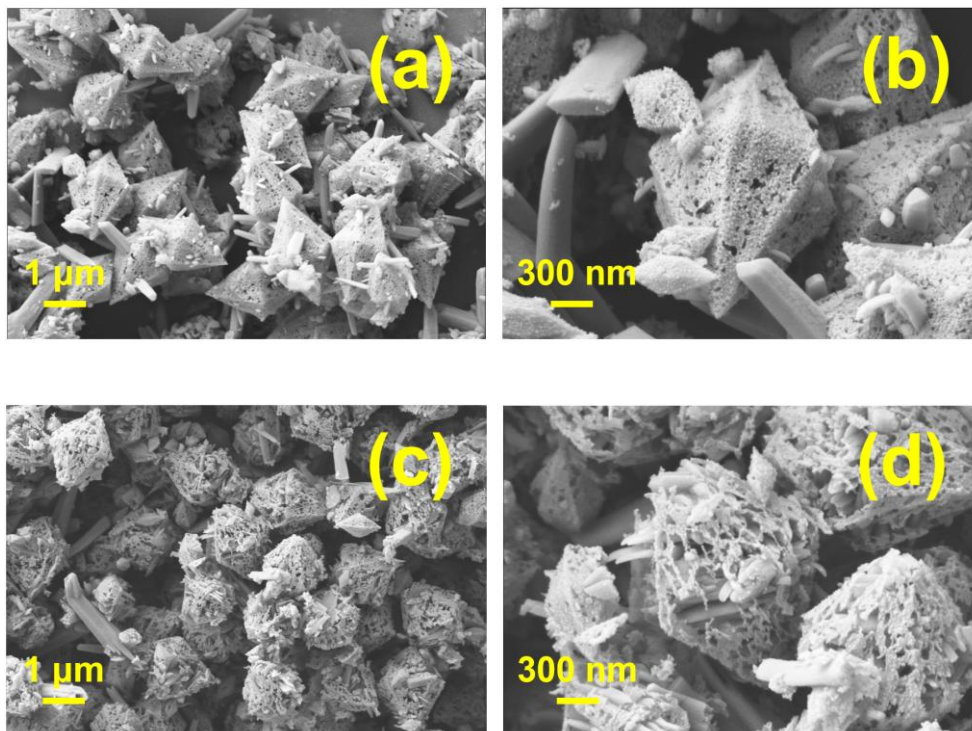


Figure 5.5 The XRD spectrum of as-prepared MOF-235 and Fe@C-350.



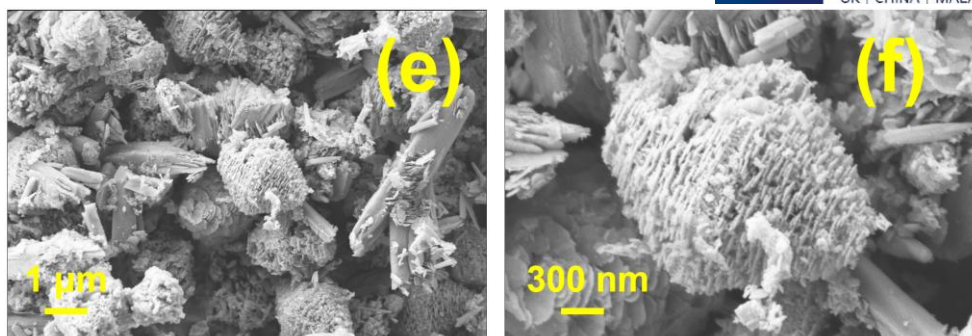


Figure 5.6 The SEM images of as-prepared (a) and (b) Fe@C-330, (c) and (d) Fe@C-340, (e) and (f) Fe@C-350.

As shown in Figure 5.7, the nitrogen adsorption-desorption isotherms of Fe@C-350 display type IV behaviour with H3 hysteresis loops, suggesting a mesoporous structure with slit-like pores. BET results, detailed in Table 5.1, show that Fe@C-350 has a specific surface area of $30.16 \text{ m}^2 \cdot \text{g}^{-1}$, a pore volume of $0.088 \text{ cm}^3 \cdot \text{g}^{-1}$ and an average pore size of 12.5 nm, which are more favourable for adsorption than those of MOF-235. Considering the effective diameter of methyl orange, which is estimated to be 6-8 nm [182], the 12.5 nm pores of Fe@C-350 correspond well to the recommended 1.7 to 3 times molecular size for optimal adsorption [183] and provide efficient dye interaction and mass transport channels. In comparison, the finer pores of activated carbon, despite their high surface area ($1362 \text{ m}^2 \cdot \text{g}^{-1}$), do not match the molecular size of methyl orange, resulting in sub-optimal adsorption as shown in previous studies [49]. This discrepancy emphasises how important not only the surface area but also the correct pore size is for adsorption efficiency. The customised pore size of Fe@C-350 is therefore characterised by superior performance in the adsorption of methyl orange, surpassing that

of activated carbon.

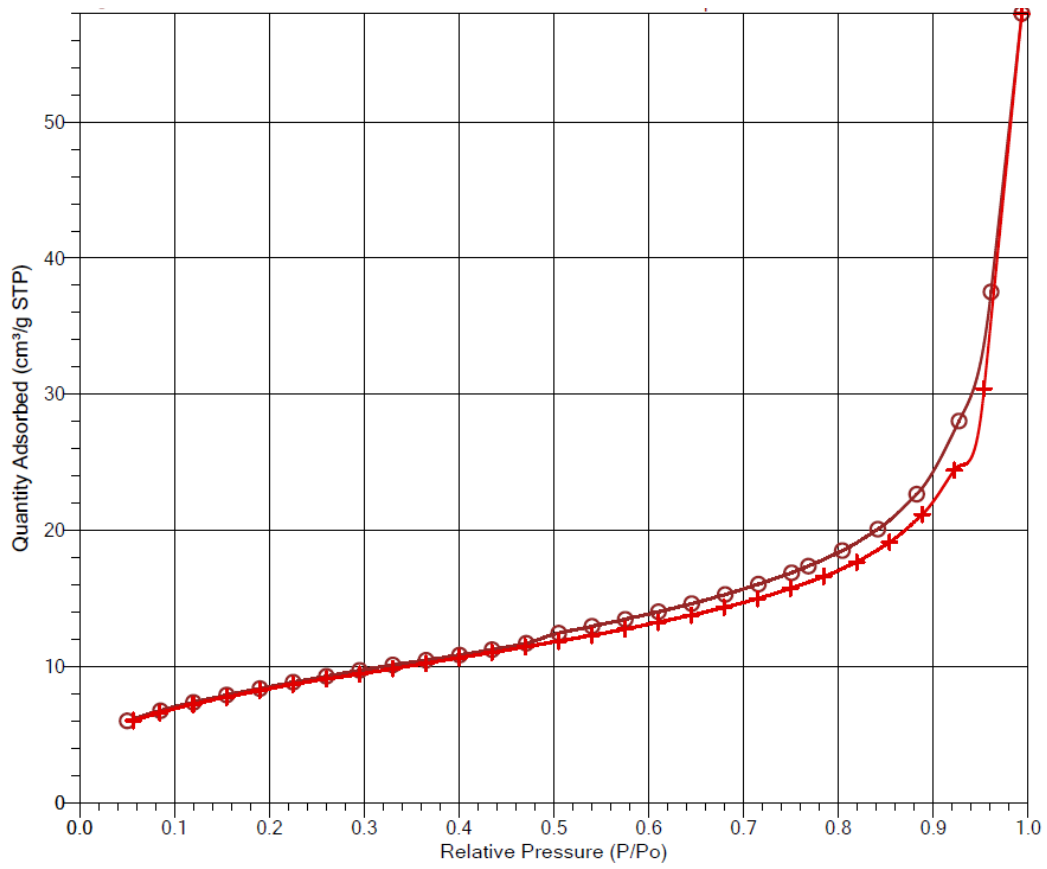


Figure 5.7 The nitrogen adsorption-desorption isotherm for Fe@C-350.

Table 5.1 BET parameters and methyl orange adsorption capacity for the carbon adsorbents and MOF adsorbents.

Adsorbent	BET surface area ($\text{m}^2 \cdot \text{g}^{-1}$)	Average pore volume ($\text{cm}^3 \cdot \text{g}^{-1}$)	Pore size (nm)	MO adsorption capacity ($\text{mg} \cdot \text{g}^{-1}$)	Ref
Active carbon	1362	1.27	3.73	238	[49]
Active carbon fiber	1278	0.81	2.39	357	[184]
MOF-235	10.95	0.027	9.93	1257.7	Chapter 4
5%GO/MIL-100(Fe)	1602	0.77	1.92	1189	[185]
Fe@C-350	30.2	0.088	12.51	1667	Chapter 5

5.7.2 Adsorption Isotherm

In the detailed study of the adsorption of methyl orange with carbonised Fe@C-350, Langmuir and Freundlich isotherm models were used to investigate the underlying thermodynamics at different temperatures. The detailed results are shown in Figure 5.8 and Table 5.2.

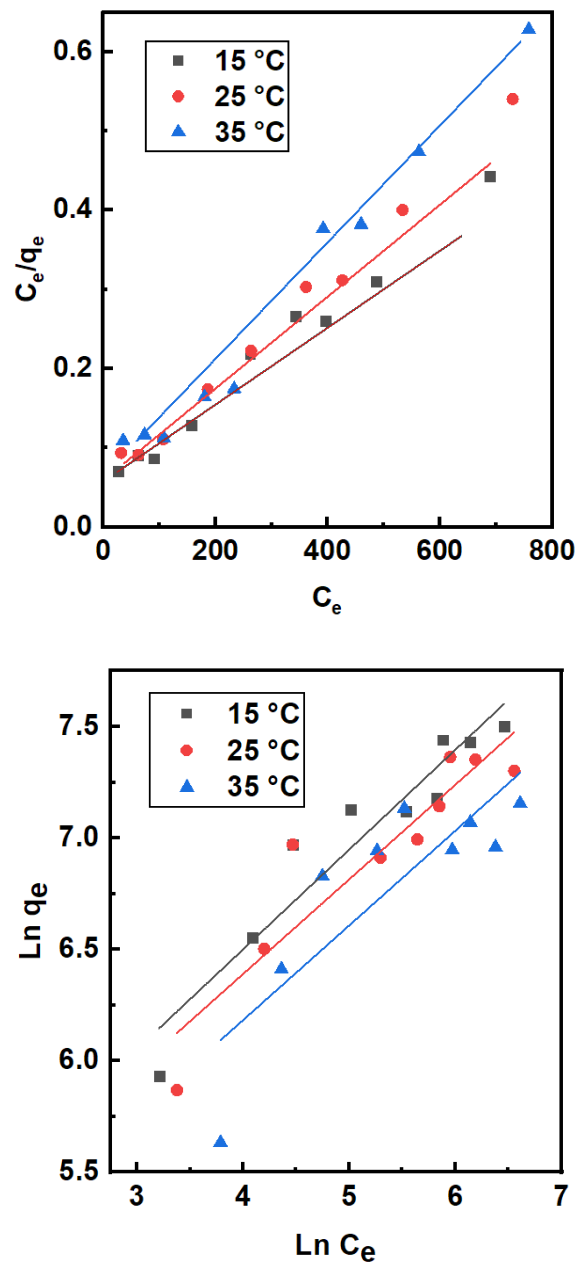


Figure 5.8 Langmuir isotherm and Freundlich isotherm models of MO on Fe@C-350 ($V = 50$ mL, $W = 10$ mg, $pH = 6.8$, adsorption time = 24 h).

This study showed that Fe@C-350 reached a maximum adsorption capacity (q_{\max}) of $1666.7 \text{ mg} \cdot \text{g}^{-1}$ at 15°C with a Langmuir constant (K_L) of $0.012 \text{ L} \cdot \text{mg}^{-1}$, indicating a considerable capacity and a moderate binding affinity. An increase in temperature to 25°C resulted in a decreased q_{\max} of $1428.6 \text{ mg} \cdot \text{g}^{-1}$, while the K_L increased to $0.013 \text{ L} \cdot \text{mg}^{-1}$, illustrating a temperature-induced shift in adsorption site availability and affinity. At 35°C , the decreasing trend continued, with q_{\max} at $1250 \text{ mg} \cdot \text{g}^{-1}$ and K_L increasing slightly to $0.017 \text{ L} \cdot \text{mg}^{-1}$. These results show a clear correlation between temperature, adsorption capacity and binding strength and emphasise the crucial role of temperature in influencing the performance of the adsorbent in removing methyl orange from water. In addition, a consistent decrease in adsorption capacity with increasing temperature was observed at different initial concentrations. This trend confirms the exothermic nature of methyl orange adsorption on Fe@C-350, suggesting that the adsorption is primarily physical.

The adsorption of methyl orange on Fe@C-350 was evaluated using Freundlich isotherm model at 15°C , 25°C and 35°C . The Freundlich parameters derived were: $K_F = 123.5$, $n = 2.422$ at 15°C ; $K_F = 116.6$, $n = 2.500$ at 25°C ; and $K_F = 125.3$, $n = 2.677$ at 35°C . The relative constancy of K_F over the entire temperature range indicates a strong adsorption process within 15°C to 35°C . The intensity parameter n , which is above 1 at all temperatures, indicates a heterogeneous adsorption surface. Variations in n could indicate changes in the surface properties or the interactions between adsorbate and

adsorbent at changing temperatures. In addition, these Freundlich parameters provide information about the underlying adsorption mechanisms. The regression coefficient (R^2) values emphasise the effectiveness of the Langmuir model in describing adsorption dynamics, especially at lower temperatures. However, the decrease in R^2 values for both models at higher temperatures indicates complicated interactions that influence adsorption.

Table 5.2 Comparative fitting outcomes for the Langmuir and Freundlich adsorption models.

Adsorbent	Temperature (°C)	Langmuir isotherm			Freundlich isotherm			
		q_{\max} (mg·g ⁻¹)	K_L (L·mg ⁻¹)	R^2	K_F (mg·g ⁻¹) (L·mg ⁻¹) ^{1/n}	1/n	n	R^2
Fe@C-350	15	1666.7	0.012	0.986	111.10	0.412	2.422	0.881
	25	1428.6	0.013	0.993	109.18	0.400	2.500	0.855
	35	1250	0.017	0.980	88.60	0.374	2.677	0.716

5.7.3 Adsorption Kinetics

Table 5.3 summarises the parameters associated with the kinetic models comprehensively, and Figure 5.9 illustrates the plots for both the pseudo-first-order and pseudo-second-order kinetic models, highlighting the rate constants (k_1 and k_2) and their linear regression correlation coefficients (R^2). The pseudo-second-order model fits the adsorption process exceptionally well, with $R^2 = 1$ for samples with an initial concentration of $200 \text{ mg}\cdot\text{L}^{-1}$. This suggests that the pseudo-second-order kinetic model better characterises the adsorption kinetics of methyl orange on Fe@C-350 than the pseudo-first-order model. Compared to other MOF materials used for methyl orange adsorption, Fe@C-350 has significant performance advantages. It outperforms its MOF precursor MOF-235 ($k_2=0.0009 \text{ g}\cdot\text{mg}^{-1}\cdot\text{min}^{-1}$) [5], and similar carbon materials such as N-NC-800 ($k_2=0.0081 \text{ g}\cdot\text{mg}^{-1}\cdot\text{min}^{-1}$) [186] by its superior adsorption rate and larger adsorption capacity [186].

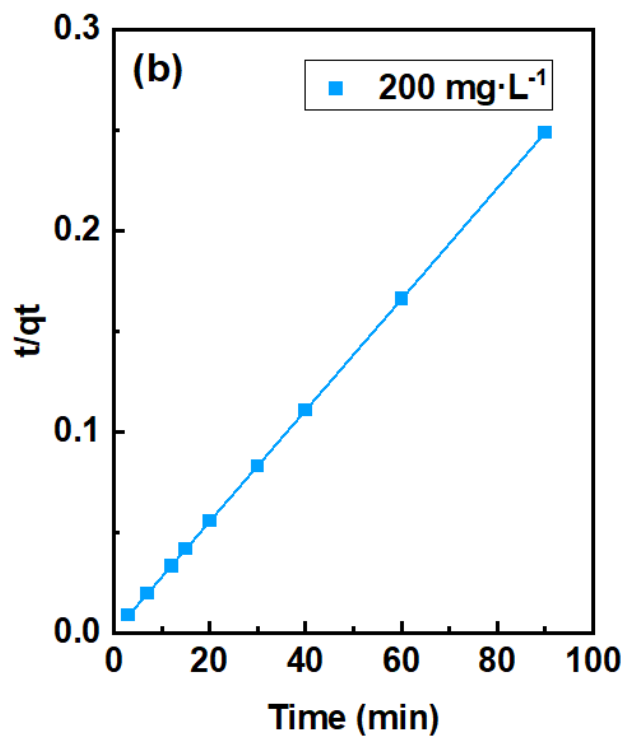
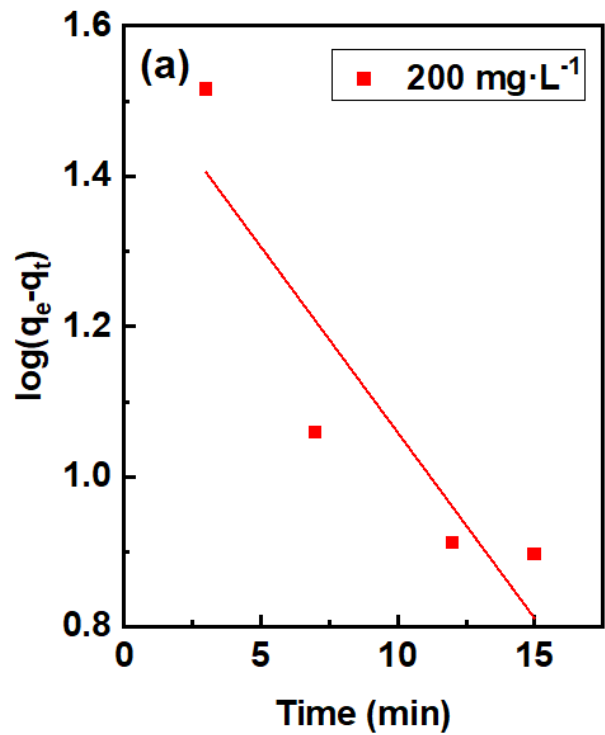


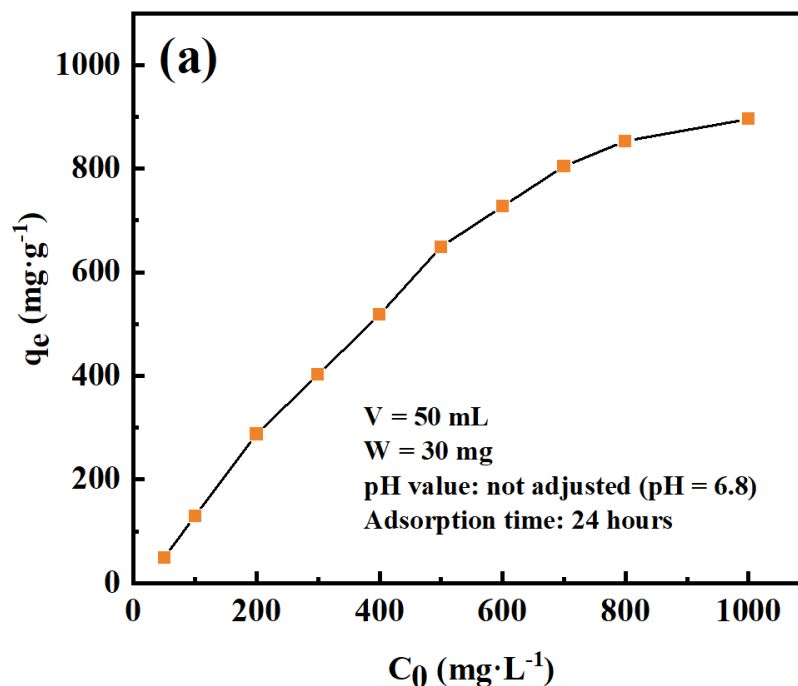
Figure 5.9 (a) Pseudo-first-order kinetic and (b) pseudo-second kinetic models of methyl orange on Fe@C-350 ($V = 100$ mL, $W = 50$ mg, temperature = 25 °C, pH = 6.8).

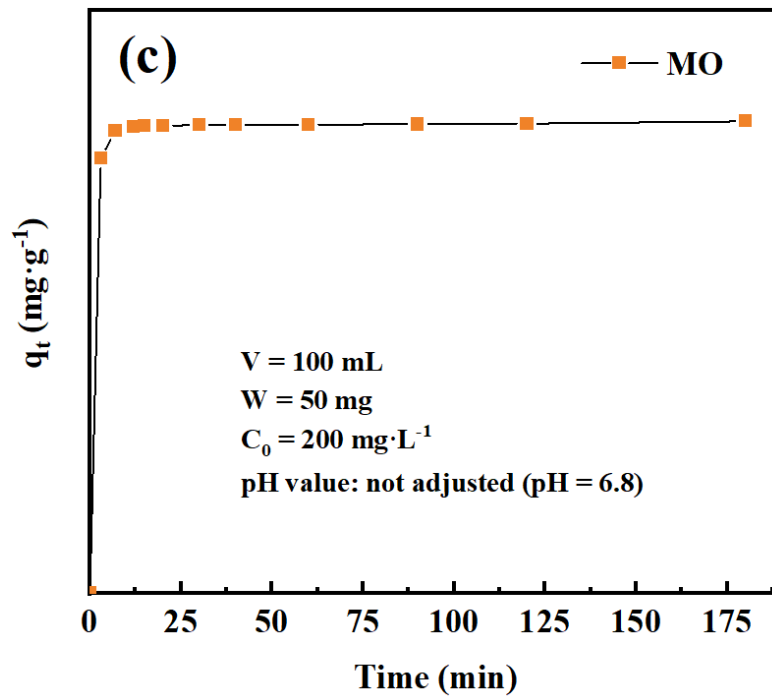
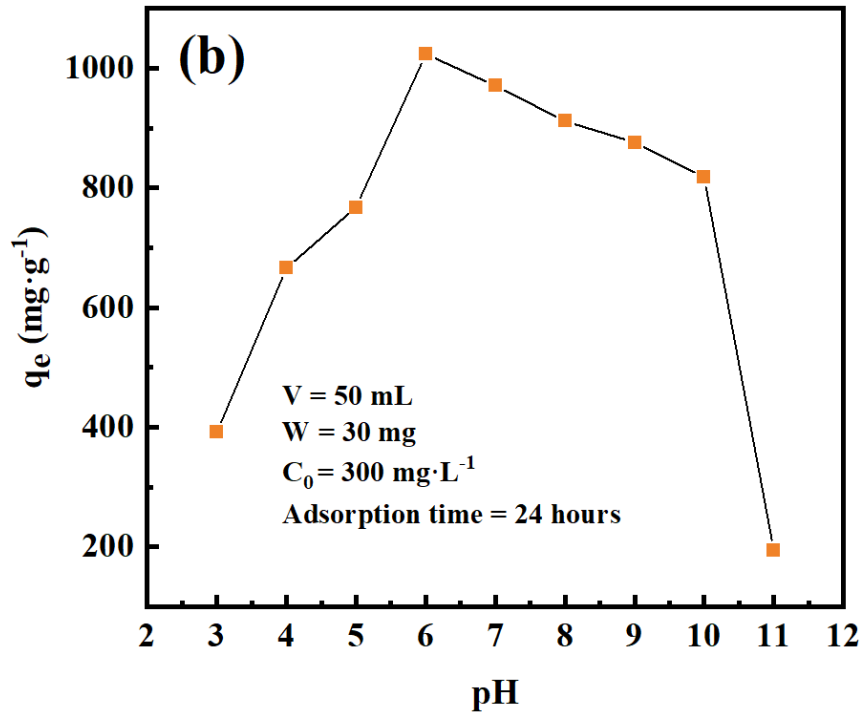
Table 5.3 Comparative fitting outcomes for the Pseudo-first-order kinetic and Pseudo-second-order kinetic models.

Initial concentration (mg·L ⁻¹)		Pseudo-first-order model		Pseudo-second-order model	
	Exp. q _e (mg·g ⁻¹)	k ₁ (min ⁻¹)	R ²	k ₂ (g·mg ⁻¹ ·min ⁻¹)	R ²
Adsorption of methyl orange					
200	368.5	0.114	0.826	0.025	1

5.7.4. Adsorption Performance

Figure 5.10 illustrates how different initial methyl orange concentrations affect the adsorption performance of Fe@C-350 at a constant temperature of 25°C. The adsorption capacity of Fe@C-350 is observed to rise proportionally with initial methyl orange concentrations ranging from 50 to 1000 mg·L⁻¹. This increase is due to the higher driving force at higher methyl orange concentrations, which increases the adsorption rate by overcoming the mass transfer resistance between the liquid and solid phases. This trend is consistent with the results of other adsorbent-adsorbate studies. However, a deviation from this trend is seen as the initial concentrations approach the 800 to 1000 mg·L⁻¹ mark, where the adsorption capacity reaches a plateau. This flattening means that the active sites on Fe@C-350 are saturated, indicating that an equilibrium state has been reached. This behaviour illustrates the finite number of active sites available for adsorption and shows the typical equilibrium state for such systems when all available sites are occupied.





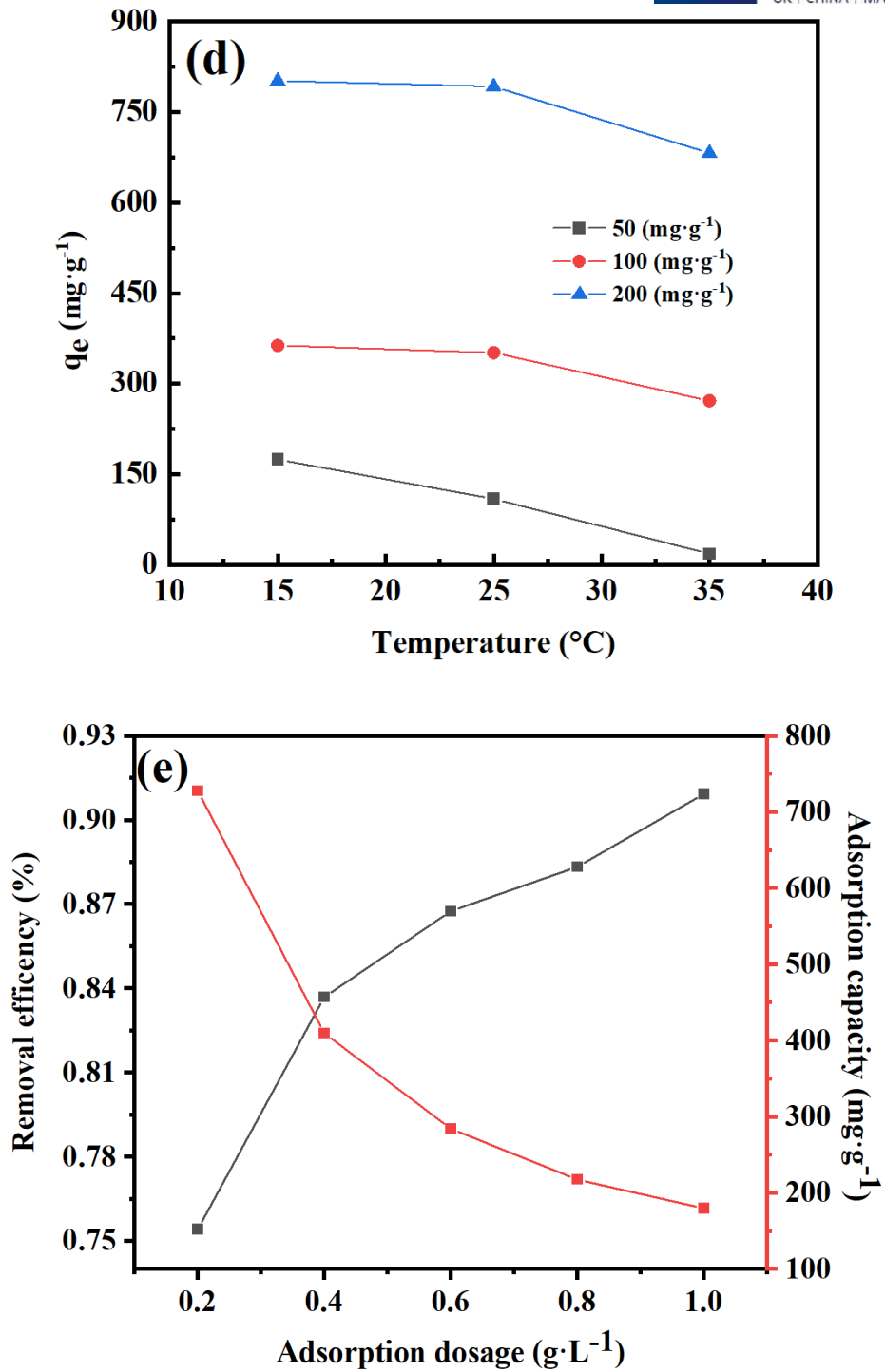


Figure 5.10 Effect of (a) initial concentration, (b) pH on adsorption performance, (c) adsorption time, (d) environment temperature and (e) adsorbents dosage.

The study investigated the influence of the initial pH of the solution on the adsorption of methyl orange dyes by Fe@C-350 and revealed a complex relationship between the acidity of the solution and the adsorption capacity of the dye. Optimal adsorption occurred at pH 6, where methyl orange removal peaked at $1023.8 \text{ mg}\cdot\text{g}^{-1}$. It is noteworthy that the adsorption capacity remained high between pH 6 and 10 and decreased slightly to $818.2 \text{ mg}\cdot\text{g}^{-1}$ at pH 10. At pH 11, a sharp decrease to $193.9 \text{ mg}\cdot\text{g}^{-1}$ was observed, which can be attributed to an increased hydroxyl ion concentration reducing the electrostatic attraction between the Fe@C-350 and the methyl orange molecules. This phenomenon is consistent with the results of previous studies [23], which confirm that methyl orange adsorption is optimal at pH 6 and is significantly hindered at pH 11 due to competition from hydroxide ions. In contrast to the original MOF-235 material, which requires a highly acidic environment (pH 3), Fe@C-350 shows robust methyl orange removal capabilities over the typical pH range of industrial wastewater. The improved performance of Fe@C-350 in a broader pH range reduces the need for pH modification and thus strengthens its practical application in methyl orange adsorption processes.

The effects of contact time and solution temperature on the removal efficiency of methyl orange with Fe@C-350 were systematically investigated. The results showed that Fe@C-350 adsorbs methyl orange rapidly, reaching 90% of its maximum uptake capacity within only 3 minutes and approaching saturation after 12 minutes when started at an methyl orange concentration of $200 \text{ mg}\cdot\text{L}^{-1}$ in a 100 ml solution using 50 mg of adsorbent. This rapid adsorption is due to the many active sites on Fe@C-350 and its optimal pore

structure, which favours the diffusion and subsequent uptake of the dye molecules. The study also showed that the adsorption effect of Fe@C-350 decreases with increasing temperature. In particular, the maximum adsorption capacity of Fe@C-350 was found to be more than five times higher at a cooler temperature of 15°C than at 35°C. This confirms that lower temperatures improve the adsorption efficiency due to the increased energetic interactions between the dye and the adsorbent. These results demonstrate the fast adsorption rate of Fe@C-350 and make it a promising candidate for methyl orange decontamination in wastewater treatment processes.

Figure 5.10 (e) illustrates that increasing the adsorbent dosage from 0.2 g·L⁻¹ to 1.0 g·L⁻¹ resulted in a significant decrease in the equilibrium adsorption capacity of methyl orange, from 727.8 mg·L⁻¹ to 179.9 mg·L⁻¹. This decrease can be attributed to the aggregation of Fe@C-350 particles, which decreases the effective surface area and increases the diffusion distance for methyl orange molecules [187]. While the adsorption efficiency per gram of adsorbent decreases, the overall removal efficiency of methyl orange increased from 75.4% to 90.9%. This demonstrates that a higher Fe@C-350 dosage provides more available adsorption sites, thereby increasing the overall removal efficiency [188].

The adsorption capabilities of Fe@C-350 for methyl orange removal were compared with other reported methods in Table 5.5. Compared to the previously investigated techniques, it exhibits higher adsorption capacity and faster equilibrium time. These improvements are due to the high density of accessible adsorption sites on the carbonised Fe@C-350 surface and pore

sizes that are well adapted to the molecular size of methyl orange. The combination of these structural properties significantly increases the efficiency of methyl orange deposition.

Table 5.4 Comparison of methyl orange adsorption capacity and efficiency of different MOF-based adsorbents.

Dye	Adsorbents	Adsorption capacity ($\text{mg}\cdot\text{g}^{-1}$)	Adsorption time	Ref.
Methyl orange	MIL-100(Fe)@GO	1189	48 h	[185]
	MIL-101(Al)-NH ₂	188±9	200 min	[189]
	PCN-222(Zr)	1022	15 min	[190]
	SCNU-Z1-Cl	285	26 min	[191]
	UiO-66@Ce	639.6	24 h	[192]
	ZIF-67	1342.8	150 min	[193]
	MOF-235	501	150 min	[5]
	Fe@C-350	1666.7	3 – 10 min (90% of adsorption capacity)	This study

5.7.5. Cyclic Adsorption-desorption Test

For adsorbents to be used in practise, their regenerability is the key to cost-efficient, large-scale use [194]. Fe@C-350 was tested through several methyl

orange adsorption-desorption cycles to assess its regenerability. Figure 5.11 shows the retention of the adsorption capacity of Fe@C-350 over 10 cycles, where the label 'x' indicates the cycle number. Remarkably, Fe@C-350 retained approximately 98% of its initial adsorption capacity after 10 cycles, demonstrating its regenerability. An initial increase to 102% capacity in the third cycle was noted, which was likely due to variations in adsorbent or methyl orange concentration during sample analysis, resulting in some experimental error.

Figure 5.12 shows the constant adsorption capacity of Fe@C-350 for methyl orange over ten regeneration cycles by pictures. It is noteworthy that the adsorption capacity of Fe@C-350 is almost unchanged after the tenth cycle compared to the first cycle. UV-vis analysis shows that the concentration of methyl orange solution after adsorption in the tenth cycle was $20.9 \text{ mg}\cdot\text{L}^{-1}$, compared to $18.3 \text{ mg}\cdot\text{L}^{-1}$ in the first regeneration cycle, emphasising the durability of the adsorbent with repeated use. The consistent performance of Fe@C-350 over multiple cycles underlines its effectiveness as a reusable adsorbent for the treatment of methyl orange effluents and highlights its potential for practical environmental remediation applications.

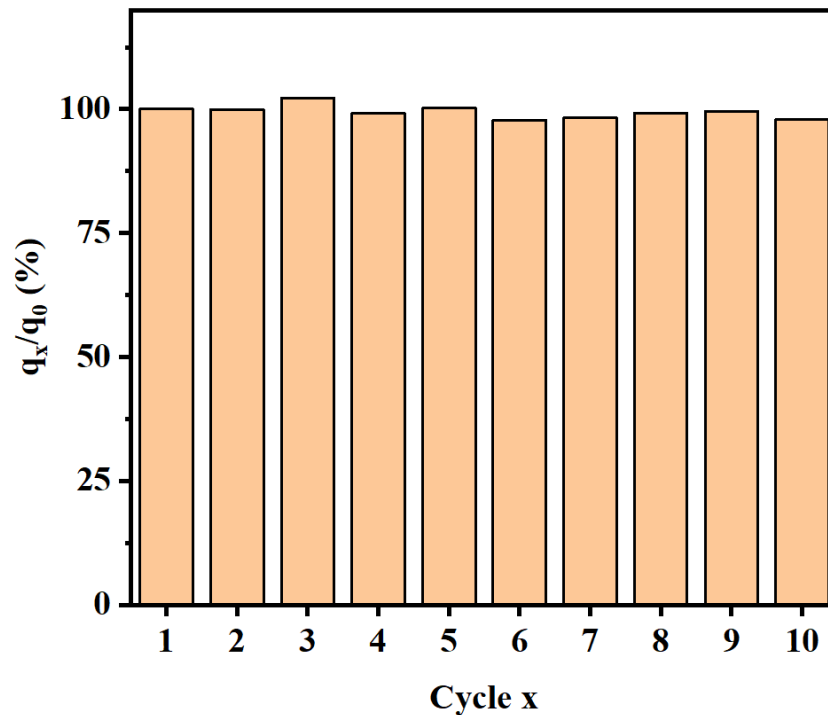


Figure 5.11 Recyclability of Fe@C-350 after 10 cycles (x = the number of thermal regeneration cycles).

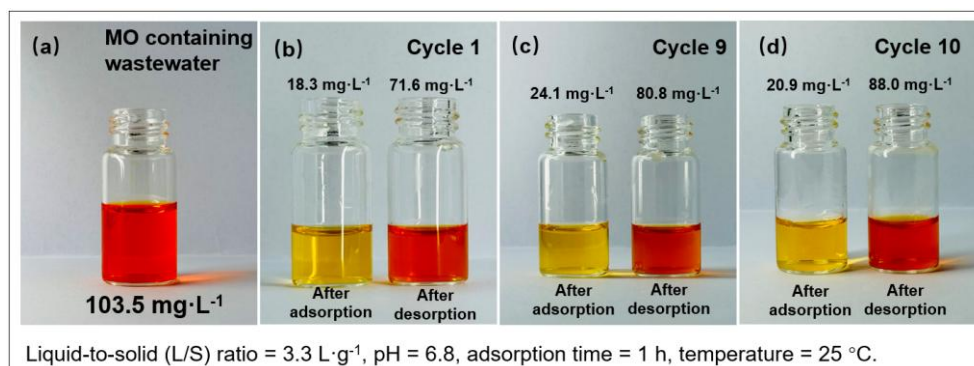


Figure 5.12 (a) The initial methyl orange sample and the methyl orange samples after adsorption and desorption in (b) the first regeneration cycle, (c) the ninth regeneration cycle and (d) the tenth regeneration cycle.

FTIR was performed on Fe@C-350 before and after methyl orange adsorption. After adsorption, the FTIR spectra showed characteristic methyl orange peaks at 1600 cm^{-1} and 1450 cm^{-1} attributed to the azo bonds ($-\text{N}=\text{N}-$)

and aromatic structures, respectively, as shown in Figure 5.13. These results confirm the adsorption of methyl orange on Fe@C-350.

Desorption studies involving repeated heating of a 100 mL methyl orange solution with Fe@C-350 indicated a physical adsorption mechanism. The presence of the dye in the supernatant, recognisable by the orange colouration and a prominent absorption peak at 465 nm identified by UV-vis spectroscopy, proves the release of methyl orange from the adsorbent during thermal treatment. After ten regeneration cycles, the methyl orange concentration in the solution after desorption was 72% of its original level, as shown in Figure 5.14. This partial desorption at 60°C indicates that some methyl orange molecules remained bound to the adsorbent, possibly due to the experimental conditions. Sampling for the concentration measurements may also have led to slight deviations.

The observed increase in methyl orange desorption at higher temperatures is probably due to increased entropy, which weakens the interactions between adsorbate and adsorbent. From this, it can be concluded that the adsorption process of Fe@C-350 for methyl orange is primarily based on physical adsorption. The preferential adsorption behaviour of Fe@C-350 is probably due to hydrophobic interactions and electrostatic interactions between the electron-rich dye and the porous carbon structure.

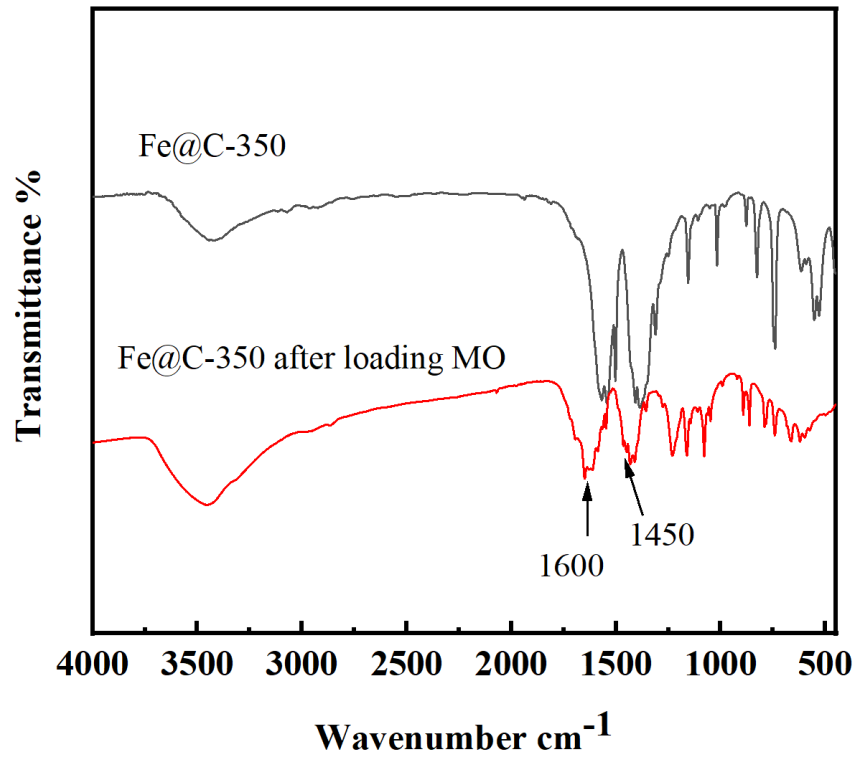


Figure 5.13 FT-IR spectra of Fe@C-350 and MO-loaded Fe@C-350.

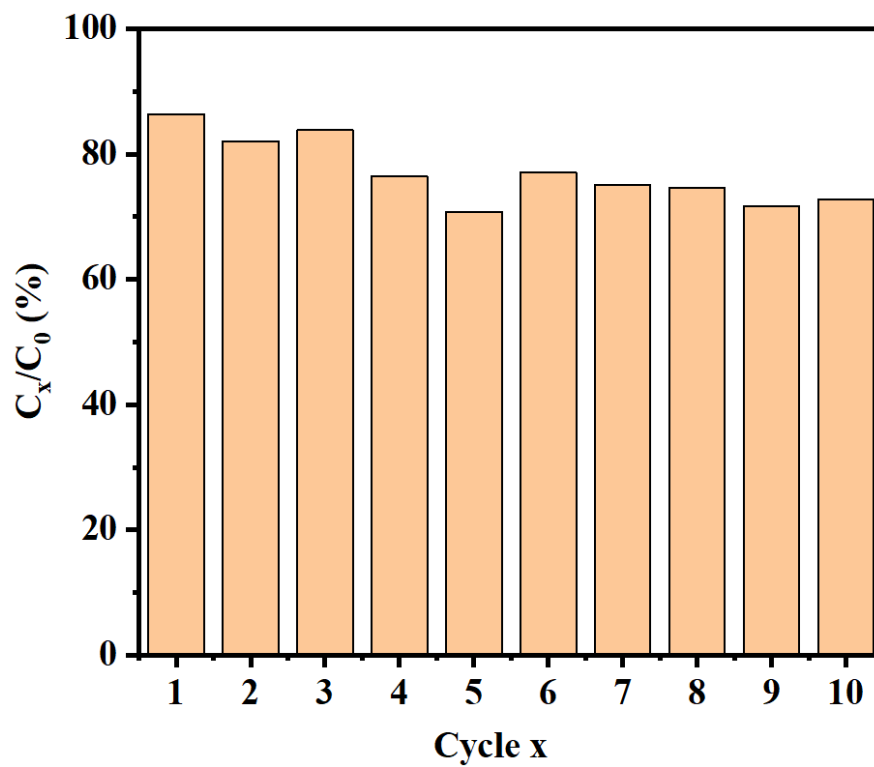


Figure 5.14 The ratio of the desorbed methyl orange solution to the initial concentration ($100\text{mg}\cdot\text{L}^{-1}$) after 10 cycles (x = the number of thermal regeneration cycles).

5.8. Conclusions

In this chapter, a porous carbon adsorbent Fe@C-350. was synthesised by the pyrolysis of the metal-organic framework MOF-235 in an argon atmosphere. The Fe@C-350 adsorbent obtained after carbonisation has a larger surface area and pore size, both of which are well suited for the adsorption of methyl orange. Kinetic studies showed the fast adsorption rate of Fe@C-350 with $k_2 = 0.114 \text{ min}^{-1}$. Fe@C-350 showed a high methyl orange adsorption capacity of $1666.7 \text{ mg}\cdot\text{g}^{-1}$. In addition, Fe@C-350 retained approximately 98% of its original adsorption capacity after 10 adsorption-desorption cycles. The adsorption was found to a monolayer physical adsorption. It can therefore be concluded that the carbonaceous material Fe@C-350 derived from MOF-235 is a highly efficient adsorbent with considerable potential for wastewater containing dyes. However, it is also necessary to investigate the application of Fe@C-350 in the removal of a broader range of contaminants.

Chapter 6.

Recycled PET Derived Carbon for Highly Efficient Heterogeneous Fenton-like Degradation of Methyl Orange

6.1. Introduction

Azo dyes are used extensively in the textile industry as well as in applications such as food colouring and cosmetics. Current data reveal that the global textile industry consumes more than 10,000 tonnes of dye each year, with approximately 100 tonnes being discharged into water streams annually [195]. This situation led to severe environmental pollution that has become one of the most pressing global problems. Methyl orange is an azo dye widely used in the dyeing industry and is used as a typical pH indicator. Its release poses a significant risk to human health. To ensure environmental safety and maintain ecological balance, it is therefore necessary to effectively remove methyl orange from water.

Advanced Oxidation Processes have recently attracted considerable attention due to their effectiveness in dye [37]. In particular, there has been increasing interest in heterogeneous Fenton reactions in which organic pollutants are degraded to less toxic molecules and even mineralised to CO₂ and H₂O [196, 197]. This method has the potential to overcome the typical limitations of conventional Fenton reactions, such as the requirement to operate in an

extremely low pH range ($\text{pH} < 3$) and the generation of significant sludge.

However, the current degradation rate of methyl orange with the heterogeneous Fenton reaction is insufficient. For example, previous studies have shown that the $\text{Fe}_3\text{O}_4/\text{MWCNTs} + \text{H}_2\text{O}_2$ system has the most significant reduction in methyl orange concentration and achieves almost complete removal within 40 minutes [198]. Therefore, the urgent need to develop a more efficient catalyst is emphasised.

In recent years, metal organic framework materials consisting of metal cations (or clusters) and organic ligands have attracted considerable attention due to their special physicochemical properties, such as large specific surface areas, high and uniform porosity, structural stability and tunable pore sizes/shapes [106]. Among the various MOFs, MOF-235 is a very effective adsorbent for methyl orange [5]. In addition, MOFs are considered as promising sacrificial templates and precursors for the synthesis of advanced porous carbon materials due to their high carbon content and uniform distribution of metal clusters and organic ligands [140]. Due to their more favourable properties in terms of structural stability, surface area, porosity, functionality and hydrophobicity, MOF-derived porous carbon materials have shown excellent potential for heterogeneous Fenton degradation of various organic dyes [199]. However, the use of MOF-235-derived carbon materials as catalysts in heterogeneous Fenton reactions for the treatment of wastewater containing methyl orange has not yet been explored.

Although MOFs and MOF-derived carbon materials offer significant advantages, their high cost, especially due to the expensive organic ligands

such as terephthalic acid, limits their industrial application. This problem can be solved by replacing commercially available ligands with those recycled from polyethylene terephthalate (PET) waste. Tertiary or chemical recycling, which involves the complete depolymerisation of PET, is crucial to produce high-quality terephthalic acid. Among the various chemical recycling methods — methanolysis, glycolysis, ammonolysis and hydrolysis — alkaline hydrolysis is particularly effective for the recovery of terephthalic acid from contaminated PET waste and yields high-purity (>99 wt%) acid suitable for MOF synthesis. While terephthalic acid from PET has been widely studied for MOF synthesis, its use for the synthesis of MOF-235 and its carbonised derivatives is still unexplored.

In this study, terephthalic acid obtained from PET waste was used as an organic base ligand for the synthesis of MOF-235, which was subsequently carbonised in situ to produce ferrous porous carbon (PD-Fe@C350). The photo-Fenton performance of PD-Fe@C350 was tested with methyl orange as a target organic pollutant. The structure and physicochemical properties of the porous carbon materials were characterised and various parameters, including pH, initial dye concentration and H₂O₂ dosage, were thoroughly investigated. Kinetic analysis was performed to study the adsorption rate and the catalytic mechanism of PD-Fe@C350 was also investigated. Meanwhile, the mechanism of photo-Fenton process was investigated.

6.2. Chemicals

The waste PET bottles used as raw materials in this study were obtained from Sam's Supermarket, Wal-Mart Department Store Co., Ltd. The chemical

reagents utilized in the experimental procedures included potassium hydroxide (KOH), ethylene glycol (AR grade, 99% purity), ferric chloride hexahydrate ($\text{FeCl}_3 \cdot 6\text{H}_2\text{O}$), N,N-dimethylformamide (DMF, 99%), ethanol (99%), terephthalic acid (BDC, 99%), hydrogen peroxide (H_2O_2 , 30%), and hydrochloric acid (HCl, 37%). All chemical reagents were sourced from Aladdin Chemical Reagent Co., Ltd. (Shanghai, China) and used as received without additional purification.

6.3. Synthesis

6.3.1. Depolymerization of waste PET Plastic Bottle

The method of depolymerization was followed by previous study [100]. Prior to depolymerization, the collected PET bottles were cleaned to remove all labels, caps, and extraneous attachments. To enhance depolymerization, the PET bottles were fragmented into small pieces. The depolymerization process commenced by combining 2 g of the PET fragments with 3.68 g of KOH in 46 mL of ethylene glycol (EG) inside a double-layered three-necked flask equipped with a water-jacketed condenser. This reaction vessel was partially submerged in an oil bath device heated to 180 °C and held at condensation reflux for 3 hours. Then, the reacted mixture was transferred to a round bottom flask and diluted with 80.33 mL of deionized water while maintaining the temperature at 80 °C with constant stirring. Concurrently, 5M H_2SO_4 was added to adjust the solution's pH to 3, which was then sustained for a further 30 minutes. The end product was rinsed with ethanol and left to dry overnight, yielding the terephthalic acid powder.

6.3.2. Synthesis of PD-MOF-235

The synthesis of PET derived MOF-235 was accomplished utilizing the conventional solvothermal technique [5]. A solution was prepared by dissolving 0.6 g of $\text{FeCl}_3 \cdot 6\text{H}_2\text{O}$ and 0.6 g of terephthalic acid (derived from PET) in 180 mL of DMF. This solution was continuously stirred for an hour until complete clarity of solution was achieved. Subsequently, 60 mL of ethanol was added. The combined mixture was then transferred to a double-layered three-necked flask with an oil bath device, maintaining in 80 °C with constant stirring for 24 hours. The orange product was washed with a mixture of ethanol and DMF and desiccated in a vacuum oven overnight. Upon cooling, the resulting product was named as PD-MOF-235.

6.3.3. Synthesis of PD-Fe@C350

As illustrated in Figure 6.1, the carbonisation of PET-derived MOF-235 was performed in a tube furnace under an argon atmosphere. The sample was subjected to a controlled heating rate of 2 °C·min⁻¹ until it reached a final temperature of 350 °C, where it was maintained for 2 hours. After cooling, the carbonised product was named as PD-Fe@C350.

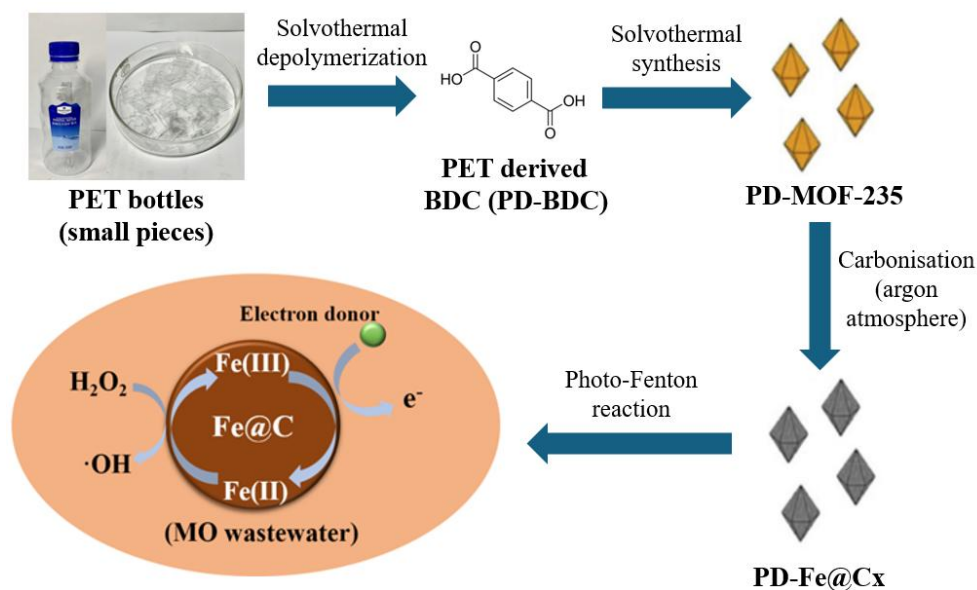


Figure 6.1 Sustainable synthesis of PD-Fe@C and its application in the Fenton reaction.

6.4. Characterisation

The crystal structures of both obtained and PET-derived BDC, PD-MOF-235 and PD-Fe@C350, were characterised using an X-ray Diffractometer (XRD) (Smart Lab (3 KW), Rigaku, Japan). Fourier Transform Infrared Spectroscopy (FT-IR, Nicolet iS50 FT-IR, Thermo Scientific, USA) was employed to analyse the surface functional groups of these materials. The surface composition and chemical states of PD-Fe@C350 were further investigated through X-ray Photoelectron Spectroscopy (XPS) using a Kratos XSAM800 system. Scanning Electron Microscopy (SEM, Regulus 8100, Hitachi, Japan) was utilized to ascertain the surface morphology and average diameter of the terephthalic acid samples and both PD-MOF-235 and PD-Fe@C350. The concentration of methyl orange was quantified via UV-vis spectrophotometry (PerkinElmer, Lambda 365) at a wavelength of 465 nm.

6.5. Photo-Fenton Performance Test

The photo-Fenton degradation performance of the catalysts synthesised in this study for methyl orange was investigated [197]. This evaluation focused on the Fenton degradation performance by examining various fundamental physicochemical parameters. These included the initial concentration of the dye, the initial solution pH, and the dosage of H₂O₂. The photo-Fenton reaction for degrading methyl orange using PD-Fe@C nanoparticles was conducted in a dark box, utilizing a xenon lamp (Perfectlight, PLS-SXE300+) equipped with a steady-current power supply. The experiment commenced with 100 ml of a 100 mg·L⁻¹ methyl orange solution. Subsequently, the solution's pH was carefully adjusted to a predetermined level using both 0.1 M and 1 M solutions of H₂SO₄ and NaOH. Following this, 20 mg of PD-Fe@C particles was added into the methyl orange solution and stirred in darkness for two hours to attain adsorption-desorption equilibrium. Once the mixture was thoroughly homogenized, it was swiftly transferred to the dark box. The photo-Fenton reaction was then initiated by introducing 1 ml of H₂O₂ at a specific concentration, along with light of a precise wavelength. The extent of photo-Fenton degradation was achieved by controlling the reaction time. After completion of the reactions at different time intervals, the samples were removed from the parallel reaction tubes and the solid particles were separated by centrifugation. The concentration of methyl orange remaining in the supernatant was accurately quantified using a UV-vis spectrophotometer with a wavelength of 465 nm to determine the efficiency of the decolourisation process.

The degradation of methyl orange followed a pseudo-first-order reaction, with the kinetics described by the equation,

$$\ln\left(\frac{C_e}{C_t}\right) = kt \quad (15)$$

where k is the observed rate constant (min^{-1}), and C_0 and C_t ($\text{mg}\cdot\text{L}^{-1}$) denote the initial concentration after adsorption-desorption equilibrium and the concentration after t minutes of reaction time, respectively.

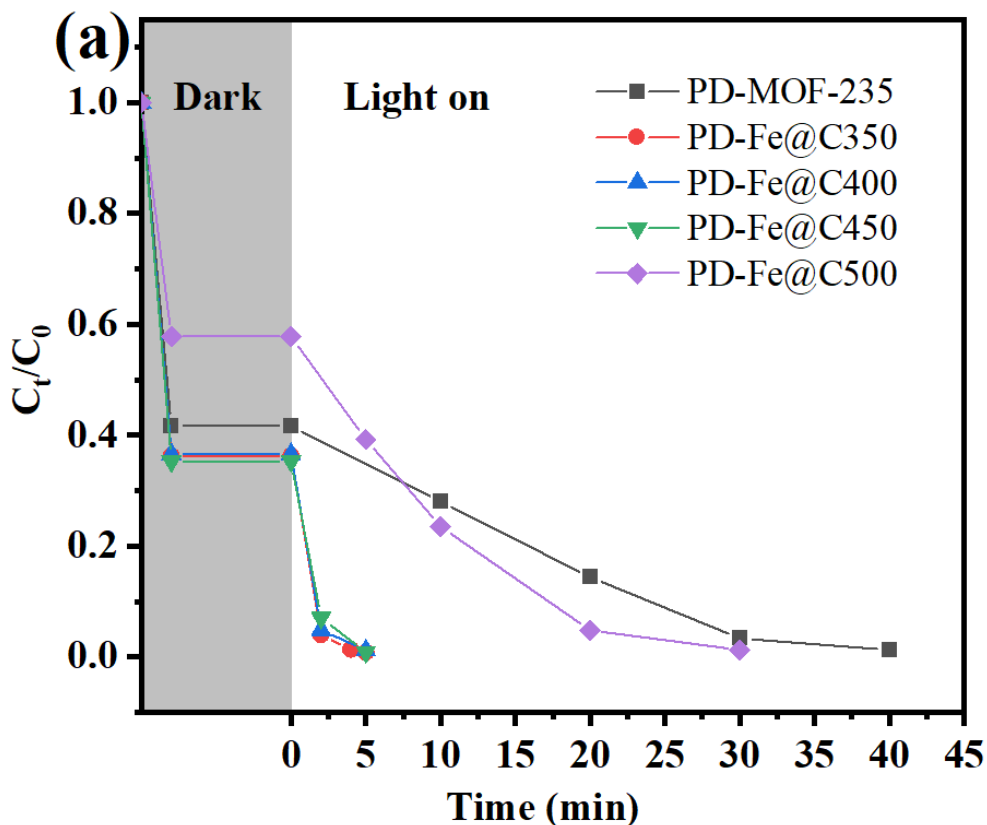
6.6. Results and discussion

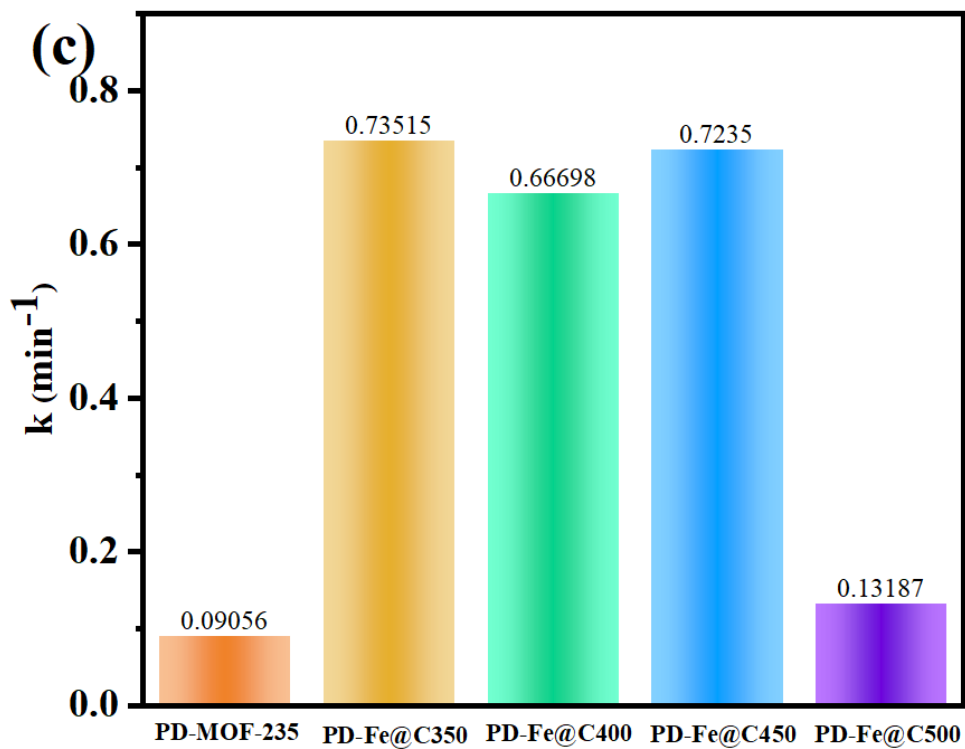
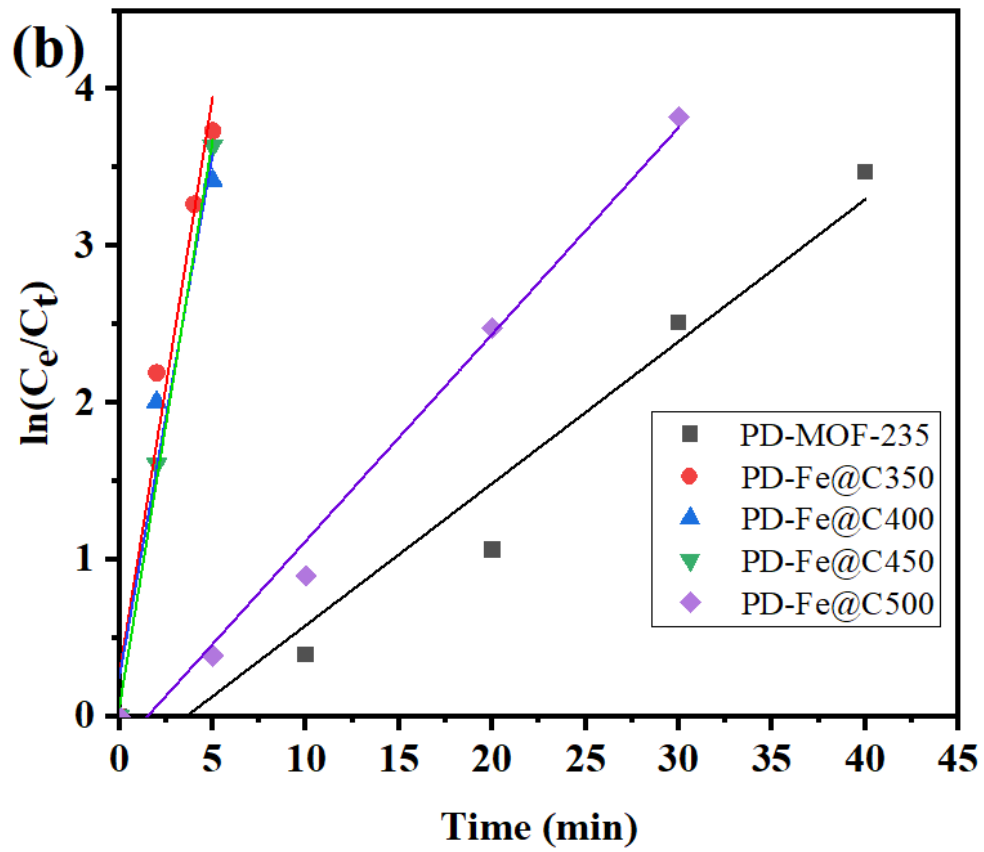
6.6.1. Carbonisation Condition

To determine the optimal carbonisation temperature for photo-Fenton efficiency, this study compared the original PD-MOF-235 with its carbonised variants, all tested under same reaction conditions. The methyl orange degradation trends (Figure 6.2 a)) and kinetic modelling were analysed. It was found that the catalysts carbonised at 350, 400, and 450°C exhibited similar adsorption and catalytic performance, each achieving a 62% methyl orange adsorption rate in the dark. Upon exposure to light and H_2O_2 , these catalysts demonstrated a degradation efficiency of over 99% in less than 5 minutes. In contrast, the non-carbonised PD-MOF-235 showed a lower adsorption rate of 41% in the dark and required 30 minutes to reach 99% degradation with light and H_2O_2 . At a carbonisation temperature of 500°C, the catalytic efficiency decreased significantly, taking 40 minutes to achieve 99% degradation.

The comparison of kinetic rates (Figure 6.2 (b) and (c)) shows that PD-Fe@C350 has the highest photocatalytic activity among all catalysts, with a

rate of 0.735 min^{-1} , which is 8.17 times higher than that of its precursor PD-MOF-235, followed by PD-Fe@C450 and PD-Fe@C400, with PD-Fe@C500 having progressively lower kinetic rates. PD-MOF-235 has the lowest overall photocatalytic performance. It is noteworthy that the kinetic rates of PD-Fe@C450 and PD-Fe@C400 are almost identical to those of PD-Fe@C350. The TGA results for PD-MOF-235 (Figure 6.2 (d)) suggest that this change in efficiency is related to the complete decomposition of the organic components and the formation of a stable carbon structure within the 350 to 450°C range. Beyond 500°C, excessive pyrolysis compromised the material's structure, leading to reduced dye uptake, as shown in the SEM images. Thus, the range of 350-450°C was identified as the optimal carbonisation window. With a focus on energy saving, PD-Fe@C350 was selected as the catalyst for further investigations.





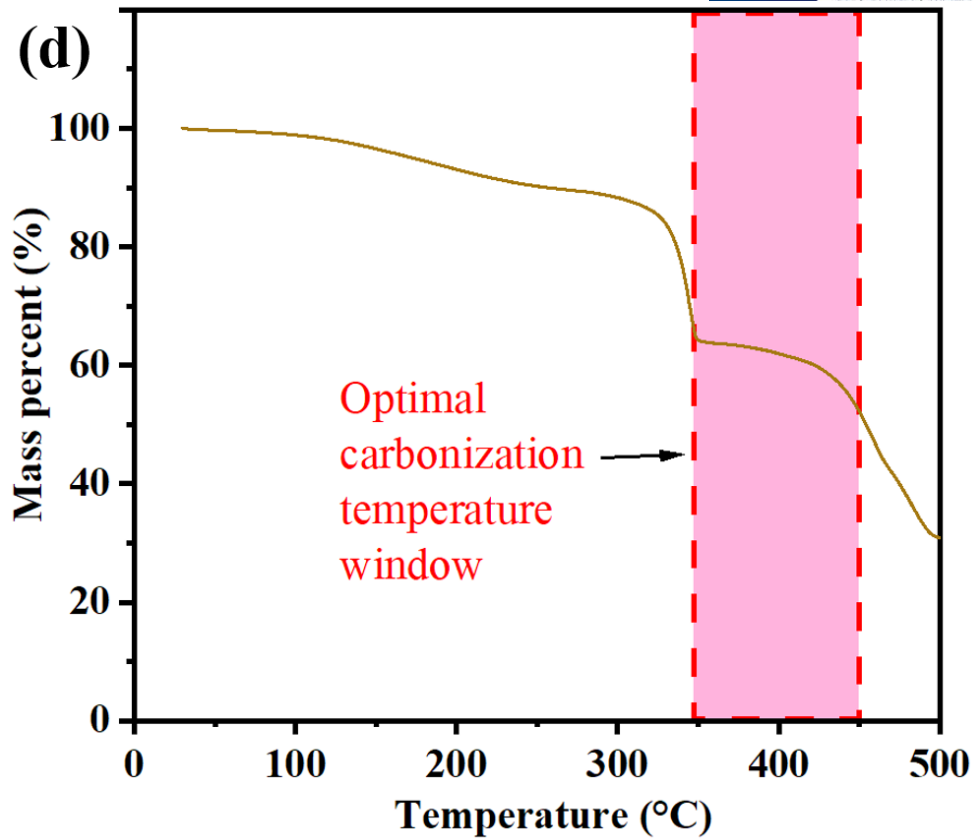


Figure 6.2 (a) Comparison of the adsorption and degradation performance of methyl orange at different carbonisation temperatures, (b) fitting kinetic curves, (c) kinetic rates of PD-MOF-235 and its carbonised derivatives, and (d) TGA results of PD-MOF-235.

6.6.2. Characterisation

6.6.2.1. Morphological Analysis

Figure 6.3 shows that terephthalic acid derived from the depolymerisation of PET waste bottles (Figure 6.3 (b)) exhibits smaller particle sizes than commercially available terephthalic acid (Figure 6.3 (a)). This phenomenon may be due to the increased reaction rate made by the continuous stirring during depolymerisation. The MOF-235 crystals depicted in Figure 6.3 (c)

are spindle-shaped, uniform in size, and have a smooth surface, with an average particle size of 800 nm. Upon processing at 350°C, these crystals transform into Fe@C-350 particles with a distinctive, pinecone-like, flaky surface morphology (Figure 6.3 (d)). The presence of these in-plane pores increases the porosity of the samples, thereby providing a greater number of active sites. Similar transformations at 400°C, resulting in the formation of carbon flakes from the pyrolysis of organic ligands, were described in Chapter 5. SEM analysis highlights the significant impact of carbonisation temperature on the morphology of the synthesised MOF derived carbon materials.

Further examination of the PD-Fe@C350's microstructure was conducted using TEM. These tests confirmed the presence of micropores (approximately 10 nm in size) within PD-Fe@C350, as shown in Figure 6.4. Together, these analyses validate the successful synthesis of the PD-Fe@C350 catalyst using discarded PET plastic bottles as the raw material.

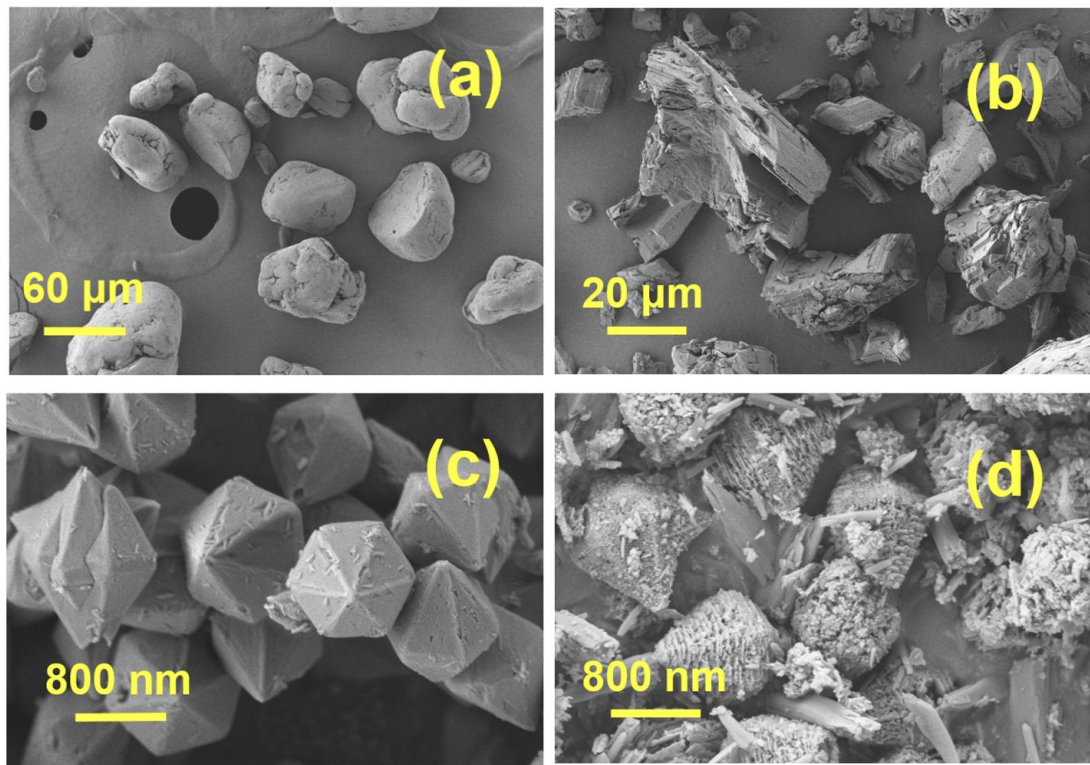


Figure 6.3 SEM images of a) purchased terephthalic acid, b) terephthalic acid obtained from the depolymerisation of PET waste bottles, c) PD-MOF-235, d) PD-Fe@C350.

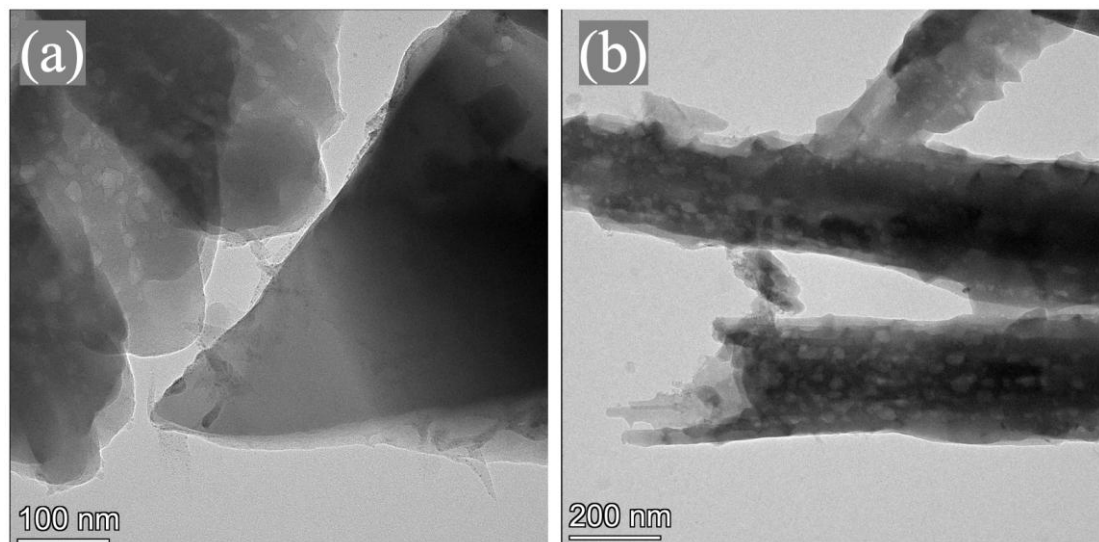


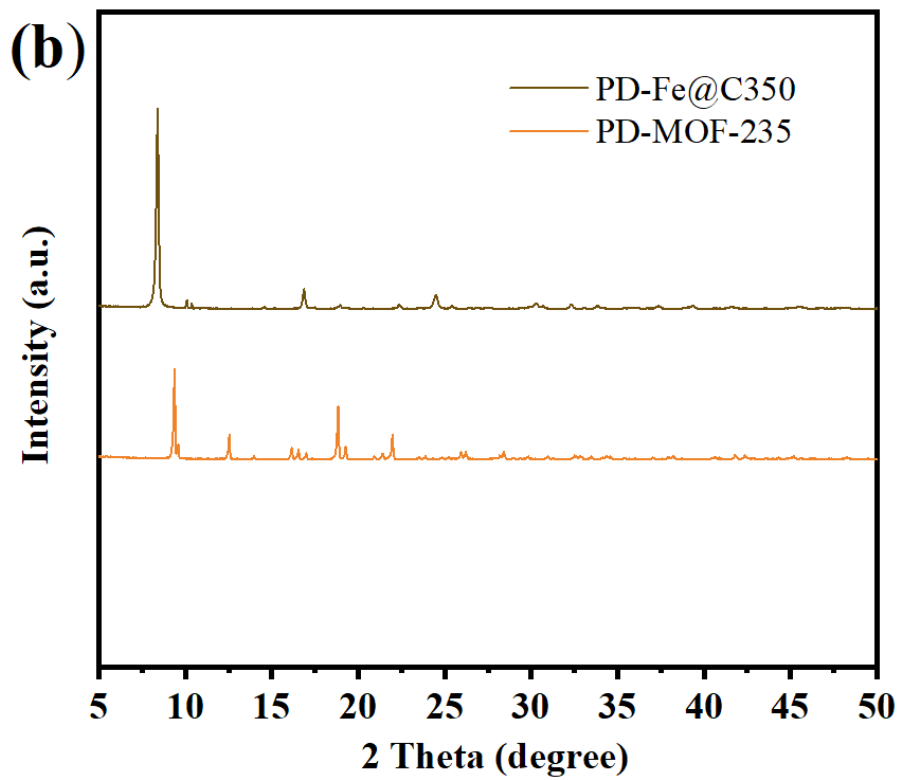
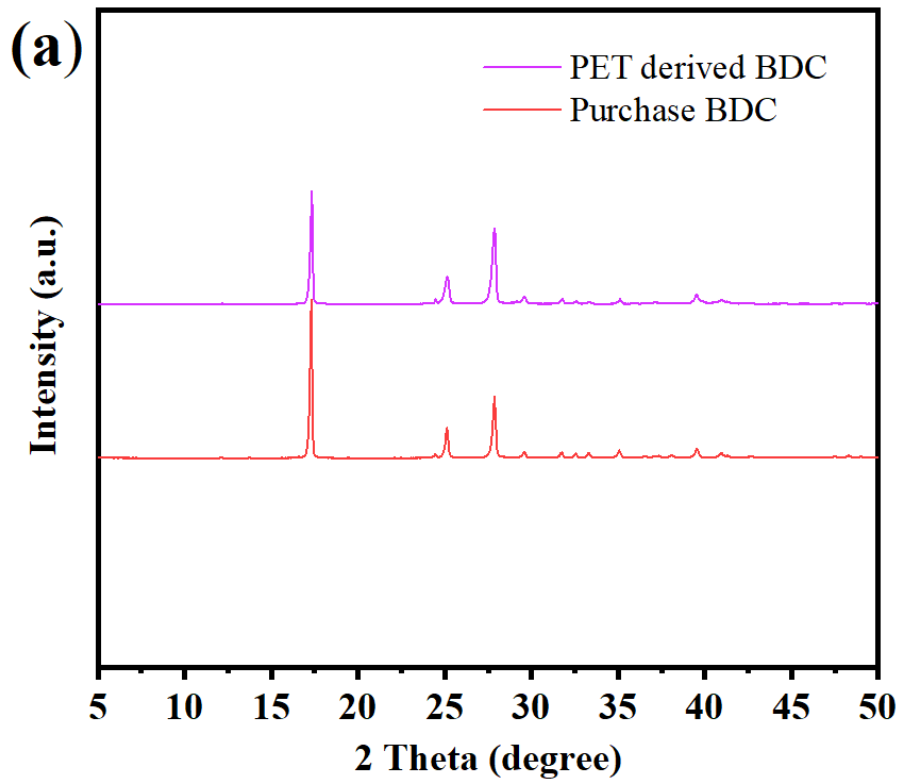
Figure 6.4 TEM images PD-Fe@C350.

6.6.2.2. Phase Analysis

Powder XRD was utilized to investigate the crystallographic structures of both waste PET bottle-derived and commercially obtained terephthalic acid, along with the eco-friendly produced PD-MOF-235 and its carbonised counterpart, PD-Fe@C350, within the 5 to 50° 2 θ range. The resulting XRD patterns, as presented in Figure 6.5, show that the peak angles of terephthalic acid from waste PET closely mirror those from commercial sources, with minor variations in peak intensities. This similarity confirms the effective extraction of high-purity terephthalic acid organic precursors from waste PET in this research. Moreover, the XRD profiles of PD-MOF-235 and conventional MOF-235 display notable parallels [157]. Additionally, the XRD results for PD-Fe@C350 indicate a prominent maghemite phase, consistent with previous studies on iron-infused carbon materials [181]. A significant observation is the near absence of the characteristic diffraction peaks of the original PD-MOF-235 structure in PD-Fe@C350's XRD pattern. This phenomenon is linked to the thermal breakdown of organic ligands, resulting in the conversion of Fe³⁺ ions from PD-MOF-235 to Fe₂O₃·H₂O in PD-Fe@C350, identifiable by peaks at 2 θ = 8.1° and 2 θ = 24.3°. Additionally, the presence of Fe₂O₃ (maghemite) in PD-Fe@C350 is verified, though its diminished intensity at 2 θ = 30.2° indicates a lower concentration. While XRD analyses often exhibit overlapping spectral signatures of Fe₂O₃ and Fe₃O₄, prevailing research suggests that the dominant phase in the carbonised PD-MOF-235 is Fe₂O₃, rather than Fe₃O₄ [181].

FTIR analysis was utilized to perform an in-depth comparison between terephthalic acid obtained from waste PET bottles and commercially sourced terephthalic acid, and to elucidate the molecular structures and identify the organic functional groups in PD-MOF-235 and PD-Fe@C350. Displayed in Figure 6.4 (c) and (d) are the spectra resulting from this analysis. Notably, the FTIR spectrum for PD-MOF-235 shows a pronounced broad peak at 3440 cm^{-1} , indicative of the O-H stretching vibrations typically associated with surface-bound water molecules. A peak of lesser intensity at 2931 cm^{-1} is also observed, correlating to the C-H stretching vibrations in the bonded DMF molecules. In contrast, following the high-temperature treatment, PD-Fe@C350 is characterized by the significant reduction of the characteristic DMF peaks. For the sample of PD-MOF 235, absorption peaks at 1663, 1597, 1390, 1016, and 750 cm^{-1} were detected, which are primarily linked to carboxylate vibrations, consistent with data found in existing literature. Specifically, the sharp peaks at 1597 and 1390 cm^{-1} correspond to asymmetric (C=O) and symmetric (C-O) vibrations of the carboxyl groups, hinting at the presence of dicarboxylic acid esters within the framework. Additionally, the peak at 750 cm^{-1} , which is indicative of C-H bending vibrations in the benzene ring, confirms the compound's identification as MOF-235 [5]. The diminished and broadened peaks seen in the PD-Fe@C350 spectrum are indicative of the successful thermal decomposition of the organic components from the original MOF during the carbonisation process. In conclusion, the collective findings from XRD and FTIR analyses, reinforced by SEM imaging, confirm that high-purity terephthalic acid was successfully derived from waste PET bottles in this study. Furthermore, the sustainable synthesis

of PD-MOF-235 and PD-Fe@C350 was achieved, with both materials exhibiting high purity and uniform morphology.



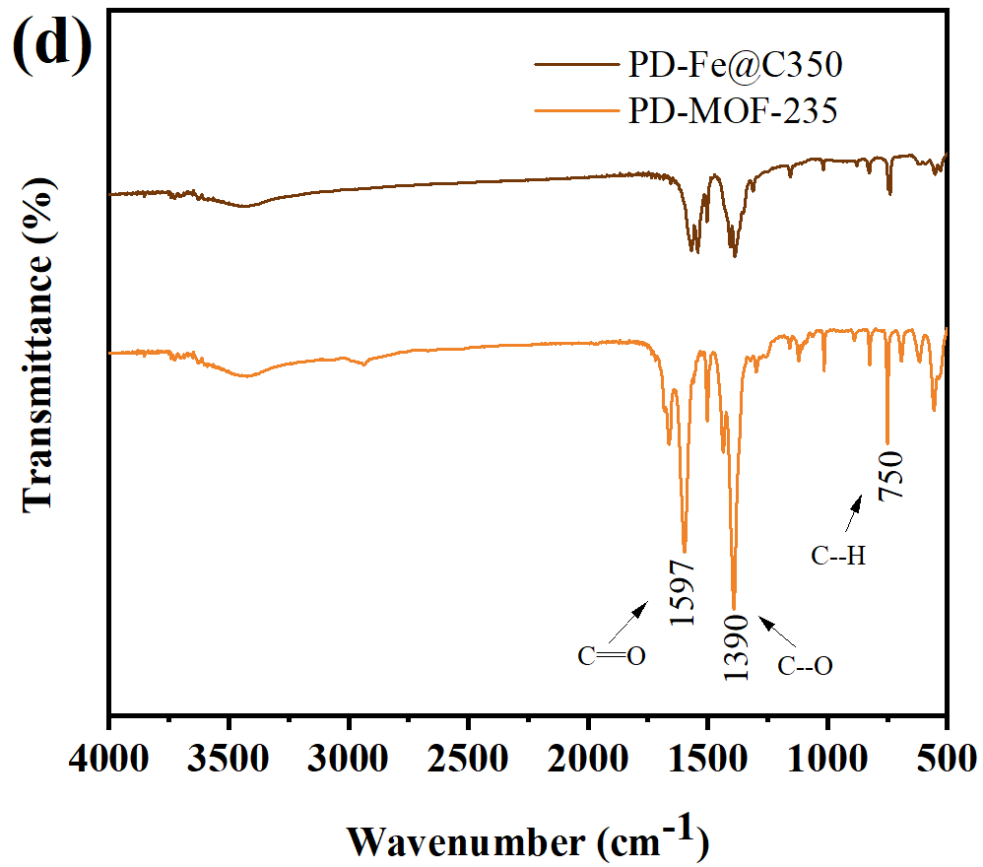
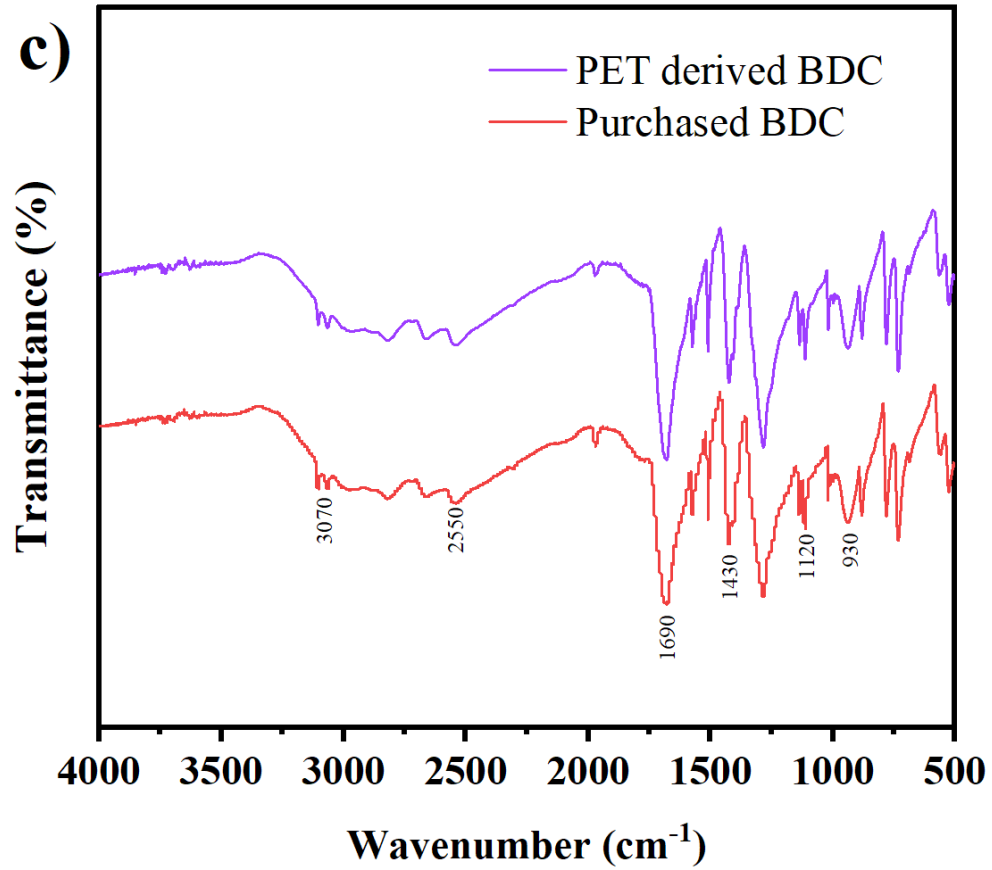


Figure 6.5 XRD patterns of a) PET derived terephthalic acid and purchased terephthalic acid and b) PD-Fe@C350 and PD-MOF-235, FTIR patterns of c) PET derived terephthalic acid and purchased terephthalic acid, d) PD-Fe@C350 and PD-MOF-235.

6.6.3. Photocatalytic Performance

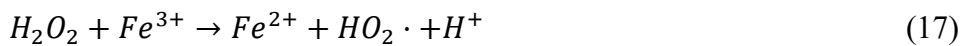
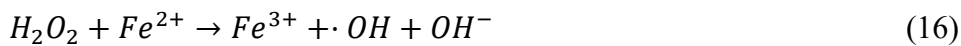
The photocatalytic performance of the synthesized PD-Fe@C350 catalyst on methyl orange was investigated under different conditions. Figure 6.6 (a) illustrates the methyl orange degradation curve. It shows a significant increase in degradation efficiency when the catalyst is combined with visible light and H₂O₂. When the catalyst is only irradiated with visible light without H₂O₂, the methyl orange removal efficiency reaches a peak value of about 80% after 8 minutes, which is mainly due to the surface adsorption properties of PD-Fe@C350 under dark conditions. However, the combined use of light and H₂O₂ significantly accelerates the degradation of methyl orange in wastewater, reaching an efficiency of more than 99% within the same time period. This enhanced photocatalytic degradation emphasizes the synergistic effect of light and H₂O₂ with the photocatalyst, which significantly improves the degradation of methyl orange in wastewater.

Figure 6.6 (b) shows the effects of different concentrations of methyl orange between 50 and 200 mg·L⁻¹ on the removal efficiency of the PD-Fe@C350 catalyst. At a lower methyl orange concentration of 50 mg·L⁻¹, the adsorption efficiency under dark conditions is around 40 %, well below the efficiency of over 80 % observed at concentrations of 100 and 200 mg·L⁻¹. This decrease in efficiency at lower concentrations is primarily due to the reduced mass

transfer. Remarkably, at initial concentrations of 50 and 100 mg·L⁻¹, a degradation efficiency of 99% is achieved within only 6 minutes, with lower concentrations showing higher reaction rate constants. In contrast, methyl orange degradation is not complete at 200 mg·L⁻¹, resulting in a reverse colouration effect. This phenomenon is probably due to an insufficient supply of H₂O₂, resulting in suboptimal decolourisation and incomplete degradation of the chromophore in the methyl orange molecule. The efficiency of the Fenton reaction is closely related to the pH of the solution, especially due to the pH-dependent utilisation of H₂O₂. Insufficient H₂O₂ content can lead to ineffective pH regulation during the reaction and thus reduce the overall efficiency. In addition, a lower pH can acidify the methyl orange stock solution and increase its red colour. These results highlight the critical interplay between dye concentration and pH in the Fenton process and emphasise the need to fine-tune these parameters to maximise the efficiency of wastewater treatment with PD-Fe@C350.

Figure 6.6 (c) illustrates the effects of different H₂O₂ concentrations on the photo-Fenton process for the degradation of methyl orange. First, different dye solution samples were equilibrated for adsorption-desorption under constant conditions. Then 1 mL of H₂O₂ was added at different concentrations, followed by activation of the light source. The results show significant differences in the oxidation-removal efficiency of methyl orange at different H₂O₂ doses. In particular, a lower H₂O₂ concentration of 0.5 M leads to a peak removal efficiency of 95%, followed by a reverse colouration over time, similar to the phenomenon observed in Figure 23. Increasing the H₂O₂ concentration to 1.0 M leads to a reaction rate constant of about 0.019. If you

further increase the H₂O₂ concentration to 1.5 M, the time required for methyl orange degradation decreases significantly. You achieve 99% degradation in 8 minutes with a reaction rate constant of 0.034. This observation is consistent with previous studies indicating that higher doses of H₂O₂ can accelerate the degradation of organic dyes, mainly due to the increased production of free radicals, which are essential for oxidative degradation. However, increasing the H₂O₂ concentration to 2.0 M and 2.5 M paradoxically reduces the degradation efficiency, with the reaction rate constants decreasing to 0.01 and 0.02, respectively. At these higher concentrations, excess hydrogen peroxide can act as a scavenger of hydroxyl radicals ($\cdot\text{OH}$), the primary oxidising agents in the Fenton reaction, as explained in the following equations:



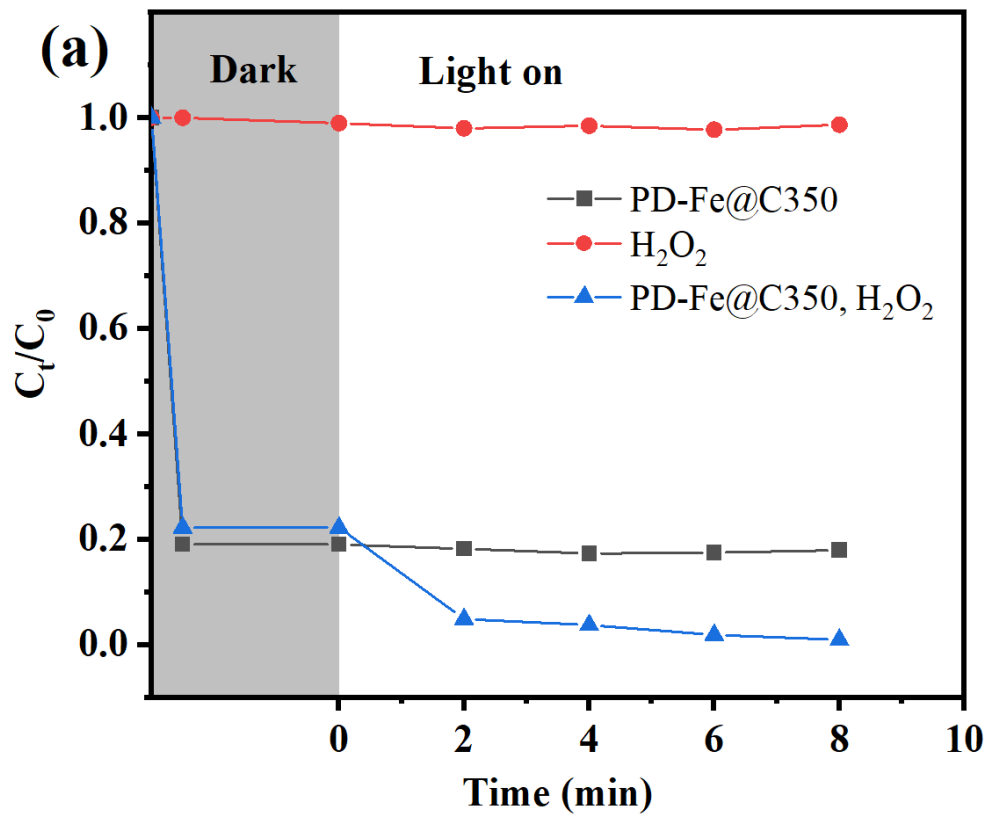
The scavenging effect inherent in the reaction environment reduces the availability of hydroxyl radicals, which are crucial for the oxidation of dye molecules. After careful consideration of the cost-effectiveness and kinetics of the reaction, it was determined that the optimal dosage of hydrogen peroxide (H₂O₂) is 1 ml of a 1.5 M solution when used together with 20 mg of catalyst. This specific dosage is chosen to achieve a delicate balance between maximising degradation efficiency and maintaining practical considerations such as overall cost and operating efficiency.

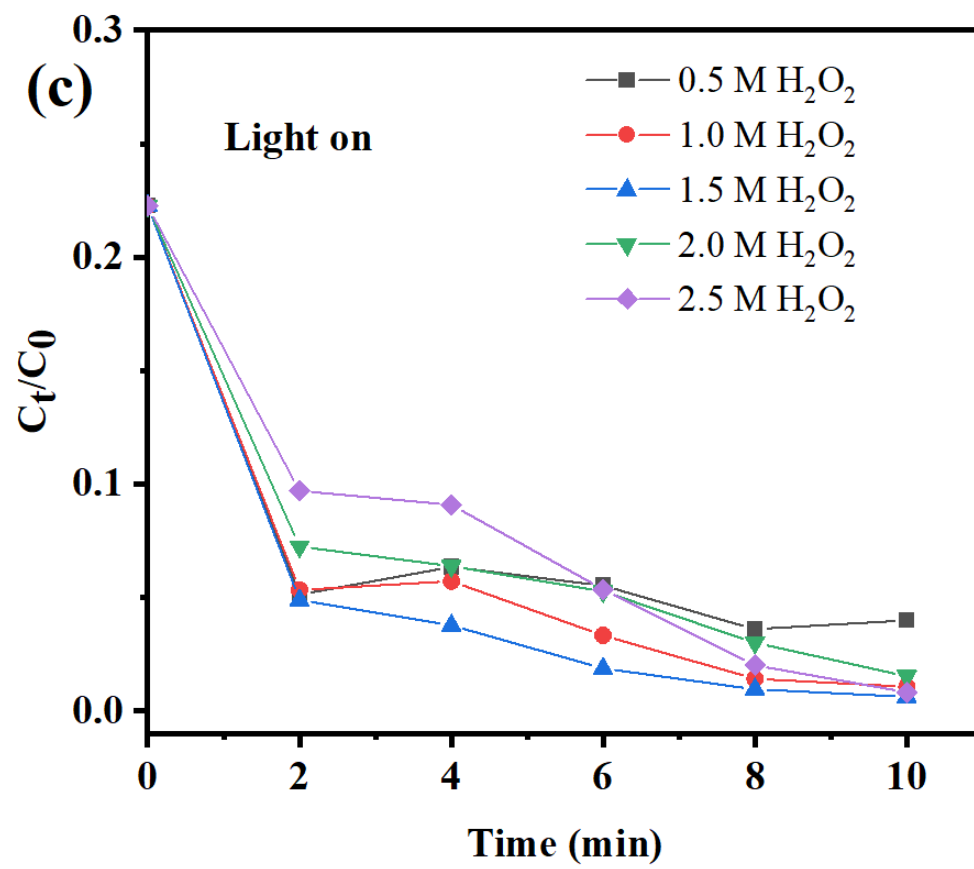
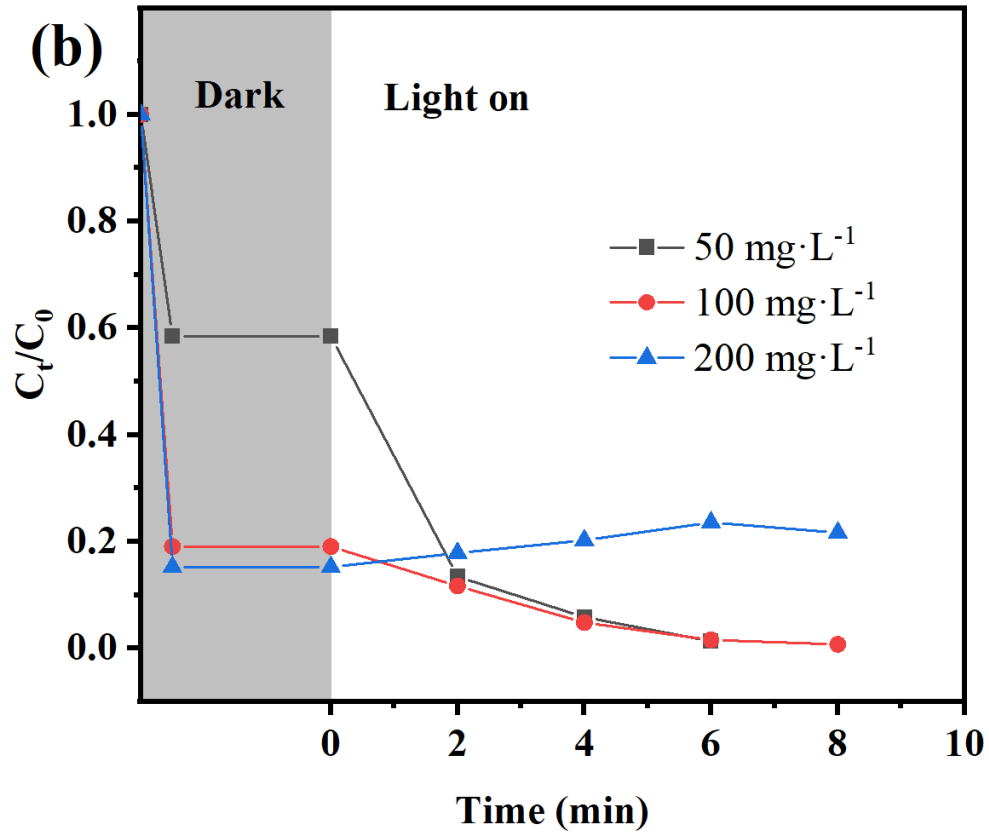
As can be seen in Figure 6.6 (d), PD-Fe@C350 shows remarkable efficacy in the Fenton oxidation process over a pH spectrum of 3 to 7, consistently

achieving degradation rates of over 99%. Remarkably, at a pH of 3, the degradation of methyl orange proceeds exceptionally fast and is completed within only 3 minutes with the highest kinetic rate of 1.171 min^{-1} . In contrast, at a pH of 7, where the concentration at adsorption-desorption equilibrium is only 25% of the initial value, the time to reach 99% degradation is extended to 13 minutes ($k = 0.227 \text{ min}^{-1}$). This observation emphasises that PD-Fe@C350 exhibits improved photo-Fenton catalyst performance under more acidic conditions. It is well known that heterogeneous iron-based Fenton-like catalysts exhibit lower efficiency in neutral environments [200]. However, PD-Fe@C350 is unique in that it contains Fe(III) chloride, which dissociates into Fe^{3+} and Cl^- ions when the catalyst is introduced. These Fe^{3+} ions are hydrolysed, forming hydrated Fe^{3+} ions and releasing H^+ ions, which slightly acidify the solution. This process increases the formation of hydroxyl radicals and thus intensifies the Fenton reaction.

In addition, PD-Fe@C350 shows excellent adsorption performance for methyl orange. Under certain conditions ($C_0 = 100 \text{ mg}\cdot\text{L}^{-1}$, $W = 0.2 \text{ g}\cdot\text{L}^{-1}$, $T = 25^\circ\text{C}$), this material can adsorb about 80 % of methyl orange a pH of 5 to 7, which significantly increases its efficiency in the photo-Fenton catalysis process. Consequently, PD-Fe@C350 shows excellent Fenton oxidation capabilities under both slightly acidic and neutral conditions. The efficiency of the catalyst in a wide pH range indicates its potential for various real-world applications in wastewater treatment. Through a comprehensive series of photo-Fenton experiments, this research has described the optimal conditions for the degradation of methyl orange with PD-Fe@C350, paving the way for

potential industrial-scale applications and significantly improving the practicality of this method.





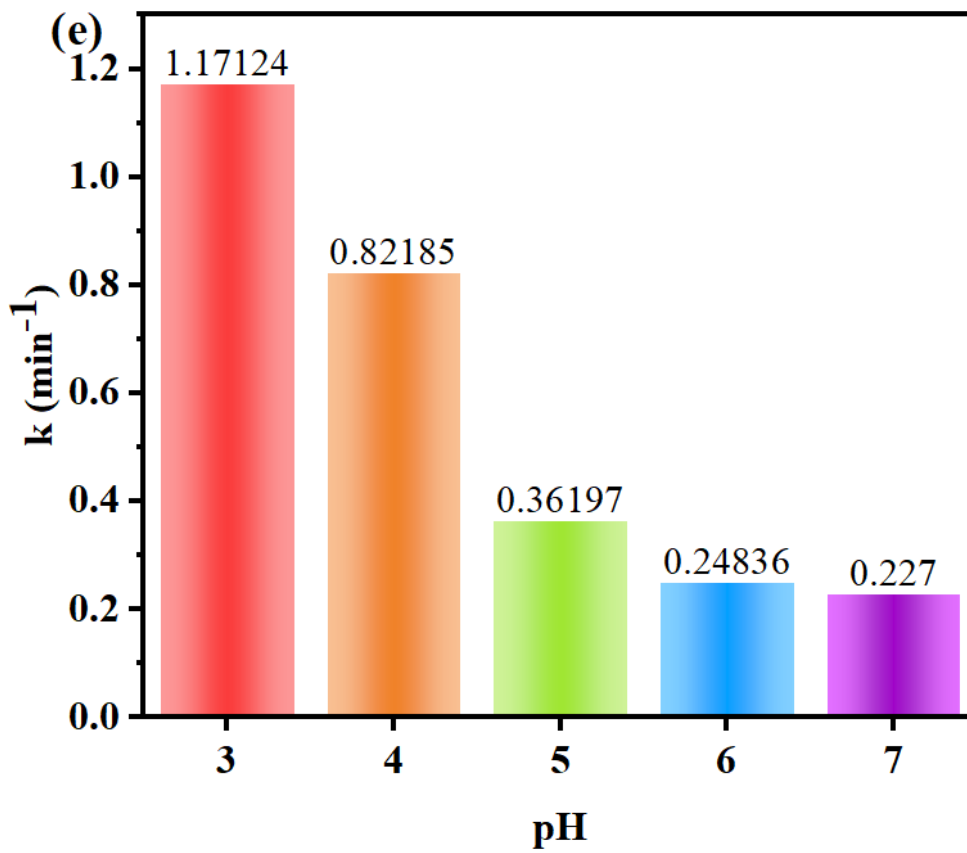
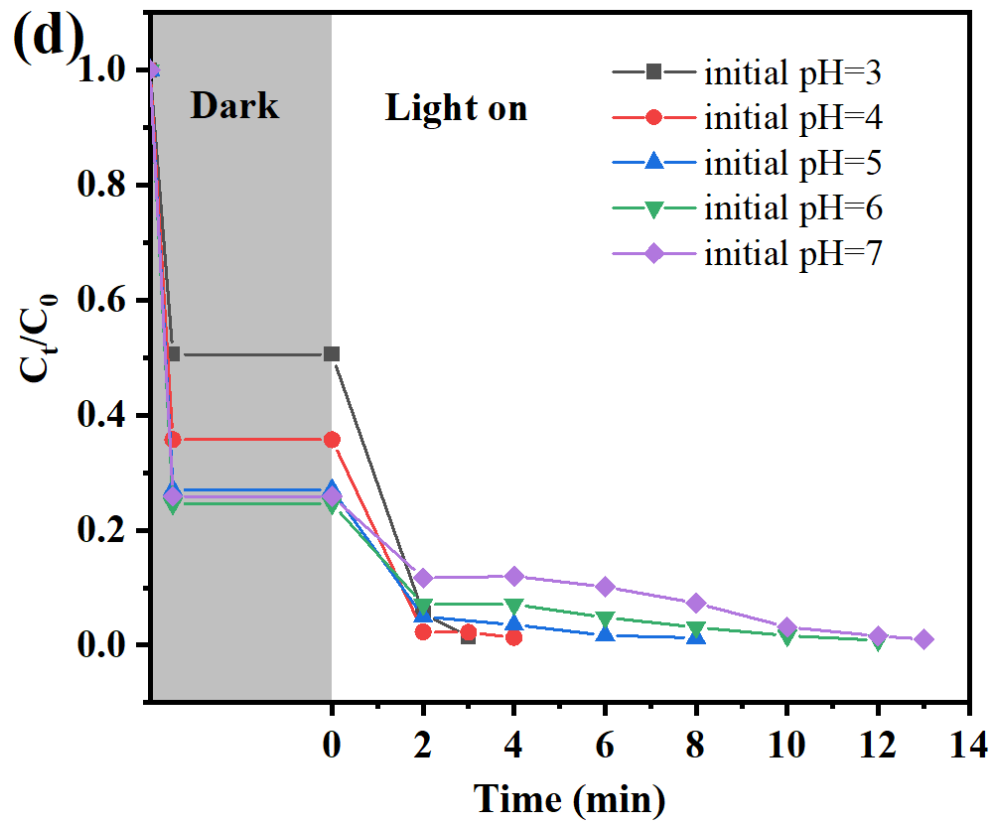


Figure 6.6 Effect of key parameters on degradation the methyl orange: a) H_2O_2 and catalyst existence; b) initial methyl orange concentration and c) H_2O_2 dosage; d) initial solution pH, and (e) kinetic rates of PD-Fe@C350 in the pH range from 3 to 7.

Table 6.1 shows the excellent performance of the photocatalyst PD-Fe@C350 in the degradation of methyl orange. At a concentration of $100 \text{ mg}\cdot\text{L}^{-1}$ of methyl orange and only $0.2 \text{ g}\cdot\text{L}^{-1}$ of catalyst under visible light, this photocatalyst achieved an impressive degradation rate of 99.9% in only 3 minutes. Compared to other listed photocatalysts, which required significantly longer times (between 10 and 300 minutes) and used different light sources such as UV or UV-B irradiation, PD-Fe@C350 is characterised by its fast and highly efficient performance under visible light.

Table 6.1 Comparison of the methyl orange degradation rate between the PD-Fe@C350 and other reported photocatalysts.

Photocatalyst	Initial methyl orange concentration	Catalyst amount (g·L ⁻¹)	Light source	Time (min)	Degradation rate (%)	Ref.
Modified fly ash mixed with TiO ₂	0.05 mM	0.4	Visible light	300	75	[201]
Mill scale	0.1 mM	0.5	UV irradiation	60	80	[202]
South African Ilmenite Sands	10 mg·L ⁻¹	2.0	UV-B	45	100	[203]
Iron-modified Laponite @diatomite composites	200 mg·L ⁻¹	0.3	UV irradiation	240	100	[204]
α-Fe ₂ O ₃ nanoparticles	200 mg·L ⁻¹	1.0	UV irradiation	10	99.55	[205]
PD-Fe@C350	100 mg·L⁻¹	0.2	Visible light	3	99.9	This work

6.7. Mechanism

The photo-Fenton reaction mechanism was investigated in this study by comparing the XPS results of fresh PD-Fe@C350 with those of PD-Fe@C350 after the photocatalytic reaction. As shown in Figure 6.7 (a), the peaks at 711 eV, 532 eV and 284 eV correspond to Fe 2p, O 1s and C 1s signals, respectively, indicating the presence of Fe, O and C elements in PD-Fe@C350 both before and after the reaction [206]. In the Fe 2p spectrum (Figure 6.7 (b)), two prominent peaks at about 724.5 eV and 710 eV represent Fe 2p_{1/2} and Fe 2p_{3/2}, respectively. The Fe 2p_{3/2} spectrum shows two broad peaks at 710.5 eV and 712.3 eV and a small shoulder peak at 708.4 eV, which are characteristic of Fe³⁺ and Fe²⁺, respectively [207]. A comparison of the Fe ion content in PD-Fe@C350 before and after the reaction shows a significant consumption of Fe(II/III) during the photo-Fenton process. The consumed Fe(II/III) and the added H₂O₂ as reactants interact under visible light to form a photo-Fenton reaction in which additional hydroxyl radicals (\cdot OH) are formed. This increased radical production enhances the efficiency of the oxidative degradation of methyl orange. The experimental results show that the addition of H₂O₂ not only facilitates the continuous generation of \cdot OH, but also further accelerates the degradation of methyl orange through the photo-Fenton reaction.

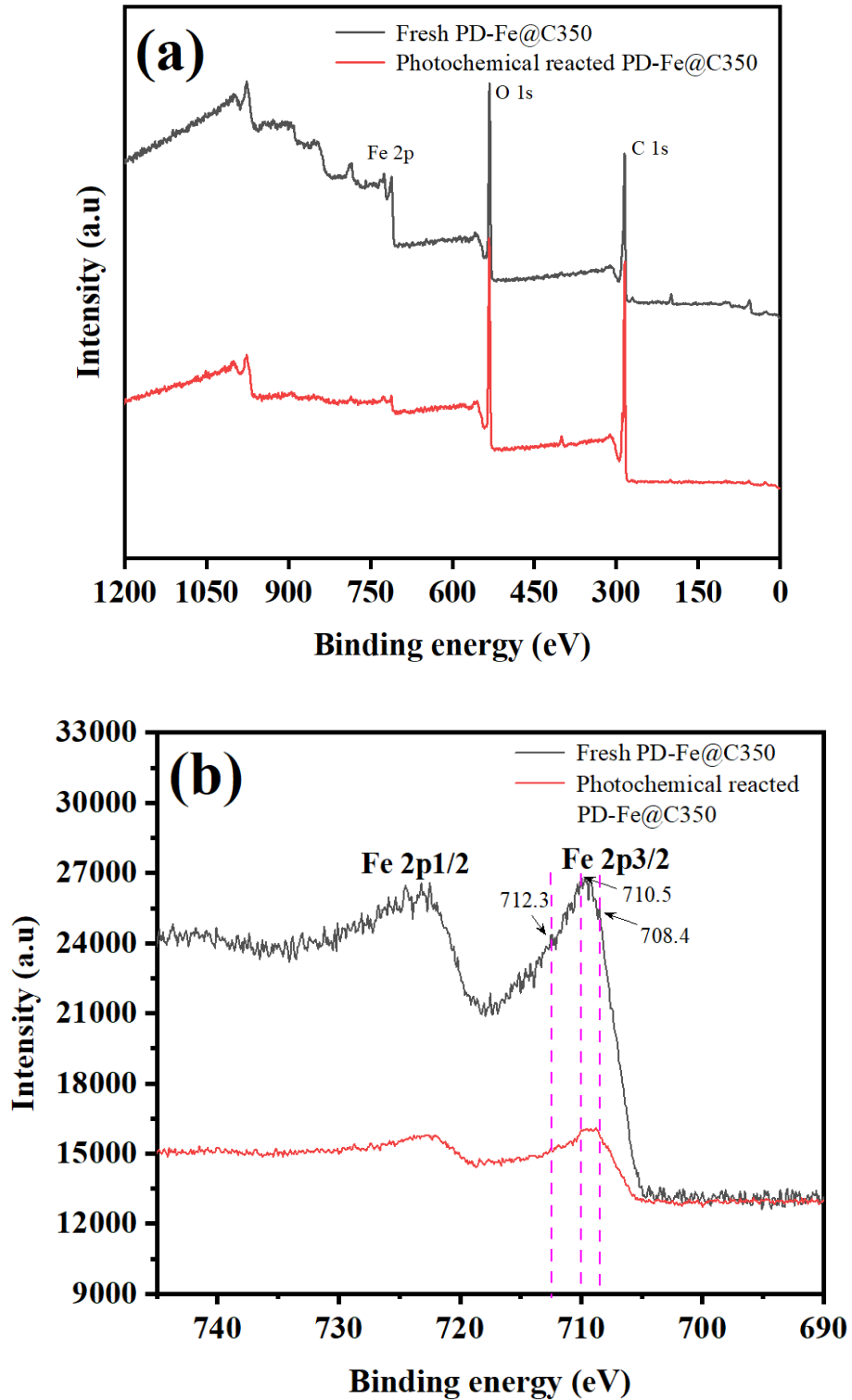
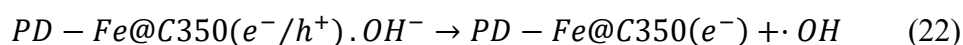
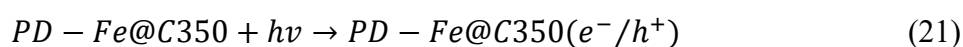
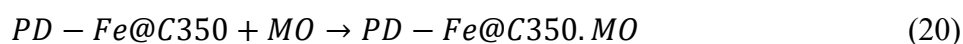
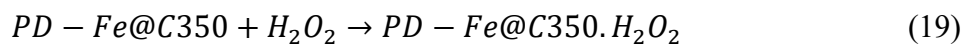
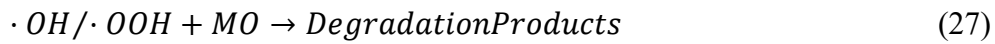
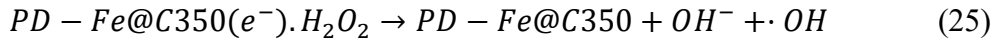
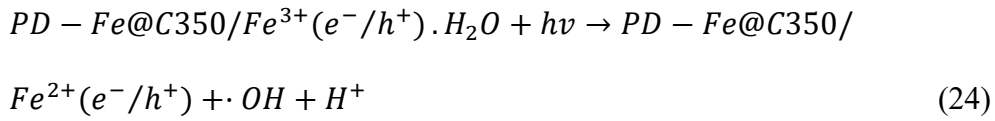
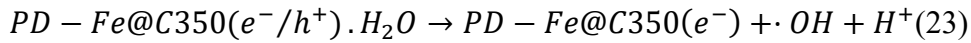


Figure 6.7 (a) XPS survey spectrum of fresh PD-Fe@C350 and photochemical reacted PD-Fe@C350, and (b) Fe 2p spectra of fresh PD-Fe@C350 and photochemical reacted PD-Fe@C350.

In this study, the photocatalytic degradation mechanism of methyl orange dye using the PD-Fe@C350 catalyst was investigated under the influence of H₂O₂ and visible light. The MOF structure within the PD-Fe@C350 particles increases the surface area and provides additional adsorption sites, improving the adsorption of the dye and the overall degradation efficiency. The experiments showed that the degradation process mainly occurs through hydroxyl radicals ($\cdot\text{OH}$). The mechanism takes place in several steps: First, both H₂O₂ and methyl orange are adsorbed onto the surface of PD-Fe@C350 (Eq (19,20)). When the catalyst is irradiated with visible light, it is activated and generates electron/hole pairs (Eq (21)) [208]. The holes (h^+) oxidise hydroxyl groups and water molecules on the surface and generate additional $\cdot\text{OH}$ (Eq (22,23)) [209]. The heterogeneous Fenton-like reaction oxidises Fe²⁺ to Fe³⁺ [210], which is then regenerated back to Fe²⁺ by photo-induced electrons (Eq (24)), increasing the efficiency of the photo-Fenton reaction [211]. In addition, excess H₂O₂ traps the electrons generated by light in the catalyser, leading to the production of further $\cdot\text{OH}$ or direct photolysis (Eq (25,26)). During the photo-Fenton process, methyl orange reacts with $\cdot\text{OH}$, undergoing cleavage and oxidation, and ultimately decomposes into carbon dioxide, water, and inorganic salts (Eq (27)). The specific photocatalytic reaction processes are outlined by the following equations.





6.8. Conclusions

In this chapter, various PD-Fe@Cx nanocomposites were prepared using terephthalic acid from the pyrolysis of PET waste bottles as the main raw material. The study identified 350°C as the optimum carbonisation temperature. It was also found that the amounts of catalyst, H₂O₂ dosage and the initial pH of the solution significantly affect the efficiency of PD-Fe@C350 in the catalytic degradation of methyl orange. Oxidative degradation experiments showed that PD-Fe@C350 exhibited excellent heterogeneous photo-Fenton catalytic performance among a wide range of pH. Under the conditions of pH 3, with 2 mg·L⁻¹ catalyst and 1 mL of 1.5 M H₂O₂, it achieved a 99.9 wt% degradation rate for 100 mg·L⁻¹ methyl orange solution, with a rate constant of k = 1.171 min⁻¹. These results indicate that PD-Fe@C350 is an effective high-performance photo-Fenton catalyst for the degradation of methyl orange in water.

Chapter 7.

Conclusions and Future Work

This chapter summarises the main findings of the study and highlights the main conclusions drawn from the research. It also identifies possible directions for future work and suggests areas where further research could improve the understanding and application of the materials and techniques investigated. These future research directions aim to build on the findings of the current study and explore new ways to improve the efficiency and sustainability of dye removal processes in aqueous environments. The chapter emphasises the importance of ongoing research in advancing this field and addressing the challenges associated with the industrial and environmental applications of these technologies.

7.1. Conclusions

This study investigated the feasibility and efficacy of using MOF-235 as a precursor for the preparation of uniform size adsorbents and photo-Fenton catalysts. Numerous reaction tests were conducted to investigate the influence of various factors such as temperature, pH, contact time and initial concentration on dye removal efficiency. Characterisation studies were carried out to elucidate the possible adsorption and photo-Fenton catalyst mechanisms. It was found that:

- 1) A controlled synthesis method was developed for MOF-235, which is characterised by a uniform particle size distribution and significantly improves the yield. Analytical studies showed that MOF-235 mainly adsorbs methyl orange by electrostatic adsorption processes. Remarkably, MOF-235 exhibited an adsorption efficiency of $1257.7 \text{ mg}\cdot\text{g}^{-1}$, indicating its superior performance. These properties highlight the potential of MOF-235 as an effective adsorbent for the treatment of wastewater contaminated with organic dyes and represent a significant advance in the field of environmental remediation technologies.
- 2) The porous carbon adsorbent Fe@C-350 was synthesised through the pyrolysis of MOF-235 in an argon atmosphere. This material exhibited a rapid adsorption rate, characterised by a first-order kinetic rate constant of 0.849 min^{-1} , and demonstrated a notable methyl orange adsorption capacity of $1666.7 \text{ mg}\cdot\text{g}^{-1}$. Furthermore, Fe@C-350 retained approximately 98% of its initial capacity after 10 adsorption-desorption cycles, highlighting its robust reusability. The adsorption process was

identified as single-layer physical adsorption. These findings underscore the potential of this derived carbonaceous material for effective and sustainable commercial use in environmental remediation.

- 3) The synthesis of various PD-Fe@C-x nanocomposites uses terephthalic acid derived from the pyrolysis of discarded PET bottles, with PD-MOF-235 serving as a precursor under argon protection. The pyrolysis temperature plays a crucial role in determining the structure and morphology of these nanocomposites. Additionally, the catalytic degradation efficiency of methyl orange by PD-Fe@C350 is significantly influenced by factors such as the catalyst and H₂O₂ amounts, as well as the initial pH. Oxidation degradation experiments reveal that PD-Fe@C350 demonstrates optimal heterogeneous photo-Fenton catalytic activity, with a removal efficiency of 99.9 wt% for 100 mL of a 100 mg·L⁻¹ methyl orange solution within 2 minutes at a pH of 4, using 2 mg·L⁻¹ catalyst and 1 mL of 1.5 M H₂O₂. These results underscore the efficacy of synthesising magnetic carbon nanocomposites from PD-MOF-235 at optimal pyrolysis temperatures as an effective approach for developing high-performance photo-Fenton catalysts for the degradation of organic pollutants in aqueous solutions.

7.2. Future Work

Although considerable progress has been made in the development of uniform adsorbents and catalysts based on MOF-235 and the clarification of their mechanisms, significant challenges still need to be overcome in further research.

- 1) Future work will include conducting zeta potential experiments for the controlled synthesis of MOF-235 to better understand the mechanism of change in adsorption capacity for methyl orange at different pH values. In addition, UV-vis analysis in the photo-Fenton experiments should be extended to a broader wavelength range to detect potential shifts around 275 nm, which may help confirm the reduction of methyl orange as photo-induced electrons are generated. In addition, the iron leaching data in the photo-Fenton experiments should be monitored as this is an important indicator of the stability of the catalyst. Controlling the leaching rates will not only prolong the life of the catalyst but also reduce treatment costs and environmental risks.

- 2) The controlled synthesis techniques developed in this study can also be applied to other MOFs such as MIL-101. These techniques can significantly improve the yield and enhance the adsorption and catalytic properties of MOFs and their carbon derivatives. Such improvements are important to advance MOF applications in areas such as environmental remediation and industrial catalysis, where high efficiency in adsorption and catalysis is very important.

- 3) Density functional theory (DFT) calculations play an important role in understanding the mechanisms and reaction pathways of active sites with different sizes. These calculations provide useful information about the electronic structure and catalytic behaviour of active sites. They also help to identify the best configurations for adsorption and catalytic processes. By studying interactions at the molecular level, DFT calculations can

guide the design and improvement of MOF materials. This enables the development of better catalysts with higher performance. This approach is particularly important when tailoring the properties of MOF-235 and its derivatives to specific industrial applications to ensure that they work efficiently and effectively in real-world applications.

- 4) Further studies are needed to test how well MOF-235 and its derivatives can remove various anionic dyes. These studies should focus on understanding the adsorption mechanisms, efficiency and capacity of these materials for different dyes. It is also important to investigate their potential for industrial use. This includes testing their scalability, cost-effectiveness and stability under conditions similar to those of large-scale water treatment processes. Understanding these factors is key to deciding whether these materials can be used in real-world applications, especially in industries where the management of dye wastewater is a major challenge.
- 5) In order to industrialise and commercialise the investigated adsorbents and catalysts, future work should focus on improving synthesis methods that are scalable and cost-efficient. It must be ensured that these materials remain stable and durable under industrial conditions, such as resistance to fouling, extreme pH values and mechanical stress during repeated cycles. The development of reactors for continuous adsorption and catalytic processes will also help to integrate these technologies into existing wastewater treatment systems. Finally, life cycle analyses and cost-benefit analyses will assess the environmental and economic impact

to ensure that these technologies are sustainable and suitable for practical use.

References

1. Pahlow, M., et al., *Increasing pressure on freshwater resources due to terrestrial feed ingredients for aquaculture production*. Science of The Total Environment, 2015. **536**: p. 847-857.
2. Chatterjee, S., et al., *Application of Response Surface Methodology for Methylene Blue dye removal from aqueous solution using low cost adsorbent*. Chemical Engineering Journal, 2012. **181-182**: p. 289-299.
3. Houas, A., et al., *Photocatalytic degradation pathway of methylene blue in water*. Applied Catalysis B: Environmental, 2001. **31**(2): p. 145-157.
4. Gad, H.M.H. and A.A. El-Sayed, *Activated carbon from agricultural by-products for the removal of Rhodamine-B from aqueous solution*. Journal of Hazardous Materials, 2009. **168**(2): p. 1070-1081.
5. Haque, E., J.W. Jun, and S.H. Jhung, *Adsorptive removal of methyl orange and methylene blue from aqueous solution with a metal-organic framework material, iron terephthalate (MOF-235)*. Journal of Hazardous Materials, 2011. **185**(1): p. 507-511.
6. Mohammadi, N., et al., *Adsorption process of methyl orange dye onto mesoporous carbon material—kinetic and thermodynamic studies*. Journal of Colloid and Interface Science, 2011. **362**(2): p. 457-462.

7. Hussain, S., et al., *Adsorption, kinetics and thermodynamics studies of methyl orange dye sequestration through chitosan composites films*. International Journal of Biological Macromolecules, 2021. **168**: p. 383-394.
8. Oladoye, P.O., et al., *Toxicity and decontamination strategies of Congo red dye*. Groundwater for Sustainable Development, 2022. **19**: p. 100844.
9. Ahmad, M.A., et al., *Sorption studies of methyl red dye removal using lemon grass (Cymbopogon citratus)*. Chemical Data Collections, 2019. **22**: p. 100249.
10. Dadfarnia, S., et al., *Methyl red removal from water by iron based metal-organic frameworks loaded onto iron oxide nanoparticle adsorbent*. Applied Surface Science, 2015. **330**: p. 85-93.
11. Mittal, A., et al., *Adsorption of hazardous dye crystal violet from wastewater by waste materials*. Journal of Colloid and Interface Science, 2010. **343**(2): p. 463-473.
12. Ahmad, R., *Studies on adsorption of crystal violet dye from aqueous solution onto coniferous pinus bark powder (CPBP)*. Journal of Hazardous Materials, 2009. **171**(1): p. 767-773.
13. Kishor, R., et al., *Ecotoxicological and health concerns of persistent coloring pollutants of textile industry wastewater and treatment approaches for environmental safety*. Journal of Environmental Chemical Engineering, 2021. **9**(2): p. 105012.

14. Yagub, M.T., T.K. Sen, and H.M. Ang, *Equilibrium, Kinetics, and Thermodynamics of Methylene Blue Adsorption by Pine Tree Leaves*. *Water, Air, & Soil Pollution*, 2012. **223**(8): p. 5267-5282.
15. Murugesan, A., et al., *Cobalt and nickel oxides supported activated carbon as an effective photocatalysts for the degradation Methylene Blue dye from aquatic environment*. *Sustainable Chemistry and Pharmacy*, 2021. **21**: p. 100406.
16. Renita, A.A., et al., *Effective removal of malachite green dye from aqueous solution in hybrid system utilizing agricultural waste as particle electrodes*. *Chemosphere*, 2021. **273**: p. 129634.
17. Mittal, A., et al., *Studies on the adsorption kinetics and isotherms for the removal and recovery of Methyl Orange from wastewaters using waste materials*. *Journal of Hazardous Materials*, 2007. **148**(1): p. 229-240.
18. Liang, J., et al., *Toxicity evaluation of textile dyeing effluent and its possible relationship with chemical oxygen demand*. *Ecotoxicology and Environmental Safety*, 2018. **166**: p. 56-62.
19. Farhan Hanafi, M. and N. Sapawe, *A review on the water problem associate with organic pollutants derived from phenol, methyl orange, and remazol brilliant blue dyes*. *Materials Today: Proceedings*, 2020. **31**: p. A141-A150.
20. Kumari Nisha, S., S. Sivakumar, and S. Achutha, *Polyvinyl alcohol/methyl orange flexible film as reusable pH indicator*. *Materials Today: Proceedings*, 2021. **42**: p. 1008-1011.

21. Liu, Y., et al., *The reuse of nano-TiO₂ under different concentration of CO₂– using coagulation process and its photocatalytic ability in treatment of methyl orange*. Separation and Purification Technology, 2022. **282**: p. 120152.
22. Haji, S., B. Benstaali, and N. Al-Bastaki, *Degradation of methyl orange by UV/H₂O₂ advanced oxidation process*. Chemical Engineering Journal, 2011. **168**(1): p. 134-139.
23. Huo, Y., et al., *Methyl orange removal by combined visible-light photocatalysis and membrane distillation*. Dyes and Pigments, 2013. **98**(1): p. 106-112.
24. Kumar, R.V., A.K. Ghoshal, and G. Pugazhenti, *Fabrication of zirconia composite membrane by in-situ hydrothermal technique and its application in separation of methyl orange*. Ecotoxicology and Environmental Safety, 2015. **121**: p. 73-79.
25. Ince, M. and O. Kaplan Ince, *An Overview of Adsorption Technique for Heavy Metal Removal from Water/Wastewater: A Critical Review*. International Journal of Pure and Applied Sciences, 2017. **3**(2): p. 10-19.
26. Kulkarni, S. and J. Kaware, *Regeneration and recovery in adsorption- a review*. Int. J. Innov. Sci. Eng. Technol, 2014. **1**(8): p. 61-64.
27. Holkar, C.R., et al., *A critical review on textile wastewater treatments: Possible approaches*. Journal of Environmental Management, 2016. **182**: p. 351-366.

28. M'Arimi, M.M., et al., *Recent trends in applications of advanced oxidation processes (AOPs) in bioenergy production: Review*. Renewable and Sustainable Energy Reviews, 2020. **121**: p. 109669.
29. Miralles-Cuevas, S., et al., *Combination of nanofiltration and ozonation for the remediation of real municipal wastewater effluents: Acute and chronic toxicity assessment*. Journal of Hazardous Materials, 2017. **323**: p. 442-451.
30. Chowdhury, P., A. Elkamel, and A.K. Ray, *Photocatalytic Processes for the Removal of Dye*, in *Green Chemistry for Dyes Removal from Wastewater*. 2015. p. 119-137.
31. Maroudas, A., et al., *Synergetic decolorization of azo dyes using ultrasounds, photocatalysis and photo-fenton reaction*. Ultrasonics Sonochemistry, 2021. **71**: p. 105367.
32. Tariq, M., et al., *Removal of Rhodamine B dye from aqueous solutions using photo-Fenton processes and novel Ni-Cu@MWCNTs photocatalyst*. Journal of Molecular Liquids, 2020. **312**: p. 113399.
33. Babuponnusami, A. and K. Muthukumar, *A review on Fenton and improvements to the Fenton process for wastewater treatment*. Journal of Environmental Chemical Engineering, 2014. **2**(1): p. 557-572.
34. Ilhan, F., et al., *Treatability of raw textile wastewater using Fenton process and its comparison with chemical coagulation*. Desalin. Water Treat, 2019. **162**: p. 142-148.

35. Clarizia, L., et al., *Homogeneous photo-Fenton processes at near neutral pH: A review*. Applied Catalysis B: Environmental, 2017. **209**: p. 358-371.
36. Liu, L., et al., *Treatment of industrial dye wastewater and pharmaceutical residue wastewater by advanced oxidation processes and its combination with nanocatalysts: A review*. Journal of Water Process Engineering, 2021. **42**: p. 102122.
37. Ismail, G.A. and H. Sakai, *Review on effect of different type of dyes on advanced oxidation processes (AOPs) for textile color removal*. Chemosphere, 2022. **291**: p. 132906.
38. Iwuzor, K.O., et al., *Adsorption of methyl orange: A review on adsorbent performance*. Current Research in Green and Sustainable Chemistry, 2021. **4**: p. 100179.
39. Song, S., et al., *Sonocatalytic degradation of methyl orange in aqueous solution using Fe-doped TiO₂ nanoparticles under mechanical agitation*. Open Chemistry, 2018. **16**: p. 1283-1296.
40. Deniz, F., *Optimization of methyl orange bioremoval by Prunus amygdalus L. (almond) shell waste: Taguchi methodology approach and biosorption system design*. Desalination and Water Treatment, 2013. **51**: p. 7067-7073.
41. Fröse, A., et al., *Application of natural dyes on diverse textile materials*. Optik, 2019. **181**: p. 215-219.

42. Barnett, J.C., *Synthetic organic dyes, 1856–1901: an introductory literature review of their use and related issues in textile conservation*. *Studies in Conservation*, 2007. **52**(sup1): p. 67-77.
43. Hunger, K., *Industrial Dyes: Chemistry, Properties, Applications*. 2007: Wiley.
44. Chung, K.-T., *Azo dyes and human health: A review*. *Journal of Environmental Science and Health, Part C*, 2016. **34**(4): p. 233-261.
45. Kim, K.-H., E. Kabir, and S.A. Jahan, *The use of personal hair dye and its implications for human health*. *Environment International*, 2016. **89-90**: p. 222-227.
46. Tkaczyk, A., K. Mitrowska, and A. Posyniak, *Synthetic organic dyes as contaminants of the aquatic environment and their implications for ecosystems: A review*. *Science of The Total Environment*, 2020. **717**: p. 137222.
47. Salleh, M.A.M., et al., *Cationic and anionic dye adsorption by agricultural solid wastes: A comprehensive review*. *Desalination*, 2011. **280**(1): p. 1-13.
48. Azam, K., et al., *A review on activated carbon modifications for the treatment of wastewater containing anionic dyes*. *Chemosphere*, 2022. **306**: p. 135566.
49. Chen, S., et al., *Equilibrium and kinetic studies of methyl orange and methyl violet adsorption on activated carbon derived from *Phragmites australis**. *Desalination*, 2010. **252**(1): p. 149-156.

50. Piaskowski, K., R. Świdarska-Dąbrowska, and P.K. Zarzycki, *Dye Removal from Water and Wastewater Using Various Physical, Chemical, and Biological Processes*. Journal of AOAC INTERNATIONAL, 2018. **101**(5): p. 1371-1384.
51. Yagub, M.T., et al., *Dye and its removal from aqueous solution by adsorption: A review*. Advances in Colloid and Interface Science, 2014. **209**: p. 172-184.
52. Allen, S. and B. Koumanova, *Decolourisation of water/wastewater using adsorption*. Journal of the university of chemical technology and metallurgy, 2005. **40**(3): p. 175-192.
53. Li, H., et al., *Cu@Co-MOFs as a novel catalyst of peroxymonosulfate for the efficient removal of methylene blue*. RSC Advances, 2019. **9**(17): p. 9410-9420.
54. Nandi, B.K., A. Goswami, and M.K. Purkait, *Removal of cationic dyes from aqueous solutions by kaolin: Kinetic and equilibrium studies*. Applied Clay Science, 2009. **42**(3): p. 583-590.
55. Liu, W., et al., *Kinetics and thermodynamics characteristics of cationic yellow X-GL adsorption on attapulgite/rice hull-based activated carbon nanocomposites*. Environmental Progress & Sustainable Energy, 2013. **32**(3): p. 655-662.
56. Alqadami, A.A., et al., *Adsorptive performance of MOF nanocomposite for methylene blue and malachite green dyes: Kinetics, isotherm and mechanism*. Journal of Environmental Management, 2018. **223**: p. 29-36.

57. Katheresan, V., J. Kannedo, and S.Y. Lau, *Efficiency of various recent wastewater dye removal methods: A review*. Journal of Environmental Chemical Engineering, 2018. **6**(4): p. 4676-4697.
58. Mhamdi, M., et al., *Adsorption of lead onto smectite from aqueous solution*. Environmental Science and Pollution Research, 2013. **20**(3): p. 1686-1697.
59. Mohammadi, A.A., et al., *Metal-organic framework Uio-66 for adsorption of methylene blue dye from aqueous solutions*. International Journal of Environmental Science and Technology, 2017. **14**(9): p. 1959-1968.
60. Jun, B.-M., et al., *Comprehensive evaluation on removal of lead by graphene oxide and metal organic framework*. Chemosphere, 2019. **231**: p. 82-92.
61. Moawed, E.A., H.A. Kiwaan, and M.M. Elshazly, *Application of polyurethane@salvadora persica composite for detection and removal of acidic and basic dyes from wastewater*. Journal of the Taiwan Institute of Chemical Engineers, 2017. **80**: p. 894-900.
62. Monte Blanco, S.P.D., et al., *Kinetic, equilibrium and thermodynamic phenomenological modeling of reactive dye adsorption onto polymeric adsorbent*. Chemical Engineering Journal, 2017. **307**: p. 466-475.
63. Huo, S.-H. and X.-P. Yan, *Metal-organic framework MIL-100(Fe) for the adsorption of malachite green from aqueous solution*. Journal of Materials Chemistry, 2012. **22**(15): p. 7449.

64. Zhang, J., F. Li, and Q. Sun, *Rapid and selective adsorption of cationic dyes by a unique metal-organic framework with decorated pore surface*. Applied Surface Science, 2018. **440**: p. 1219-1226.
65. Liu, X., et al., *Selective adsorption performance of H₆P₂Mo₁₅W₃O₆₂-based Cu₃(BTC)₂ composite in treatment of simulated cationic dye wastewater*. Chemical Research in Chinese Universities, 2017. **33**(2): p. 268-273.
66. Silvani, L., G. Cornelissen, and S.E. Hale, *Sorption of α -, β -, γ - and δ -hexachlorocyclohexane isomers to three widely different biochars: Sorption mechanisms and application*. Chemosphere, 2019. **219**: p. 1044-1051.
67. Oberoi, A.S., et al., *Insights into the Fate and Removal of Antibiotics in Engineered Biological Treatment Systems: A Critical Review*. Environmental Science & Technology, 2019. **53**(13): p. 7234-7264.
68. Qiao, X.X., et al., *Engineered nanoscale schwertmannites as Fenton-like catalysts for highly efficient degradation of nitrophenols*. Applied Surface Science, 2021. **548**: p. 149248.
69. Ganiyu, S.O., et al., *Coupling of membrane filtration and advanced oxidation processes for removal of pharmaceutical residues: A critical review*. Separation and Purification Technology, 2015. **156**: p. 891-914.
70. Jain, B., et al., *Treatment of organic pollutants by homogeneous and heterogeneous Fenton reaction processes*. Environmental Chemistry Letters, 2018. **16**(3): p. 947-967.

71. Zhang, Y., et al., *Coupling of heterogeneous advanced oxidation processes and photocatalysis in efficient degradation of tetracycline hydrochloride by Fe-based MOFs: Synergistic effect and degradation pathway*. Chemical Engineering Journal, 2019. **369**: p. 745-757.
72. Mohammadifard, Z., et al., *Heterogeneous photo-Fenton degradation of formaldehyde using MIL-100(Fe) under visible light irradiation*. Environmental Pollution, 2019. **251**: p. 783-791.
73. Xiao, J., et al., *Fenton-Like Reaction: Recent Advances and New Trends*. Chemistry – A European Journal, 2024. **30**(24): p. e202304337.
74. Liu, N., et al., *Ultrathin graphene oxide encapsulated in uniform MIL-88A(Fe) for enhanced visible light-driven photodegradation of RhB*. Applied Catalysis B: Environmental, 2018. **221**: p. 119-128.
75. Mei, W., et al., *Effect of electronic migration of MIL-53(Fe) on the activation of peroxymonosulfate under visible light*. Chemical Physics Letters, 2018. **706**: p. 694-701.
76. Cao, J., Z. Xiong, and B. Lai, *Effect of initial pH on the tetracycline (TC) removal by zero-valent iron: Adsorption, oxidation and reduction*. Chemical Engineering Journal, 2018. **343**: p. 492-499.
77. Yilmaz, E., E. Sert, and F.S. Atalay, *Synthesis, characterization of a metal organic framework: MIL-53 (Fe) and adsorption mechanisms of methyl red onto MIL-53 (Fe)*. Journal of the Taiwan Institute of Chemical Engineers, 2016. **65**: p. 323-330.

78. Gao, Y., et al., *Integrated adsorption and visible-light photodegradation of aqueous clofibric acid and carbamazepine by a Fe-based metal-organic framework*. Chemical Engineering Journal, 2017. **330**: p. 157-165.
79. Hu, H., et al., *Enhanced photocatalysis degradation of organophosphorus flame retardant using MIL-101(Fe)/persulfate: Effect of irradiation wavelength and real water matrixes*. Chemical Engineering Journal, 2019. **368**: p. 273-284.
80. MacDonald, M.J., et al., *Photo-Fenton abatement of aqueous organics using metal-organic frameworks: An advancement from benchmark zeolite*. Science of The Total Environment, 2018. **644**: p. 389-397.
81. Ahmad, N., et al., *Visible light-conducting polymer nanocomposites as efficient photocatalysts for the treatment of organic pollutants in wastewater*. Journal of Environmental Management, 2021. **295**: p. 113362.
82. Du, C., et al., *Fe-based metal organic frameworks (Fe-MOFs) for organic pollutants removal via photo-Fenton: A review*. Chemical Engineering Journal, 2022. **431**: p. 133932.
83. Lin, J., et al., *Fabrication of GO@MIL-101(Fe) for enhanced visible-light photocatalysis degradation of organophosphorus contaminant*. Journal of Water Process Engineering, 2020. **33**: p. 101010.
84. Liu, W., et al., *Enhancing electronic transfer by magnetic iron materials and metal-organic framework via heterogeneous Fenton-*

- like process and photocatalysis*. *Materials Science in Semiconductor Processing*, 2021. **135**: p. 106096.
85. Wu, Y., et al., *2D/2D FeNi-layered double hydroxide/bimetal-MOFs nanosheets for enhanced photo-Fenton degradation of antibiotics: Performance and synergetic degradation mechanism*. *Chemosphere*, 2022. **287**: p. 132061.
86. Xu, W., et al., *Morphology controlled synthesis of α -Fe₂O_{3-x} with benzimidazole-modified Fe-MOFs for enhanced photo-Fenton-like catalysis*. *Applied Catalysis B: Environmental*, 2021. **291**: p. 120129.
87. Jiao, L., et al., *Metal–organic frameworks: Structures and functional applications*. *Materials Today*, 2019. **27**: p. 43-68.
88. Lee, Y.-R., J. Kim, and W.-S. Ahn, *Synthesis of metal-organic frameworks: A mini review*. *Korean Journal of Chemical Engineering*, 2013. **30**(9): p. 1667-1680.
89. Safaei, M., et al., *A review on metal-organic frameworks: Synthesis and applications*. *TrAC Trends in Analytical Chemistry*, 2019. **118**: p. 401-425.
90. Stock, N. and S. Biswas, *Synthesis of Metal-Organic Frameworks (MOFs): Routes to Various MOF Topologies, Morphologies, and Composites*. *Chemical Reviews*, 2012. **112**(2): p. 933-969.
91. Ding, M., X. Cai, and H.-L. Jiang, *Improving MOF stability: approaches and applications*. *Chemical Science*, 2019. **10**(44): p. 10209-10230.

92. Maru, K., S. Kalla, and R. Jangir, *Dye contaminated wastewater treatment through metal–organic framework (MOF) based materials*. *New Journal of Chemistry*, 2022. **46**(7): p. 3054-3072.
93. Jiang, D., et al., *The application of different typological and structural MOFs-based materials for the dyes adsorption*. *Coordination Chemistry Reviews*, 2019. **380**: p. 471-483.
94. Rubio-Martinez, M., et al., *New synthetic routes towards MOF production at scale*. *Chemical Society Reviews*, 2017. **46**(11): p. 3453-3480.
95. Feng, S.H. and G.H. Li, *Chapter 4 - Hydrothermal and Solvothermal Syntheses*, in *Modern Inorganic Synthetic Chemistry (Second Edition)*, R. Xu and Y. Xu, Editors. 2017, Elsevier: Amsterdam. p. 73-104.
96. Julien, P.A., C. Mottillo, and T. Frišćić, *Metal–organic frameworks meet scalable and sustainable synthesis*. *Green Chemistry*, 2017. **19**(12): p. 2729-2747.
97. Chen, J., K. Shen, and Y. Li, *Greening the Processes of Metal–Organic Framework Synthesis and their Use in Sustainable Catalysis*. *ChemSusChem*, 2017. **10**(16): p. 3165-3187.
98. Fu, J. and Y.-n. Wu, *A Showcase of Green Chemistry: Sustainable Synthetic Approach of Zirconium-Based MOF Materials*. *Chemistry – A European Journal*, 2021. **27**(39): p. 9967-9987.
99. El-Sayed, E.-S.M. and D. Yuan, *Waste to MOFs: sustainable linker, metal, and solvent sources for value-added MOF synthesis and applications*. *Green Chemistry*, 2020. **22**(13): p. 4082-4104.

100. Shanmugam, M., et al., *Upcycling hazardous metals and PET waste-derived metal–organic frameworks: a review on recent progresses and prospects*. *New Journal of Chemistry*, 2022. **46**(33): p. 15776-15794.
101. Cheng, S., et al., *Waste PET-derived MOF-5 for high-efficiency removal of tetracycline*. *Separation and Purification Technology*, 2024. **339**: p. 126490.
102. Li, J., et al., *Facile synthesis of accordion-like porous carbon from waste PET bottles-based MIL-53(Al) and its application for high-performance Zn-ion capacitor*. *Green Energy & Environment*, 2024. **9**(7): p. 1138-1150.
103. Al-Enizi, A.M., et al., *Waste polyethylene terephthalate plastic derived Zn-MOF for high performance supercapacitor application*. *Journal of King Saud University - Science*, 2024. **36**(5): p. 103179.
104. Nabgan, B., et al., *Pellet size dependent steam reforming of polyethylene terephthalate waste for hydrogen production over Ni/La promoted Al₂O₃ catalyst*. *International Journal of Hydrogen Energy*, 2017. **42**(34): p. 21571-21585.
105. Beniah Obinna, I. and E.C. Ebere, *A review: Water pollution by heavy metal and organic pollutants: Brief review of sources, effects and progress on remediation with aquatic plants*. *Analytical Methods in Environmental Chemistry Journal*, 2019: p. 5-38.
106. Rojas, S. and P. Horcajada, *Metal–Organic Frameworks for the Removal of Emerging Organic Contaminants in Water*. *Chemical Reviews*, 2020. **120**(16): p. 8378-8415.

107. Mukherjee, D., B. Van der Bruggen, and B. Mandal, *Advancements in visible light responsive MOF composites for photocatalytic decontamination of textile wastewater: A review*. *Chemosphere*, 2022. **295**: p. 133835.
108. Li, S., et al., *Water Purification: Adsorption over Metal-Organic Frameworks*. *Chinese Journal of Chemistry*, 2016. **34**(2): p. 175-185.
109. Ihsanullah, I., *Applications of MOFs as adsorbents in water purification: Progress, challenges and outlook*. *Current Opinion in Environmental Science & Health*, 2022. **26**: p. 100335.
110. Zhu, Y., et al., *Recent progress in developing 2D MOFs/COFs/Zeolites nanosheets membranes for water purification*. *Separation and Purification Technology*, 2024. **337**: p. 126404.
111. Hu, T., et al., *Metal-organic frameworks (MOFs) and their derivatives as emerging catalysts for electro-Fenton process in water purification*. *Coordination Chemistry Reviews*, 2022. **451**: p. 214277.
112. Li, Y., et al., *Synthesis and shaping of metal-organic frameworks: a review*. *Chemical Communications*, 2022. **58**(82): p. 11488-11506.
113. Hashemi, L., M.Y. Masoomi, and H. Garcia, *Regeneration and reconstruction of metal-organic frameworks: Opportunities for industrial usage*. *Coordination Chemistry Reviews*, 2022. **472**: p. 214776.
114. Haque, E., et al., *Adsorptive removal of methyl orange from aqueous solution with metal-organic frameworks, porous chromium-*

- benzenedicarboxylates*. Journal of Hazardous Materials, 2010. **181**(1-3): p. 535-542.
115. Wang, X., et al., *Fe-Based Metal-Organic Frameworks: From Various Synthesis, Diverse Structures to Multifunctional Applications*. Chinese Journal of Chemistry, 2023. **41**(24): p. 3772-3791.
116. Viswanathan, V.P., et al., *Exploring the Effect of Morphologies of Fe(III) Metal-Organic Framework MIL-88A(Fe) on the Photocatalytic Degradation of Rhodamine B*. ChemistrySelect, 2020. **5**(25): p. 7534-7542.
117. Wang, X., et al., *Fe-Based Metal-Organic Frameworks: From Various Synthesis, Diverse Structures to Multifunctional Applications*. Chinese Journal of Chemistry, 2023. **41**(24): p. 3772-3791.
118. Wu, Q., et al., *Fe-based metal-organic frameworks as Fenton-like catalysts for highly efficient degradation of tetracycline hydrochloride over a wide pH range: Acceleration of Fe(II)/ Fe(III) cycle under visible light irradiation*. Applied Catalysis B: Environmental, 2020. **263**: p. 118282.
119. Xing, D., et al., *Two-dimensional π -d conjugated metal-organic framework $Fe_3(\text{hexaiminotriphenylene})_2$ as a photo-Fenton like catalyst for highly efficient degradation of antibiotics*. Applied Catalysis B: Environmental, 2021. **290**: p. 120029.

120. Feng, L., et al., *Destruction of Metal–Organic Frameworks: Positive and Negative Aspects of Stability and Lability*. *Chemical Reviews*, 2020. **120**(23): p. 13087-13133.
121. Wang, C., et al., *New Strategies for Novel MOF-Derived Carbon Materials Based on Nanoarchitectures*. *Chem*, 2020. **6**(1): p. 19-40.
122. Liu, D., et al., *Recent advances in MOF-derived carbon-based nanomaterials for environmental applications in adsorption and catalytic degradation*. *Chemical Engineering Journal*, 2022. **427**: p. 131503.
123. Yu, F., et al., *Recent progress on metal-organic framework-derived porous carbon and its composite for pollutant adsorption from liquid phase*. *Chemical Engineering Journal*, 2021. **405**: p. 126960.
124. Huo, Q., et al., *Cu, Zn-embedded MOF-derived bimetallic porous carbon for adsorption desulfurization*. *Chemical Engineering Journal*, 2019. **378**: p. 122106.
125. Wang, J., et al., *From metal–organic frameworks to porous carbon materials: recent progress and prospects from energy and environmental perspectives*. *Nanoscale*, 2020. **12**(7): p. 4238-4268.
126. Hu, J., et al., *Porous carbons prepared by using metal–organic framework as the precursor for supercapacitors*. *Carbon*, 2010. **48**(12): p. 3599-3606.
127. Yuan, M., et al., *Co-MOF-Derived Hierarchical Mesoporous Yolk-shell-structured Nanoreactor for the Catalytic Reduction of*

- Nitroarenes with Hydrazine Hydrate*. ChemCatChem, 2019. **11**(14): p. 3327-3338.
128. Kukulka, W., et al., *MOF-5 derived carbon as material for CO₂ absorption*. RSC Advances, 2019. **9**(32): p. 18527-18537.
129. Zhang, X., et al., *Synthesis of 3D magnetic porous carbon derived from a metal–organic framework for the extraction of clenbuterol and ractopamine from mutton samples*. The Analyst, 2020. **145**(14): p. 5011-5018.
130. Liu, B., et al., *Metal-Organic Framework as a Template for Porous Carbon Synthesis*. Journal of the American Chemical Society, 2008. **130**(16): p. 5390-5391.
131. Liu, B., et al., *Metal–organic framework (MOF) as a template for syntheses of nanoporous carbons as electrode materials for supercapacitor*. Carbon, 2010. **48**(2): p. 456-463.
132. Wei, F., et al., *In situ fabricated porous carbon coating derived from metal-organic frameworks for highly selective solid-phase microextraction*. Analytica Chimica Acta, 2019. **1078**: p. 70-77.
133. Ning, X., et al., *N-doped porous carbon supported Ni catalysts derived from modified Ni-MOF-74 for highly effective and selective catalytic hydrodechlorination of 1,2-dichloroethane to ethylene*. Chemosphere, 2020. **241**: p. 124978.
134. Banerjee, A., et al., *MOF derived porous carbon–Fe₃O₄ nanocomposite as a high performance, recyclable environmental*

- superadsorbent*. Journal of Materials Chemistry, 2012. **22**(37): p. 19694.
135. Hussain, M.Z., et al., *MOF Derived Porous ZnO/C Nanocomposites for Efficient Dye Photodegradation*. ACS Applied Energy Materials, 2018. **1**(9): p. 4695-4707.
136. Wang, F., et al., *Atomic Co/Ni active sites assisted MOF-derived rich nitrogen-doped carbon hollow nanocages for enhanced lithium storage*. Chemical Engineering Journal, 2021. **420**: p. 127583.
137. Hao, M., et al., *Recent advances on preparation and environmental applications of MOF-derived carbons in catalysis*. Science of The Total Environment, 2021. **760**: p. 143333.
138. Liang, Y., et al., *Highly efficient removal of quinolones by using the easily reusable MOF derived-carbon*. Journal of Hazardous Materials, 2022. **423**: p. 127181.
139. Karimi, H., et al., *Carbonization temperature effects on adsorption performance of metal-organic framework derived nanoporous carbon for removal of methylene blue from wastewater; experimental and spectrometry study*. Diamond and Related Materials, 2020. **108**: p. 107999.
140. Chen, D., et al., *MOF-derived magnetic porous carbon-based sorbent: Synthesis, characterization, and adsorption behavior of organic micropollutants*. Advanced Powder Technology, 2017. **28**(7): p. 1769-1779.

141. Wang, C., et al., *Large-Scale Synthesis of MOF-Derived Superporous Carbon Aerogels with Extraordinary Adsorption Capacity for Organic Solvents*. *Angewandte Chemie*, 2020. **132**(5): p. 2082-2086.
142. Wang, Y., et al., *Degradation of norfloxacin by MOF-derived lamellar carbon nanocomposites based on microwave-driven Fenton reaction: Improved Fe(III)/Fe(II) cycle*. *Chemosphere*, 2022. **293**: p. 133614.
143. Tang, J. and J. Wang, *MOF-derived three-dimensional flower-like FeCu@C composite as an efficient Fenton-like catalyst for sulfamethazine degradation*. *Chemical Engineering Journal*, 2019. **375**: p. 122007.
144. Shao, W., et al., *Core-shell-structured MOF-derived 2D hierarchical nanocatalysts with enhanced Fenton-like activities*. *Journal of Materials Chemistry A*, 2020. **8**(6): p. 3168-3179.
145. Mohanty, C., et al., *Poly-m-aminophenol/CoFe₂O₄ (p-n) heterojunction: Sustainable decontamination of BPA, ciprofloxacin pollutants from water and its study of antimicrobial performance*. *Journal of Water Process Engineering*, 2024. **65**: p. 105821.
146. Munagapati, V.S., V. Yarramuthi, and D.-S. Kim, *Methyl orange removal from aqueous solution using goethite, chitosan beads and goethite impregnated with chitosan beads*. *Journal of Molecular Liquids*, 2017. **240**: p. 329-339.
147. Fan, J., et al., *Rapid decolorization of azo dye methyl orange in aqueous solution by nanoscale zerovalent iron particles*. *Journal of Hazardous Materials*, 2009. **166**(2): p. 904-910.

148. Darwish, A.A.A., M. Rashad, and H.A. Al-Aoh, *Methyl orange adsorption comparison on nanoparticles: Isotherm, kinetics, and thermodynamic studies*. *Dyes and Pigments*, 2019. **160**: p. 563-571.
149. Mokhtari, P., et al., *Removal of methyl orange by copper sulfide nanoparticles loaded activated carbon: Kinetic and isotherm investigation*. *Journal of Molecular Liquids*, 2016. **219**: p. 299-305.
150. Li, Y., et al., *Facile synthesis of MOF 235 and its superior photocatalytic capability under visible light irradiation*. *RSC Advances*, 2016. **6**(20): p. 16395-16403.
151. Jantawasu, P., T. Sreethawong, and S. Chavadej, *Photocatalytic activity of nanocrystalline mesoporous-assembled TiO₂ photocatalyst for degradation of methyl orange monoazo dye in aqueous wastewater*. *Chemical Engineering Journal*, 2009. **155**(1): p. 223-233.
152. García, E.R., et al. *Adsorption of Azo-Dye Orange II from Aqueous Solutions Using a Metal-Organic Framework Material: Iron-Benzenetricarboxylate*. *Materials*, 2014. **7**, 8037-8057 DOI: 10.3390/ma7128037.
153. Pargoletti, E., et al., *A detailed investigation of MnO₂ nanorods to be grown onto activated carbon. High efficiency towards aqueous methyl orange adsorption/degradation*. *Applied Surface Science*, 2019. **472**: p. 118-126.
154. Ayati, A., et al., *Emerging adsorptive removal of azo dye by metal-organic frameworks*. *Chemosphere*, 2016. **160**: p. 30-44.

155. Sağlam, S., F.N. Türk, and H. Arslanoğlu, *Use and applications of metal-organic frameworks (MOF) in dye adsorption: Review*. Journal of Environmental Chemical Engineering, 2023. **11**(5): p. 110568.
156. He, H., et al., *Rapid room-temperature synthesis of a porphyrinic MOF for encapsulating metal nanoparticles*. Nano Research, 2021. **14**(2): p. 444-449.
157. Simonsson, I., et al., *Experimental investigations into the irregular synthesis of iron(iii) terephthalate metal-organic frameworks MOF-235 and MIL-101*. Dalton Transactions, 2021. **50**(14): p. 4976-4985.
158. Dunne, P.W., E. Lester, and R.I. Walton, *Towards scalable and controlled synthesis of metal-organic framework materials using continuous flow reactors*. Reaction Chemistry & Engineering, 2016. **1**(4): p. 352-360.
159. Liu, Z., et al., *Preparation of a GO/MIL-101(Fe) Composite for the Removal of Methyl Orange from Aqueous Solution*. ACS Omega, 2021. **6**(7): p. 4597-4608.
160. Liu, K., et al., *Simultaneous voltammetric determination of dopamine and uric acid based on MOF-235 nanocomposite*. Inorganic Chemistry Communications, 2022. **142**: p. 109584.
161. Yang, J., et al., *Exploration of hydrogen-bonded organic framework (HOF) as highly efficient adsorbent for rhodamine B and methyl orange*. Microporous and Mesoporous Materials, 2022. **330**: p. 111624.

162. Faraki, Z. and M.A. Bodaghifard, *A Triazine-Based Cationic Covalent Organic Framework as a Robust Adsorbent for Removal of Methyl Orange*. *Polycyclic Aromatic Compounds*, 2023. **43**(7): p. 5940-5957.
163. Du, C., et al., *A novel cationic covalent organic framework as adsorbent for simultaneous removal of methyl orange and hexavalent chromium*. *RSC Advances*, 2023. **13**(34): p. 24064-24070.
164. Molavi, H., et al., *Selective dye adsorption by highly water stable metal-organic framework: Long term stability analysis in aqueous media*. *Applied Surface Science*, 2018. **445**: p. 424-436.
165. Tong, M., et al., *Influence of framework metal ions on the dye capture behavior of MIL-100 (Fe, Cr) MOF type solids*. *Journal of Materials Chemistry A*, 2013. **1**(30): p. 8534.
166. Wang, J. and R. Bai, *Formic acid enhanced effective degradation of methyl orange dye in aqueous solutions under UV-Vis irradiation*. *Water Research*, 2016. **101**: p. 103-113.
167. Parshetti, G.K., et al., *Decolorization and detoxification of sulfonated azo dye methyl orange by *Kocuria rosea* MTCC 1532*. *Journal of Hazardous Materials*, 2010. **176**(1): p. 503-509.
168. Gong, R., et al., *Adsorptive Removal of Methyl Orange and Methylene Blue from Aqueous Solution with Finger-Citron-Residue-Based Activated Carbon*. *Industrial & Engineering Chemistry Research*, 2013. **52**(39): p. 14297-14303.
169. Güyer, G.T., K. Nadeem, and N. Dizge, *Recycling of pad-batch washing textile wastewater through advanced oxidation processes*

- and its reusability assessment for Turkish textile industry.* Journal of Cleaner Production, 2016. **139**: p. 488-494.
170. Islam, M.A., et al., *Removal of dye from polluted water using novel nano manganese oxide-based materials.* Journal of Water Process Engineering, 2019. **32**: p. 100911.
171. Takeuchi, T., et al., *A pathological study of Minamata disease in Japan.* Acta Neuropathologica, 1962. **2**(1): p. 40-57.
172. Al-Tohamy, R., et al., *A critical review on the treatment of dye-containing wastewater: Ecotoxicological and health concerns of textile dyes and possible remediation approaches for environmental safety.* Ecotoxicology and Environmental Safety, 2022. **231**: p. 113160.
173. Slokar, Y.M. and A. Majcen Le Marechal, *Methods of decoloration of textile wastewaters.* Dyes and Pigments, 1998. **37**(4): p. 335-356.
174. Li, T.-T., et al., *Regulation of the surface area and surface charge property of MOFs by multivariate strategy: Synthesis, characterization, selective dye adsorption and separation.* Microporous and Mesoporous Materials, 2018. **272**: p. 101-108.
175. Duo, H., et al., *Iron-based metal–organic framework as an effective sorbent for the rapid and efficient removal of illegal dyes.* New Journal of Chemistry, 2019. **43**(38): p. 15351-15358.
176. Li, W., B. Mu, and Y. Yang, *Feasibility of industrial-scale treatment of dye wastewater via bio-adsorption technology.* Bioresource Technology, 2019. **277**: p. 157-170.

177. Abo El Naga, A.O., S.A. Shaban, and F.Y.A. El Kady, *Metal organic framework-derived nitrogen-doped nanoporous carbon as an efficient adsorbent for methyl orange removal from aqueous solution*. Journal of the Taiwan Institute of Chemical Engineers, 2018. **93**: p. Microbes and environmental management363-373.
178. Zhao, X., et al., *Synthesis of magnetic metal-organic framework (MOF) for efficient removal of organic dyes from water*. Scientific Reports, 2015. **5**(1): p. 11849.
179. Gecgel, C., et al., *Comparison of MIL-101(Fe) and amine-functionalized MIL-101(Fe) as photocatalysts for the removal of imidacloprid in aqueous solution*. Journal of the Iranian Chemical Society, 2019. **16**(8): p. 1735-1748.
180. Chen, D., et al., *Heterogeneous Fenton-like catalysis of Fe-MOF derived magnetic carbon nanocomposites for degradation of 4-nitrophenol*. RSC Adv., 2017. **7**(77): p. 49024-49030.
181. Duo, H., et al., *Metal-organic frameworks derived magnetic porous carbon for magnetic solid phase extraction of benzoylurea insecticides from tea sample by Box-Behnken statistical design*. Journal of Chromatography A, 2020. **1626**: p. 461328.
182. Wu, L., et al., *Study on the adsorption properties of methyl orange by natural one-dimensional nano-mineral materials with different structures*. Scientific Reports, 2021. **11**(1).
183. Tang, L., et al., *Sustainable efficient adsorbent: Alkali-acid modified magnetic biochar derived from sewage sludge for aqueous organic*

- contaminant removal*. Chemical Engineering Journal, 2018. **336**: p. 160-169.
184. Yang, Y. and C. Guan, *Adsorption properties of activated carbon fiber for highly effective removal of methyl orange dye*. IOP Conference Series: Earth and Environmental Science, 2018. **208**(1): p. 012005.
185. Luo, S. and J. Wang, *MOF/graphene oxide composite as an efficient adsorbent for the removal of organic dyes from aqueous solution*. Environmental Science and Pollution Research, 2018. **25**(6): p. 5521-5528.
186. Abo El Naga, A.O., S.A. Shaban, and F.Y.A. El Kady, *Metal organic framework-derived nitrogen-doped nanoporous carbon as an efficient adsorbent for methyl orange removal from aqueous solution*. Journal of the Taiwan Institute of Chemical Engineers, 2018. **93**: p. 363-373.
187. Padmavathy, K.S., G. Madhu, and P.V. Haseena, *A study on Effects of pH, Adsorbent Dosage, Time, Initial Concentration and Adsorption Isotherm Study for the Removal of Hexavalent Chromium (Cr (VI)) from Wastewater by Magnetite Nanoparticles*. Procedia Technology, 2016. **24**: p. 585-594.
188. de Souza, T.N.V., et al., *Adsorption of basic dyes onto activated carbon: Experimental and theoretical investigation of chemical reactivity of basic dyes using DFT-based descriptors*. Applied Surface Science, 2018. **448**: p. 662-670.

189. Haque, E., et al., *Dichotomous adsorption behaviour of dyes on an amino-functionalised metal–organic framework, amino-MIL-101(Al)*. *Journal of Materials Chemistry A*, 2014. **2**(1): p. 193-203.
190. Li, H., et al., *Enhanced adsorptive removal of anionic and cationic dyes from single or mixed dye solutions using MOF PCN-222*. *RSC Advances*, 2017. **7**(27): p. 16273-16281.
191. Deng, S.-Q., et al., *Hydrolytically Stable Nanotubular Cationic Metal–Organic Framework for Rapid and Efficient Removal of Toxic Oxo-Anions and Dyes from Water*. *Inorganic Chemistry*, 2019. **58**(4): p. 2899-2909.
192. Yang, J.-M., et al., *Adsorptive removal of organic dyes from aqueous solution by a Zr-based metal–organic framework: effects of Ce(III) doping*. *Dalton Transactions*, 2018. **47**(11): p. 3913-3920.
193. Zhang, Z.-h., et al., *Selective and Competitive Adsorption of Azo Dyes on the Metal–Organic Framework ZIF-67*. *Water, Air, & Soil Pollution*, 2016. **227**(12): p. 471.
194. Dai, Y., et al., *The adsorption, regeneration and engineering applications of biochar for removal organic pollutants: A review*. *Chemosphere*, 2019. **223**: p. 12-27.
195. Yagub, M.T., T.K. Sen, and H.M. Ang, *Equilibrium, Kinetics, and Thermodynamics of Methylene Blue Adsorption by Pine Tree Leaves*. *Water, Air, & Soil Pollution*, 2012. **223**(8): p. 5267-5282.

196. Zhang, Y., et al., *Heterogeneous degradation of organic contaminants in the photo-Fenton reaction employing pure cubic β -Fe₂O₃*. Applied Catalysis B: Environmental, 2019. **245**: p. 410-419.
197. Yang, R., et al., *Yolk-shell Fe₃O₄@MOF-5 nanocomposites as a heterogeneous Fenton-like catalyst for organic dye removal*. Separation and Purification Technology, 2021. **267**: p. 118620.
198. Xu, H.-Y., et al., *Heterogeneous Fenton-like discoloration of methyl orange using Fe₃O₄/MWCNTs as catalyst: kinetics and Fenton-like mechanism*. Frontiers of Materials Science, 2018. **12**(1): p. 34-44.
199. Miao, S., et al., *Metal-organic frameworks-derived CoFeN-NC materials with the enhanced catalytic activity and selectivity for the degradation of organic dyes via adsorption and heterogeneous photo-Fenton*. Applied Surface Science, 2022. **601**: p. 154028.
200. Sun, W., et al., *Characteristics and application of iron-based materials in heterogeneous Fenton oxidation for wastewater treatment: a review*. Environmental Science: Water Research & Technology, 2023. **9**(5): p. 1266-1289.
201. Visa, M. and A. Duta, *Methyl-orange and cadmium simultaneous removal using fly ash and photo-Fenton systems*. Journal of Hazardous Materials, 2013. **244-245**: p. 773-779.
202. Urmi, S.A., A.S.W. Kurny, and F. Gulshan, *Decolorization of Methyl Orange Using Mill Scale by Photo-Fenton Reaction*. Procedia Engineering, 2015. **105**: p. 844-851.

203. Butt, A.L., J.K. Mpinga, and S.M. Tichapondwa, *Photo-Fenton Oxidation of Methyl Orange Dye Using South African Ilmenite Sands as a Catalyst*. *Catalysts*, 2021. **11**(12): p. 1452.
204. Dai, N., et al., *Typical synthesis of an iron-modified Laponite @diatomite composite for photo-Fenton degradation of methyl orange dyes*. *Applied Surface Science*, 2023. **607**: p. 154886.
205. Xiang, H., et al., *A low-cost solvent-free method to synthesize α -Fe₂O₃ nanoparticles with applications to degrade methyl orange in photo-fenton system*. *Ecotoxicology and Environmental Safety*, 2020. **200**: p. 110744.
206. Wu, C., et al., *Facile synthesis of excellent Fe₃O₄@starch-derived carbon Photo-Fenton catalyst for tetracycline degradation: Rapid Fe³⁺/Fe²⁺ circulation under visible light condition*. *Separation and Purification Technology*, 2024. **329**: p. 125174.
207. Huang, M., et al., *Distinguishing homogeneous-heterogeneous degradation of norfloxacin in a photochemical Fenton-like system (Fe₃O₄/UV/oxalate) and the interfacial reaction mechanism*. *Water Research*, 2017. **119**: p. 47-56.
208. Liu, H., et al., *Highly flexible Fe₂O₃/TiO₂ composite nanofibers for photocatalysis and ultraviolet detection*. *Journal of Physics and Chemistry of Solids*, 2018. **121**: p. 236-246.
209. Zheng, X., et al., *Enhanced photo-Fenton degradation of tetracycline using TiO₂-coated α -Fe₂O₃ core-shell heterojunction*. *Journal of Industrial and Engineering Chemistry*, 2018. **68**: p. 14-23.

210. Dias, F.F., et al., *Residue-based iron catalyst for the degradation of textile dye via heterogeneous photo-Fenton*. *Applied Catalysis B: Environmental*, 2016. **186**: p. 136-142.
211. Du, D., et al., *Yolk-shell structured $Fe_3O_4@void@TiO_2$ as a photo-Fenton-like catalyst for the extremely efficient elimination of tetracycline*. *Applied Catalysis B: Environmental*, 2017. **200**: p. 484-492.